

AD-774 431

AIR CUSHION LANDING SYSTEM DROP
DYNAMICS THEORY (MECHANICAL)

Frederick C. Bauer

Air Force Institute of Technology

Prepared for:

Air Force Flight Dynamics Laboratory

December 1973

DISTRIBUTED BY:

NTIS

National Technical Information Service
U. S. DEPARTMENT OF COMMERCE
5285 Port Royal Road, Springfield Va. 22151

Unclassified

Security Classification

DOCUMENT CONTROL DATA - R & D

(Security classification of title, body of abstract and indexing annotation must be entered when the overall report is classified)

1. ORIGINATING ACTIVITY (Corporate number)

Air Force Institute of Technology (AFIT/EN)
Wright-Patterson AFB, Ohio 45433

2a. REPORT SECURITY CLASSIFICATION

Unclassified

2b. GROUP

3. REPORT TITLE

Air Cushion Landing System, Drop Dynamics Theory (Mechanical)

4. DESCRIPTIVE NOTES (Type of report and inclusive dates)

AFIT Thesis

5. AUTHOR(S) (First name, middle initial, last name)

Frederick C. Bauer, Captain, USAF

6. REPORT DATE

December 1973

7a. TOTAL NO. OF PAGES

88/103

7b. NO. OF REFS

9

8a. CONTRACT OR GRANT NO.

8b. ORIGINATOR'S REPORT NUMBER(S)

GAM/AE/73A-1

8c. PROJECT NO.

N/A

8d. OTHER REPORT NO(S) (Any other numbers that may be assigned this report)

10. DISTRIBUTION STATEMENT

Approved for public release; distribution unlimited.

11. SUPPLEMENTARY NOTES

Approved for public release; IAW AFR 190-17
JERRY C. HIX, Captain, USAF
Director of Information

12. SPONSORING MILITARY ACTIVITY

Air Force Flight Dynamics Laboratory
Wright-Patterson AFB, Ohio 45433

13. ABSTRACT

A mechanical analog Vertical Energy Absorption Model (VEAM) is developed to predict the dynamics of an Air Cushion Landing System (ACLS) in the vertical dimension. Three degrees of freedom and thus three primary modes of oscillation are investigated: heave, pitch and roll. Data from Air Force Flight Dynamics Laboratory Tests of a full-scale Australian Jindivik drone are used to develop and verify the model.

The VEAM study demonstrates that the use of a mechanical analog prediction scheme for an Air-Cushion Landing System has sufficient merit to warrant further investigation. It shows that a mechanical analog model can predict system response within the model domain of three degrees of freedom without knowledge of the numerous and varying trunk and cushion parameters if the mode spring and damper coefficients are provided. The model response correlates with Jindivik test data much better in pitch and roll than in heave. Both the pitch and roll mode spring and damper coefficients are shown to be linear in accordance with model assumptions. Model response in heave is heavily dependent upon the mode damping ratio (ζ) and the undamped natural frequency (ω_n), but the results are reasonable; that is, response frequency correlates to test data and response displacement is in the proper direction but sometimes of incorrect magnitude. The heave mode spring coefficient is shown to hold to the linear approximation. The inability to match magnitudes exactly suggests that the heave damper coefficient is non-linear.

DD FORM 1473
1 NOV 65

Unclassified

Security Classification

KEY WORDS

LINE A

6144 P

LINA C

POLE

vi 7

NOTE

W

500

W

Air Cushion Recovery System

(Continued on next page)

1-574-1000

[illegible]

1. The first of these is the fact that the Government has not been able to secure the necessary funds to carry out its policy. This is due to the fact that the Government has not been able to secure the necessary funds to carry out its policy.

AD-774431

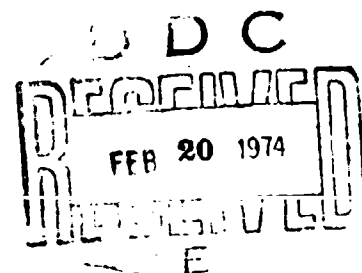
AIR CUSHION LANDING SYSTEM
DROP DYNAMICS THEORY (MECHANICAL)

THESIS

GAM/AE/73A-1

Frederick C. Bauer
Captain USAF

Reproduced by
NATIONAL TECHNICAL
INFORMATION SERVICE
U S Department of Commerce
Springfield VA 22151



Approved for public release; distribution unlimited.

AIR CUSHION LANDING SYSTEM
DROP DYNAMICS THEORY (MECHANICAL)

THESIS

Presented to the Faculty of the School of Engineering of
the Air Force Institute of Technology
Air University
by Partial Fulfillment of the
Requirements for the Degree of
Master of Science

by

Frederick C. Bauer, M.S. (SM)
Captain USAF

Graduate Aerospace-Mechanical Engineering

December 1973

Approved for public release; distribution unlimited.

it

Preface

This report is about a Vertical Energy Absorption Model (VEAM) for an Air Cushion Landing System (ACLS) that was developed from full-scale experimental tests of an Australian Jindivik drone aircraft. The tests were conducted by the Air Force Flight Dynamics Laboratory, Mechanical Branch, and selected test cases were used to verify the predictive capability of the model in its three degrees of freedom; heave, pitch and roll. It is my hope that the results of this effort will find practical use in the Flight Dynamics Laboratory and will help in the advancement of Air Cushion Technology.

I wish to express my gratitude to my academic advisor, Captain James T. Karam, Jr. for the finesse with which he managed the "care and feeding" of the student mind during the experience. His assistance and guidance were invaluable.

I am particularly grateful to Major John C. Vaughn III, Principal Scientist of the Mechanical Branch, AFFDL, for his assistance throughout the period of this study. A special note of appreciation is due to Mr. James T. Steiger, also of the Mechanical Branch, who provided much motivational and technical assistance. Without their aid this study could not have been accomplished.

My children, Scott, Kimberly, and Tiffany, will never know what they contributed toward the completion of this study, and for that I wish to thank them. My wife, Dorothy, knows, and with that knowledge she remained a fortress of patience and a fountain of understanding. She is a special person, and I want very much to thank her...for typing this thesis...for everything.

Contents

	Page
Preface	ii
List of Figures	v
List of Tables	vii
List of Symbols	viii
Abstract	xi
I. Introduction	1
Air Cushion Development	1
Air Cushion Concept and Definitions	2
Air Cushion Application	3
Background	4
Purpose	5
Scope	5
II. Model Development and Theory	6
The Jindivik Drone	6
Test Method and Data	10
The Vertical Energy Absorption Model (VEAM)	12
Model Assumptions	13
Approach to Analysis	13
Linearity of Springs	16
III. The Model Equations of Motion	17
The Force Equation	17
Perturbation from Equilibrium	18
The Heave Mode	19
The Roll Mode	19
The Pitch Mode	20
Free Fall Analysis	20
Summary.	21
IV. Analysis of Jindivik Data (Theory)	22
Analysis of Roll and Pitch Data	22
Analysis of Heave Data	23
Results.	25
V. Analysis of the Spring/Damper Units (Theory)	28
General	28
Spring/Damper Unit Evaluation	28
VI. Analysis of the Vertical Energy Absorption Model.	30
General.	30
Spring Coefficient Comparison.	30
Model Roll Response.	31
Model Pitch Response	31
Model Heave Response	34

VII. Conclusions and Recommendations	41
Conclusions.	41
Recommendations	42
Bibliography.	44
Appendix A: Analysis of Jindivik Data (Computer Solution). .	45
Appendix B: Analysis of the Equations of Motion (Computer Solution).	65
Appendix C: Justification of the Small Angle and Horizontal Displacement Assumptions in Pitch and Roll . . .	82
Appendix D: AFFDL Jindivik and Test Data	86
Vita.	88

List of Figures

Figure		Page
1	The Lake LA-4 Aircraft with ACLS	1
2	The deHavilland CC-115, Buffalo, with ACLS . . .	2
3	An ACLS Trunk - Cushion Configuration.	3
4	The Australian Jindivik Drone with ACLS	4
5	The Jindivik Drone in Test Configuration	8
6	The Jindivik with ACRS, Dimensions, and Instrumentation	9
7	The Jindivik ACRS with Dimensions	10
8	Schematic of Vertical Energy Absorption Model (VEAM)	12
9	Linearity of the Exponential Decay in Roll . . .	14
10	Schematic of Displacements	15
11	Spring Linearity	16
12	A Spring/Damper Unit in Arbitrary Deflection . .	17
13	The VEAM in Arbitrary Deflection (Heave, Pitch and Roll)	18
14	A General Underdamped Sinusoidal Response . . .	22
15	Heave Test Data.	24
16	Heave Data Analysis Coordinates	24
17	Comparison of Spring Coefficients	30
18	Model Response, Roll Test 58, Wing Tip Transducer	32
19	Model Response, Pitch Test 61, Nose Transducer .	33
20a	Model Response, Heave Test 122, CG Transducer. .	36
20b	Model Response, Heave Test 122, CG Transducer. .	37
20c	Model Response, Heave Test 122, CG Transducer. .	38
20d	Model Response, Heave Test 122, CG Transducer. .	39
21	Program DATANYL.	48
22	Program DATANYL, Subroutine DECRE	51
23	Program DATANYL, Subroutine DATAPLT	52
24	Sample Output of Program DATANYL	54
25	Data Analysis of ACRS on Jindivik Drone; Test Run 55, Roll	55
26	Data Analysis of ACRS on Jindivik Drone; Test Run 56, Roll	56

27	Data Analysis of ACRS on Jindivik Drone; Test Run 58, Roll	57
28	Data Analysis of ACRS on Jindivik Drone; Test Run 59, Pitch	58
29	Data Analysis of ACRS on Jindivik Drone; Test Run 60, Pitch	59
30	Data Analysis of ACRS on Jindivik Drone; Test Run 61, Pitch	60
31	Program RISE	63
32	Vertical Displacement for Subroutine LOCATE. . .	66
33	Program MODANYL.	68
34	Program MODANYL, Subroutines F and LOCATE. . .	71
35	Model Response, Roll Test 55, Wing Tip Transducer	72
36	Model Response, Pitch Test 60, Nose Transducer .	73
37	Model Response, Heave Test 121, CG Transducer. .	74
38	Model Response, Roll Test 56, Wing Tip Transducer	77
39	Model Response, Pitch Test 59, Nose Transducer .	78
40	Model Response, Heave Test 123, CG Transducer. .	79
41	Vertical and Translational Transducer Errors . .	83

List of Tables

Table		Page
I	AFFDL Jindivik Test Numbers	11
II	Results of Analysis of Jindivik Data	26
III	Program RISE Free Fall Computations	27
IV	Linear Spring/Damper Unit Coefficients	29
V	Zeta and ω_n Computations for Heave	34
VI	Program DATANYL - Input Data	46
VII	Program DATANYL - Output Data	47
VIII	Program RISE - Input Data	61
IX	Program RISE - Output Data	62

List of Symbols

Symbol	Description	Unit
b	span of the ACLS trunk	in
c	damper coefficient	lb \cdot sec/ft
CG	center of gravity of entire vehicle	
CP	center of pressure of ACLS trunk	
D	displacement, angular or linear	rad or in
d	logarithmic decrement	dimensionless
δ	displacement of CG from CP	in
F	Force	lb \cdot f
f_d	damped natural frequency	cyc/sec
g	gravitational constant	ft/sec ²
h	vertical axis measured from surface, positive down	in
h_c	contact height above the surface; the in ground effect condition of the ACLS and the spring neutral position of the VEAM	in
h_{CG}	vertical displacement height of the CG linear transducer (AFFDL tests)	in
h_{eq}	equilibrium (hover) height above the surface	in
h_i	initial or release height above the surface for drop tests	in
h_n	vertical displacement height of the nose transducer (AFFDL tests)	in
h_{px}	height above surface of any given damped sinusoid peak (X)	in
h_w	vertical displacement height of the wing transducer (AFFDL tests)	in
i	subscript identifier of the five spring/ damper units	
J	moment of inertia of the vehicle	slug-ft ²

K	constant in the heave analysis of \ddot{z} and ω_n	dimensionless
k	spring coefficient	lb _f /ft
l	length of the ACLS trunk between: longitudinal axis ground tangent points	in
M	moment	ft-lb _f
m	mass of the vehicle	slugs
\dot{m}_c	air mass flow rate into ACLS cushion	lb _m /sec
\dot{m}_t	air mass flow rate into ACLS trunk	lb _m /sec
P_c	ACLS cushion pressure	lb _f /in ²
P_a	atmospheric pressure	lb _f /in ²
T	period of sinusoidal oscillation	sec
t	horizontal axis, time, in the model domain	sec
t_o	initial or activation time of the model = τ_c	sec
t_{px}	time in the model domain of any given sinusoid peak (x)	sec
τ	horizontal axis, time, in the free fall domain	sec
τ_o	release time of vehicle for drop tests	sec
τ_c	contact time of vehicle in free fall domain when reaches in ground effect (IGE), = t_o	sec
τ_{px}	time in the free fall domain of any given sinusoid peak (x)	sec
ω_d	damped natural frequency	rad/sec
ω_n	undamped natural frequency	rad/sec
x	longitudinal axis of the model, CG through nose positive	
y	lateral axis of the model, CG through right wing positive	
z	vertical axis of the model, measured from the equilibrium position through the CG downward positive	
z_c	contact height of model measured from equilibrium in	

z	the deflection height of each spring/damper unit measured from the model equilibrium position	in
θ	pitch angle due to rotation about the y axis	rad
ϕ	roll angle due to rotation about the x axis	rad
ϕ'	phase angle of the general underdamped sinusoidal response	rad
γ	damping ratio	dimensionless

Abstract

A mechanical analog Vertical Energy Absorption Model (VEAM) is developed to predict the dynamics of an Air Cushion Landing System (ACLS) in the vertical dimension. Three degrees of freedom and thus three primary modes of oscillation are investigated: heave, pitch and roll. Data from Air Force Flight Dynamics Laboratory Tests of a full-scale Australian Jindivik drone are used to develop and verify the model. As part of the comparative analysis of Jindivik data, a computer program is developed that will analyze the peak data of an underdamped, second order, sinusoidal, response and evaluate the mode response characteristics, damping ratio (ζ), undamped natural frequency (ω_n) as well as the mode spring and damper coefficients. Another computer program is developed to analyze the same response characteristics using the method of peak overshoot and peak times.

The VEAM study demonstrates that the use of a mechanical analog prediction scheme for an Air-Cushion Landing System has sufficient merit to warrant further investigation. It shows that a mechanical analog model can predict system response within the model domain of three degrees of freedom without knowledge of the numerous and varying trunk and cushion parameters if the mode spring and damper coefficients are provided. The model response correlates with Jindivik test data much better in pitch and roll than in heave. Both the pitch and roll mode spring and damper coefficients are shown to be linear in accordance with model assumptions. Model response in heave is heavily dependent upon the mode damping ratio (ζ) and the undamped natural frequency (ω_n), but the results are reasonable; that is, response frequency correlates to test data and response displacement is in the proper direction but sometimes of incorrect magnitude. The heave mode spring coefficient is shown to hold to the linear approximation. The inability to match magnitudes exactly suggests that the heave damper coefficient is non-linear.

AIR CUSHION LANDING SYSTEM, DROP DYNAMICS THEORY (MECHANICAL)

I. Introduction

Air Cushion Development

The Air Cushion Landing System (ACLS) is a natural extension of the already successful application of air cushion theory to Air Cushion Vehicles (ACV) and Surface Effect Ships (SES). Bell Aerospace, a Division of Textron, Inc. and a pioneer in this field, in concert with the Air Force Flight Dynamics Laboratory (AFFDL), has developed and flight tested an ACLS on the Lake LA-4 aircraft (Figure (1)) as early as

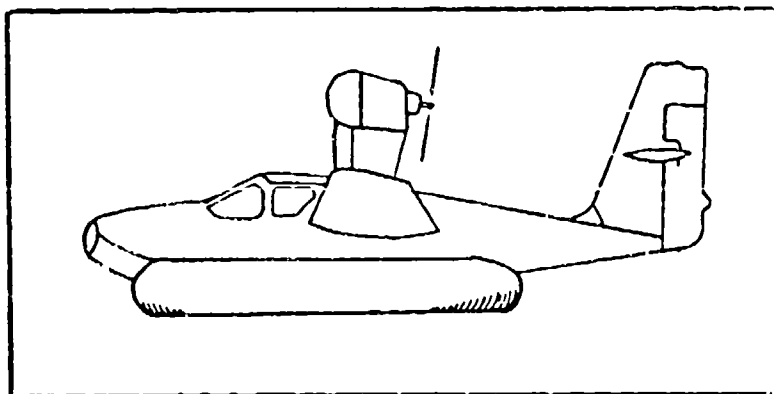


Fig. 1. The Lake LA-4 with ACLS

August 1967. These tests proved that an aircraft could takeoff, land, and ground maneuver on a cushion of air much in the same manner as the ACV's. Further, due to the large surface

"contact" area of an ACLS, vehicle weight and landing loads were widely distributed, resulting in low footprint pressures (approximately 0.5 - 3 psi). In certain cases this characteristic of the ACLS will motivate abandoning conventional landing gear on aircraft for the air cushion. The low footprint pressures free the ACLS equipped aircraft from a hard surface runway requirement and allows routine operations on unprepared surfaces, marsh land, water, and even obstacle strewn surfaces. In cooperation with the Canadian government, Bell Aerospace is currently testing an enlarged version of the LA-4 ACLS on a de Havilland CC-115, Buffalo (Figure 2). Success of the Buffalo tests is expected to result in an ACLS test series on the Lockheed C-130 Hercules.

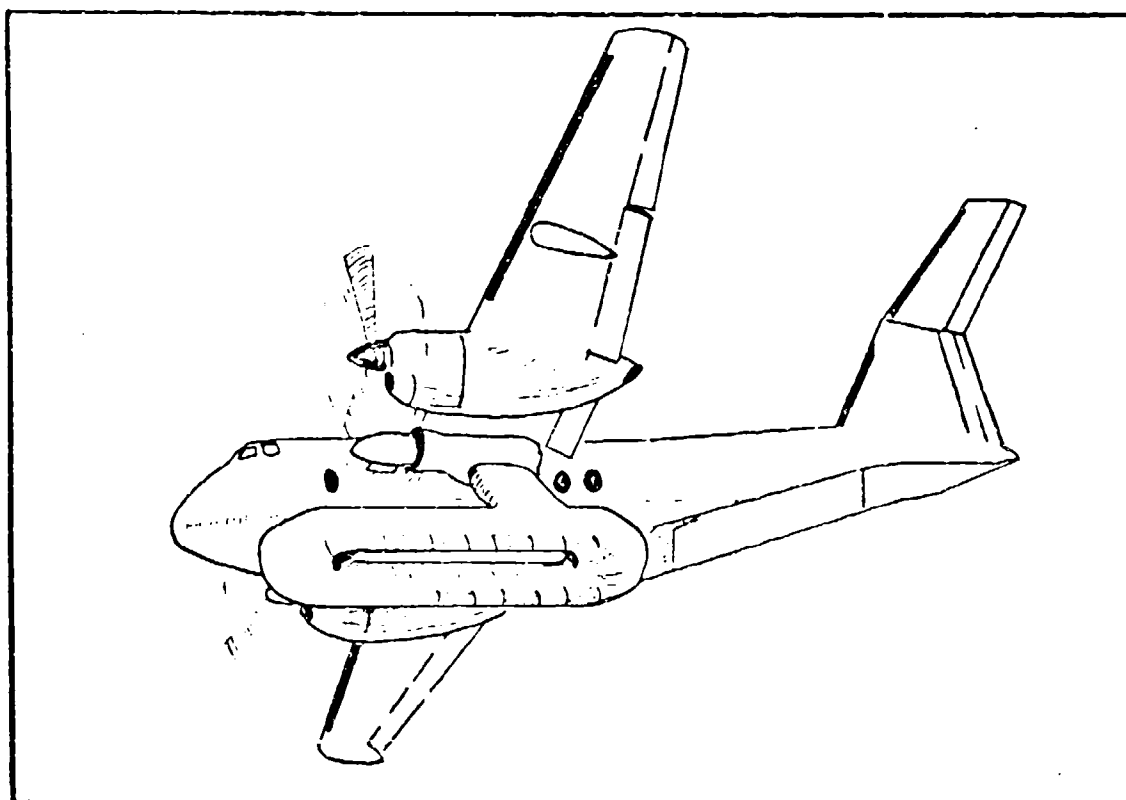


Fig. 2. The deHavilland CC-115, Buffalo, with ACLS

Air Cushion Concept and Definitions

The operation of an ACLS is not the same as the ACV. The uniqueness of the ACLS requires development of its own discipline.

The design and method of construction is in no way fixed. Many configurations are under investigation (Ref 3:26), but the one shown in Figure 3 seems to be relatively standard. The shape and material of the trunk has a significant effect on its capability.

The trunk is that peripheral portion of the system that contains the air cushion. Usually an elongated donut shaped manifold of a nylon/rubber material, it contains the flow of air around and into the cushion.

The cushion is comprised of that volume of air inside the trunk periphery; that is, the hole of the donut.

System refinements being studied are separate air flow into the cushion and a back-pressure relief valve in the trunk to reduce springiness on landing. The trunk and the cushion together absorb the vertical energy of a descending mass.

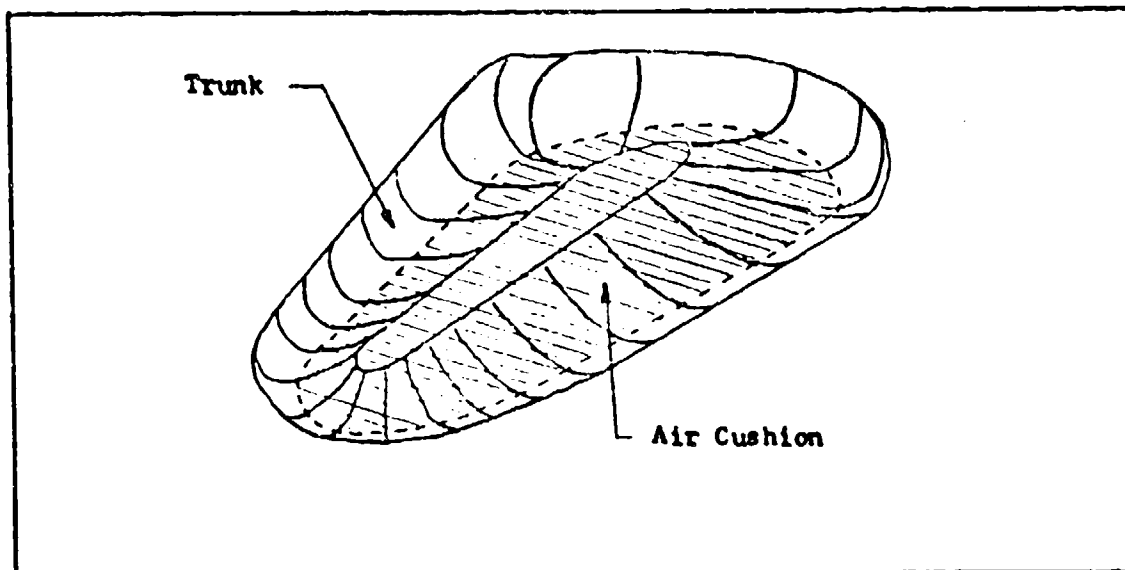


Fig. 3. An ACLS Trunk-Cushion Configuration

Early model and inexpensive trunks are made of a non-stretchable material that functions like an inflatable beach ball which maintains the same surface area whether or not inflated. More sophisticated trunks are made of a stretchable material. A trunk cannot be allowed complete freedom of stretch or, like a balloon, it will expand under pressure until fracture. An ACLS trunk must have limits, like a woman's girdle, which allows elastic expansion until it reaches the nylon thread limit. Unlike a girdle, which has a 50% stretch capability, a Bell Aerospace trunk will stretch up to 300% for its design shape limit. This kind of trunk can be installed under tension, flush to the aircraft undersurface, eliminating the need for complicated, heavy storage doors while maintaining a low drag profile when not in use.

Air Cushion Application

The Air Force, through the AFFDL, is showing great interest in applying air cushion technology to drone recovery. Most drones are in the same size and weight class as the LA-4, so feasibility has already been demonstrated. Present drone operations include surface launching from a rail, dolly, or skid, or air launching from under the wing of a mothership (C-130). Recovery methods include mid-air retrieval by helicopter or parachute descent to the surface. Costs of support

operations and limitations on the numbers of drones that can be handled simultaneously demand a better method. One serious proposal is the Air Cushion Recovery System (ACRS). A recovery system differs from a landing system in the sense that it is designed for landings only, and does not need the higher power (airflow) required for taxi and takeoff operations. It can be constructed of less expensive non-stretchable materials which can be stored in parachute fashion ready for deployment at recovery. In a current test series, the AFFDL is actively engaged in the development of an ACRS on an Australian Jindivik drone (Figure 4).

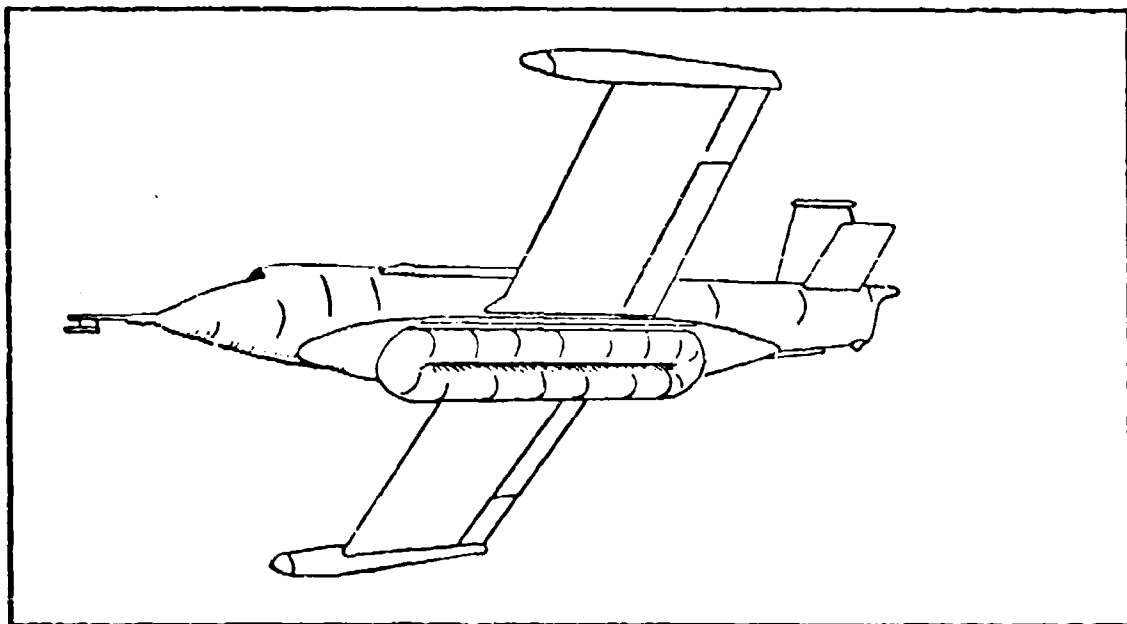


Fig. 4. The Australian Jindivik Drone with ACRS

Background

The technology of the ACLS is in its infancy. Major research efforts were the LA-4 program, the one quarter scale and the one tenth models of the CC-115, and the current, full scale CC-115 program. Throughout these efforts, the primary approach to development of a Vertical Energy Absorption Model (VEAM) has been with the emphasis on mass air flow theory (Ref 9). This approach was severely complicated by the number of variables changing simultaneously and the lack of concrete information on many of the variables. It was the initial

Jindivik tests that suggested an alternate approach; drop test data indicated that the Jindivik with ACRS was behaving like an underdamped, second order system. In April 1973, the AFFDL decided in favor of investigating a mechanical analog VEAM.

The mechanical analog promises a fast reacting prediction scheme which is needed as a computer subroutine to be joined to a larger aircraft simulation program that is being developed by the AFFDL Flight Controls Division. The ACLS portion of the program, which must eventually include forward motion with its associated aerodynamic and braking forces, is to predict the forces that the ACLS contributes to the overall dynamics of the vehicle on landing. A real-time dynamic analysis is most important in order to keep pace with other force inputs, such as pilot stick inputs, and to maintain a realistic simulation of vehicle response.

Purpose

The purpose of this study, under the sponsorship of the AFFDL, Mechanical Branch, is to develop a Vertical Energy Absorption Model using a mechanical system analog that will successfully predict the dynamics of an Air Cushion Landing System in the vertical dimension.

The investigation is to show that a mechanical analog will predict ACLS response even though the physical parameters of the trunk and cushion are not known. If a mechanical analog is successful, and if the spring and damper coefficients of the mechanical system eventually can be related to the trunk and cushion parameters, then this method of analysis promises a simplified design approach for the ACLS without the need to first design and build expensive test vehicles.

Scope

The mechanical analog was developed solely from the full scale Jindivik tests, and the model results are limited by the nature of those tests. Results are confined to cases that are restricted to three degrees of freedom; specifically, heave, pitch and roll. This feature is explicitly defined in the next chapter which describes development of the VEAM. Not an explicit part of the analysis is the understanding that the model was developed from a non-stretchable trunk of unique design.

Extension of the model to cases where a stretchable trunk is employed must be done with caution since the energy absorption capabilities and reactions of the two materials may vary significantly. The basic design of the Jindivik trunk differs from the only other trunks tested to date (the LA-4 and CC-115), in that the cushion volume is smaller (in proportion to trunk volume) than other trunks. The full effect of these differences will only become clear after more tests with different configurations.

II. Model Development and Theory

The Jindivik Drone

Tests on a full-scale Air Cushion Recovery System (ACRS) were begun by the Air Force Flight Dynamics Laboratory (AFFDL) in February 1973 at Wright-Patterson Air Force Base. An Australian drone aircraft, the Jindivik, was provided for the tests and fitted with a Sandaire designed ACRS modified by the AFFDL. These tests motivated the selection of the Jindivik drone as the basis for the Vertical Energy Absorption Model (VEAM).

The Jindivik was set in a test cell as shown in Figure 5 and modified slightly to accommodate the tests. The forward hood was removed to facilitate instrumentation and the landing skid was removed for the ACRS installation. Weights were added to simulate the internal equipment, engine, and fuel with care exercised so that the total weight and moments of inertia of the test vehicle matched its operational counterpart. Primary control of the Jindivik for the tests was achieved through the single suspension point, chain and pulley assembly, attached directly above the center of gravity.

A planform drawing of the drone in Figure 6 locates the recording instrumentation used in the AFFDL tests. Signals from this instrumentation eventually were recorded on light-sensitive paper by a Honeywell visicorder (Model 906 A) from which data was reduced. Pressures of the trunk and cushion and the displacement of the nose, wingtip, and center of gravity were measured on all tests used for development of the VEAM model.

Changes to the ACRS trunk design component fabrication, and installation were the cooperative effort of the AFFDL, Centro and Goodrich. The trunk, depicted in Figure 7, was constructed from a non-stretchable neoprene coated nylon of various weights. The lower surface of the trunk consisted entirely of brake tread made from three-eighths inch tire tread material. The heavy brake tread results in a weight penalty (one-half the weight of the entire trunk assembly), but it did facilitate precise angular positioning of the trunk nozzles for optimum efficiency. Two Tech Development TD-530 ejectors were provided

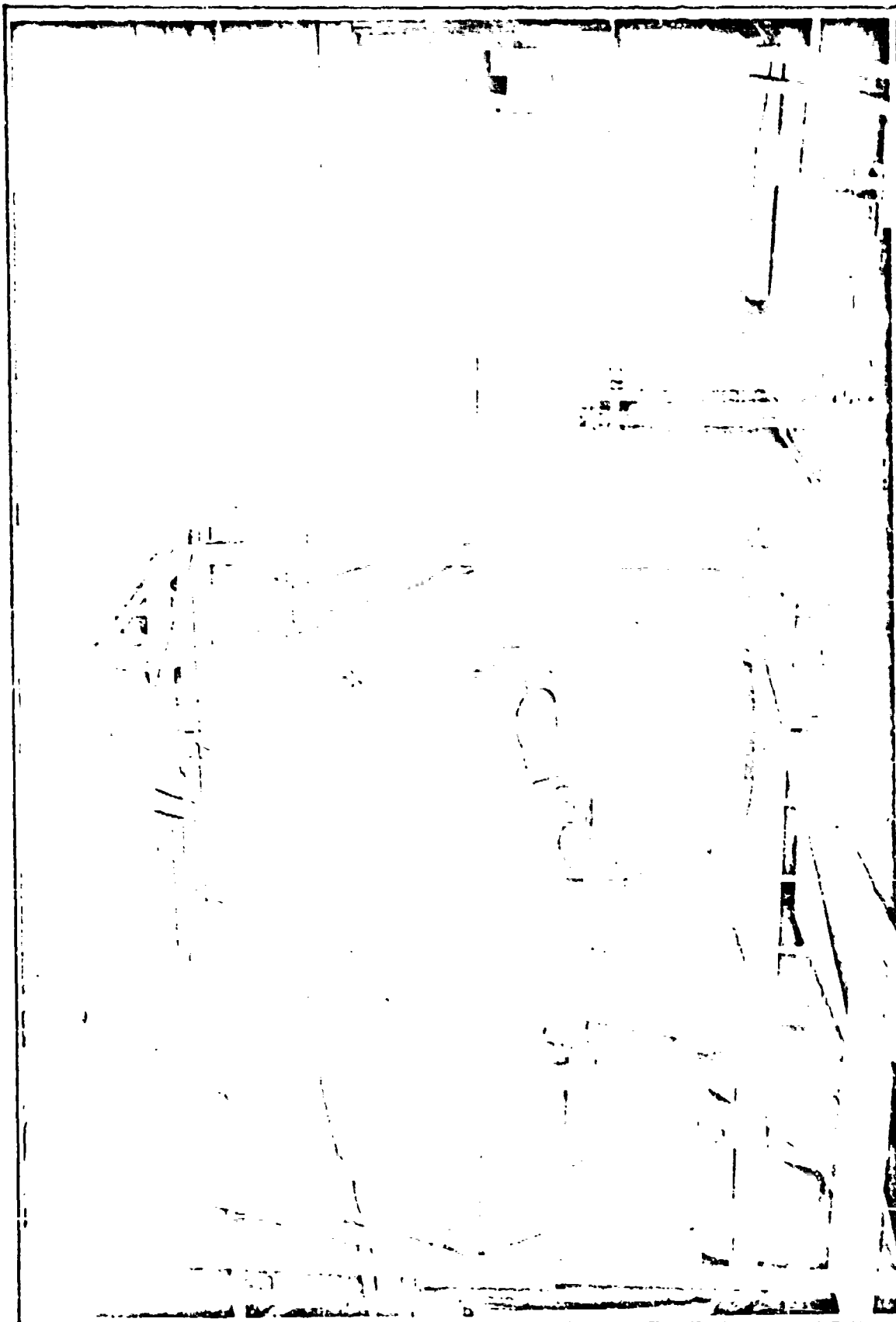


Fig. 5. The Jindivik Drone in Test Configuration

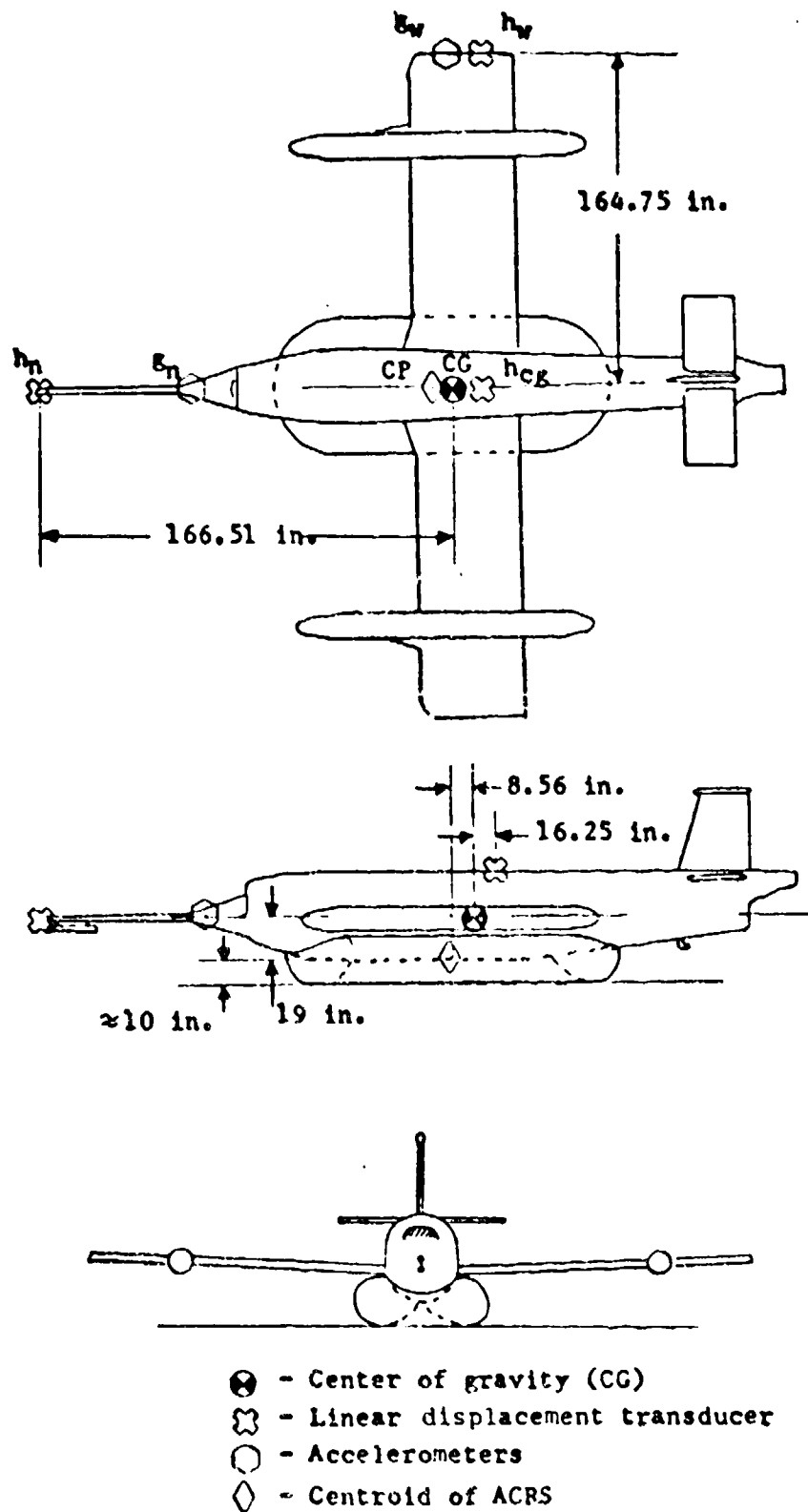


Fig. 6. The Jindivik with ACRS, Dimensions, and Instrumentation

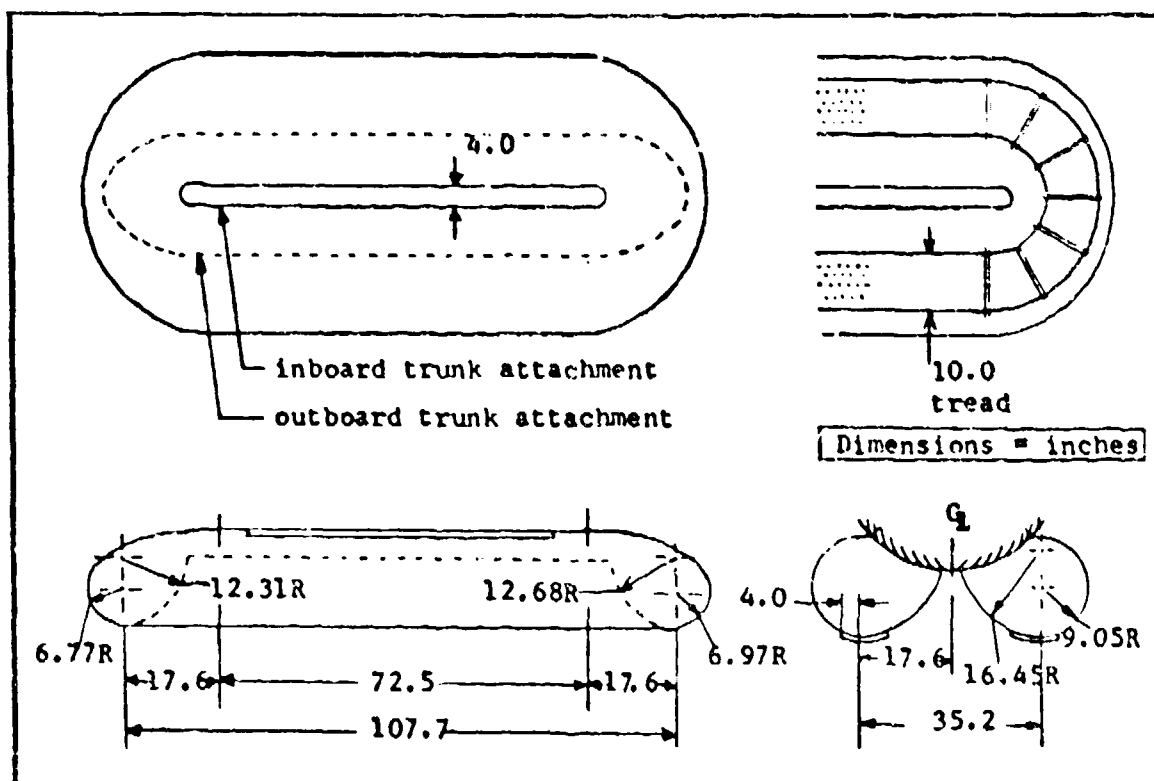


Fig. 7. The Jindivik ACRS with Dimensions

for the portion of the tests used to develop the VEAM; one provided mass flow to the trunk and the other to the cushion.

Test Method and Data

Nine AFFDL Jindivik tests were used to develop the VEAM. The tests were in the three primary modes of oscillation of the model; heave, pitch, and roll. In pitch and roll, the analysis centered on perturbation about the hover equilibrium condition, whereas in the heave case, the analysis was of Jindivik oscillation dynamics after being released from a height greater than hover equilibrium. The method of collecting data in the three modes influenced the analysis of each mode and the resulting model.

Roll Mode - One wing-tip was lowered to the surface and released at time zero (t_0). The wing-tip linear transducers recorded vertical deflections of the wing-tip as oscillations damped back to hover equilibrium. A maximum roll angle was of the order of 5 degrees.

Pitch Mode - Resistance to pitch perturbation was significant enough that the Jindivik could not be displaced easily and released,

as with the roll case. Oscillations were introduced until the pitch perturbations were of sufficient magnitude. The linear transducer, attached to the nose boom, recorded vertical deflections of the nose boom relative to hover equilibrium. A maximum pitch angle of approximately 7 degrees was experienced.

Heave Mode - The magnitude of heave stiffness was large enough to make it technically impractical to conduct perturbation testing. Thus, the Jindivik was raised to a height and released. This test method required separation of the analysis into two regions; the first, the free-fall from release until "contact" of the ACRS with the surface, and the second, the dynamic oscillations of the ACRS about the hover equilibrium condition. Since the ACRS rides on a cushion of air, "contact" does not necessarily imply the physical meeting of the trunk and the surface. Thus, "surface contact" has been defined as In Ground Effect (IGE); that is, the position at which the first distinguishable rise in trunk or cushion pressure can be detected. Experimental testing shows that trunk and cushion pressure rise within a fraction of a second of one another, and can be considered simultaneous for the purpose of defining IGE. Heave data was complicated by the fact that the heave linear transducer could not be placed at the center of gravity due to the fuselage, nor could it be placed directly above the center of gravity due to the suspension hoist. The sensor offset resulted in heave data being affected by pitch and required analytical adjustment.

A summary of the AFFDL tests in its three significant modes of oscillation and under various conditions is presented in Table 1.

TABLE I AFFDL JINDIVIK TEST NUMBERS used for the VEAM development				
Test Mode	Vent Opened $P_c \approx P_a$ $\dot{m}_c < 0$	Vent Closed $P_c = \text{unk}$ $\dot{m}_c = 0$	Flow Added $P_{cp} = 12.5 \text{ psi}$ $\dot{m}_c = \frac{1}{2} \dot{m}_t$	Flow Added $P_{cp} = 30.4 \text{ psi}$ $\dot{m}_c = \dot{m}_t$
ROLL	56	55	58	
PITCH	59	60	61	
HEAVE*	123		122	121
* Jindivik balanced so that CG is approximately over the trunk CP.				

Tests were conducted in still ambient air in an enclosed test cell, and, as described above, were limited to perturbations or vertical descent (no forward velocity). Thus, no aerodynamic lift or drag forces nor brake drag forces were present to complicate force or moment analysis.

The Vertical Energy Absorption Model (VEAM)

The model chosen for analysis is depicted in Figure 8.

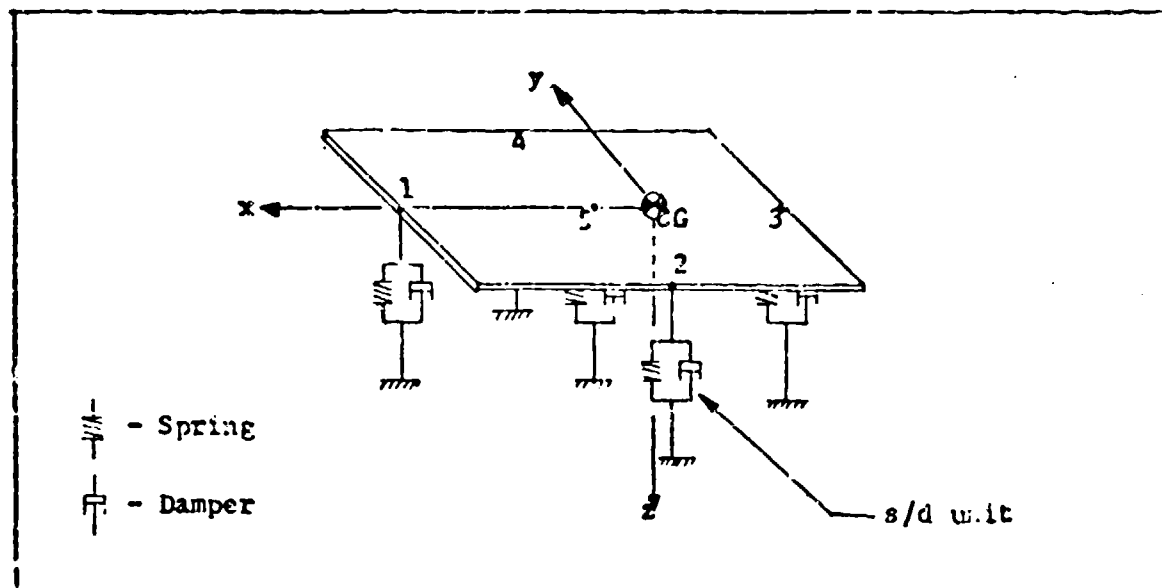


Fig. 8. Schematic of Vertical Energy Absorption Model

Normally, consideration of an object in three dimensional space results in six degrees of freedom (DOF). Jindivik testing methods allowed a reduction to 3 DOF. The elimination of air flow over the wings and forward movement of the model during the initial test series had the effect of eliminating all forces in the horizontal (x,y) plane. Consequently, it is assumed that there is no lateral displacement, and that all movement is confined to the vertical (z) axis. Because there are no lift and drag forces to create sideloads, yaw is not present. Thus, the dynamic/perturbation study is limited to the vertical mode (heave) and the pitch and roll modes. The axis system chosen, similar to a conventional Euler system with z positive down, has its origin at the center of gravity and is fixed in space with the x,y plane parallel to the surface when the center of gravity is at the hover equilibrium condition. This seeming complication to the axis is required in order

to generalize the analysis and yet allow a changing equilibrium height (relative to the surface) as the mass flow into the cushion changes.

Model Assumptions

Observation of the Jindivik oscillations in its three modes results in data which gives insight into the character of the ACRS. One of the first Jindivik dynamic tests conducted was the roll test shown in Figure 9. The plot of peak displacements suggests an underdamped second order response, which motivated the selection of a mechanical analog model for the ACRS. The period (T) is approximately constant throughout, which makes the damped natural frequency (ω_d) constant. A semi-log plot of the peak amplitude excursions from equilibrium demonstrates the linearity of the exponential decay. A complete discussion of this analysis is contained in Chapter IV.

There is a single effective spring and a single effective damper that results from each mode analysis. With the assumption that the springs and dampers are linear and time invariant, it is possible to construct spring/damper units (s/d units), each a linear spring and damper in parallel, and distribute them as depicted in Figure 8. The rotational roll spring and damper and the rotational pitch spring and damper are each divided into translational s/d units displaced at an assumed moment arm. The linear heave spring and damper are represented by the combined effect of the four peripheral s/d units and the center cushion s/d unit. The constants of proportionality for the Jindivik are determined from the experimental data (Appendix A).

As is usual with lumped linear models, analysis requires the concentration of mass at the center of gravity (point-mass assumption). The plane surface which distributes the s/d units at the proper moment arm is assumed massless. The center of gravity can be varied from the center of pressure (also the geometric center of the trunk) by the distance δ . In the model, the center of gravity and the center of pressure are in the same plane.

Approach to Analysis

When the ACRS is Out of Ground Effect (OGE), it is inoperative; that is, pressures of the trunk and cushion are constant and no forces or

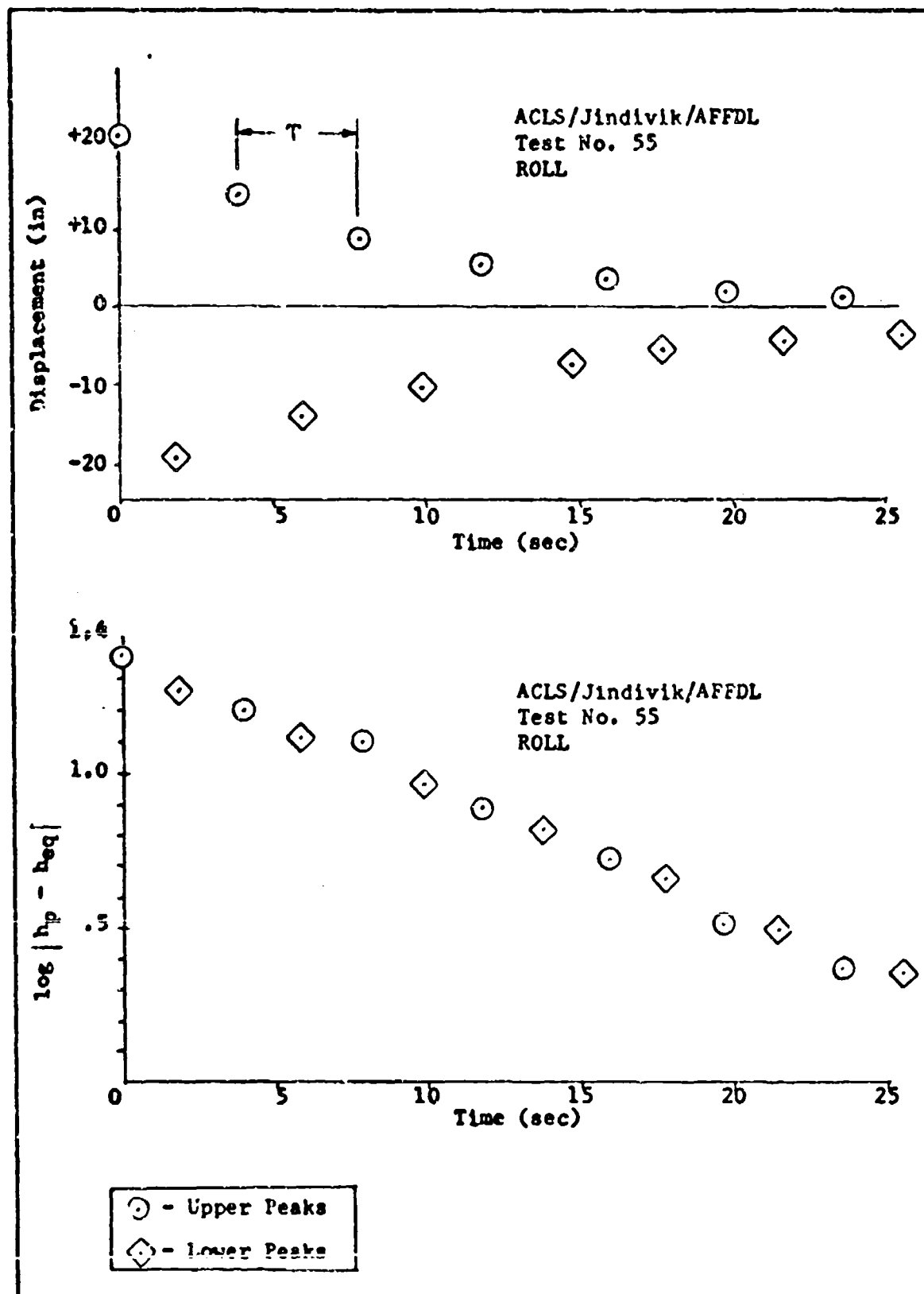


Fig. 9. Linearity of Exponential Decay in Roll

moments are present. As the ACRS descends in free fall toward the surface, it reaches the region (IGE) where reaction with the surface causes a pressure rise in both the trunk and cushion.

The instant the IGE condition is encountered marks time zero (t_0) for activation of the analytical model. This displacement corresponds to the spring-neutral position (h_c) as depicted in Figure 10.

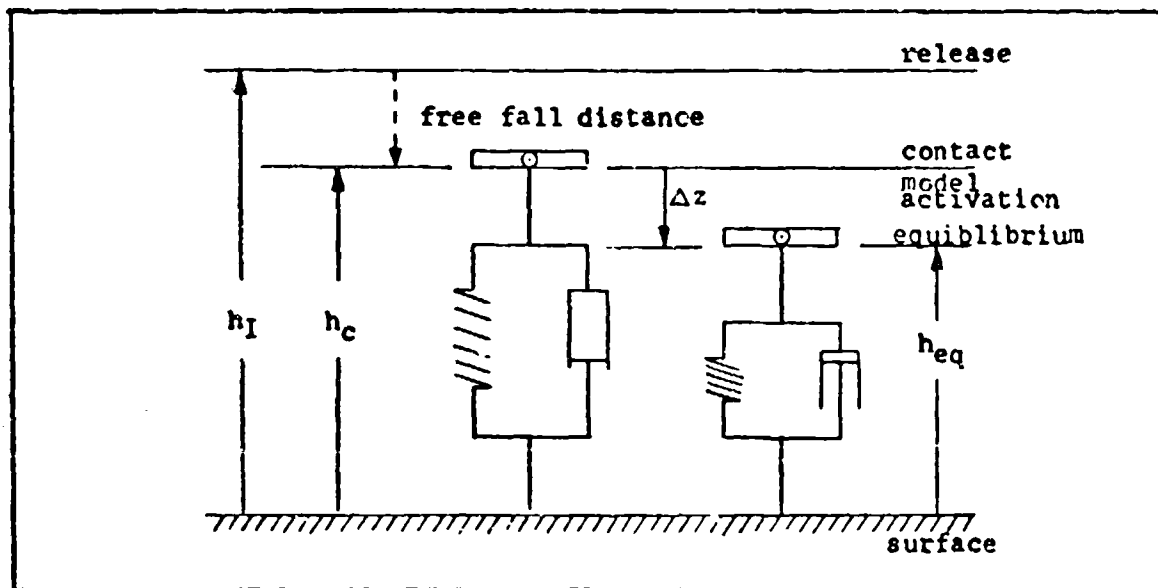


Fig. 10. Schematic of Vertical Displacements

Any further downward displacement causes reaction forces. Descent of the model continues, compressing each spring (ΔZ) until the combined upward force of the spring/damper units (s/d units) supports the weight of the model. This displacement is the equilibrium position (h_{eq}) and corresponds to equilibrium hover for the Jindivik. When the center of gravity is displaced from the center of pressure, the Jindivik longitudinal centerline will not be level with the surface. A non-zero equilibrium pitch angle (Θ_{eq}) will result so that for each s/d unit

$$\Delta Z = (\text{Moment Arm}) \sin \Theta_{eq} \quad (1)$$

The equilibrium pitch angle is non-zero due to the combined physical constraints of (1) the CG of the vehicle being aft of the trunk CP in normal configuration, (2) the assumption that the roll and the pitch spring coefficients are symmetrically placed relative to the trunk CP, and (3) the assumption that the symmetrical spring coefficients are equal in magnitude.

Linearity of Springs

The curves in Figure 11a illustrate that a linear approximation for a non-linear spring is usually valid within a small perturbation of a given position, in this case, equilibrium. Figure 11b illustrates that real spring phenomena is not infinitely linear, but that non-linearities are usually present at the extremes. For the VEAM, when it is above the contact level, no forces should exist. At this extreme the spring relationship $F = kx$ implies that $k = 0$ at displacements less than contact (x_c). At the other extreme, where the vehicle underbelly strikes the surface, the spring relationship again terminates. It is suspected that the spring goes non-linear prior to fuselage and surface contact (x_s). These two extremes define the limits of the domain for successful VEAM operations.

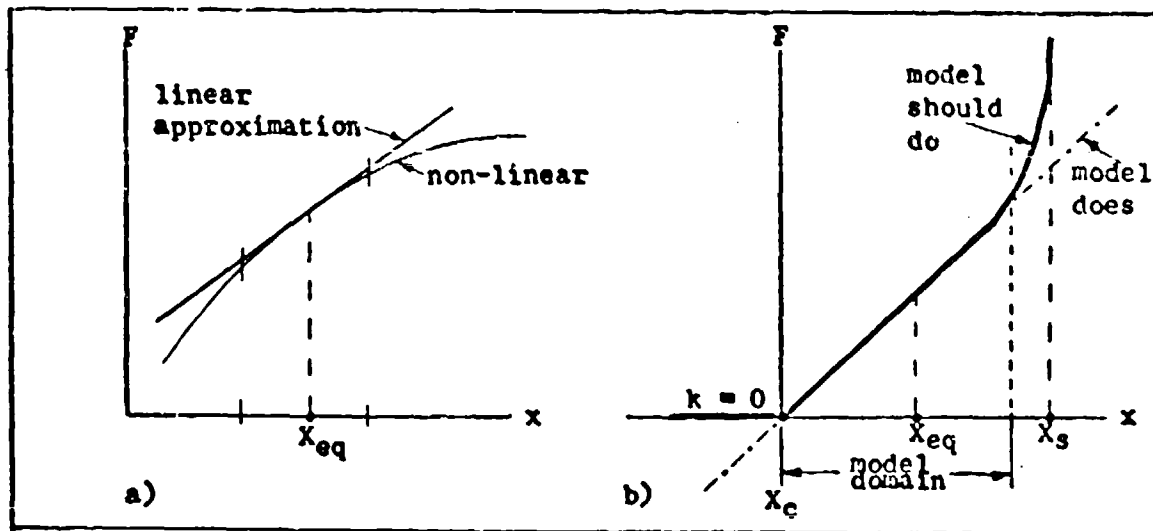


Fig. 11. Spring Linearity

III. The Model Equations of Motion

The Force Equation

In this chapter, the equations of motion that apply to the three degrees of freedom will be developed. Each spring/damper unit as

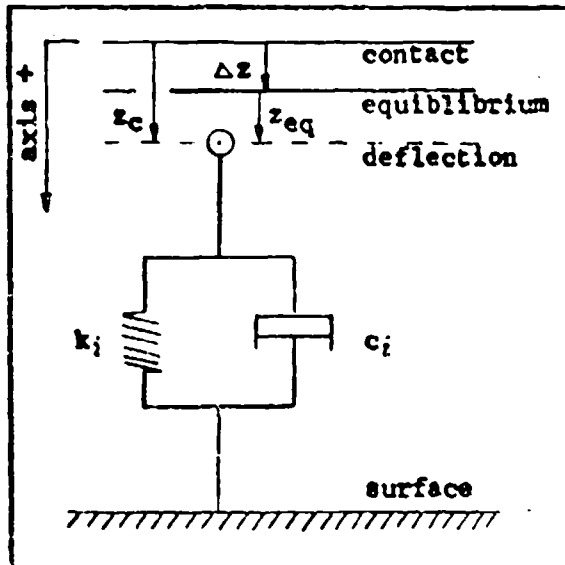


Fig. 12. A Spring/Damper Unit in Arbitrary Deflection

illustrated in Figure 12 will result in a force with constants of proportionality for displacement h_i and velocity c_i for each mode. The total force described as

$$F_i = - (h_i z_{ci} + c_i \dot{z}_{ci}) \quad (2)$$

where displacement is measured positive down from the spring-neutral or contact position.

When the model is released from the spring neutral position, which is defined as horizontal to the surface, it will settle downward due to model mass and seek an

equilibrium position so that the forces and moments for each degree of freedom are exactly balanced. This equilibrium position can vary in relation to the horizontal surface depending upon the relative location of the s/d units to the center of gravity and the center of gravity to the center of pressure of the trunk. Thus, at each s/d unit attachment point i , if the variable deflection were defined as ΔZ , then the total force at each point would be

$$F_i = - [h_i (z_{eqi} + \Delta Z_i) + c_i \dot{z}_{eqi}] \quad (3)$$

However, for any given model configuration, the forces and moments due to the deflection ΔZ from spring-neutral to equilibrium are constant so as to exactly counteract the presence of the mass at all times. If the deflection from contact to equilibrium were eliminated from an analysis, the resulting equations represent a dynamic force balance relative to the equilibrium condition where each s/d unit force contribution would be represented by

$$F_i = - (h_i z_i + c_i \dot{z}_i) \quad (4)$$

In this last equation, z_i represents the vertical deflection of each s/d unit attachment point from the equilibrium position ($z_i = Z_{q_i}$).

Perturbation from Equilibrium

Analysis of the model in its three degrees of freedom starts by considering the forces that act upon it in time (equation 4). The forces remaining after model weight is eliminated are dependent upon \dot{z} and $\dot{\theta}$. The model is given a positive deflection in heave, pitch and roll simultaneously. Allowing that all angles are small (Appendix C),

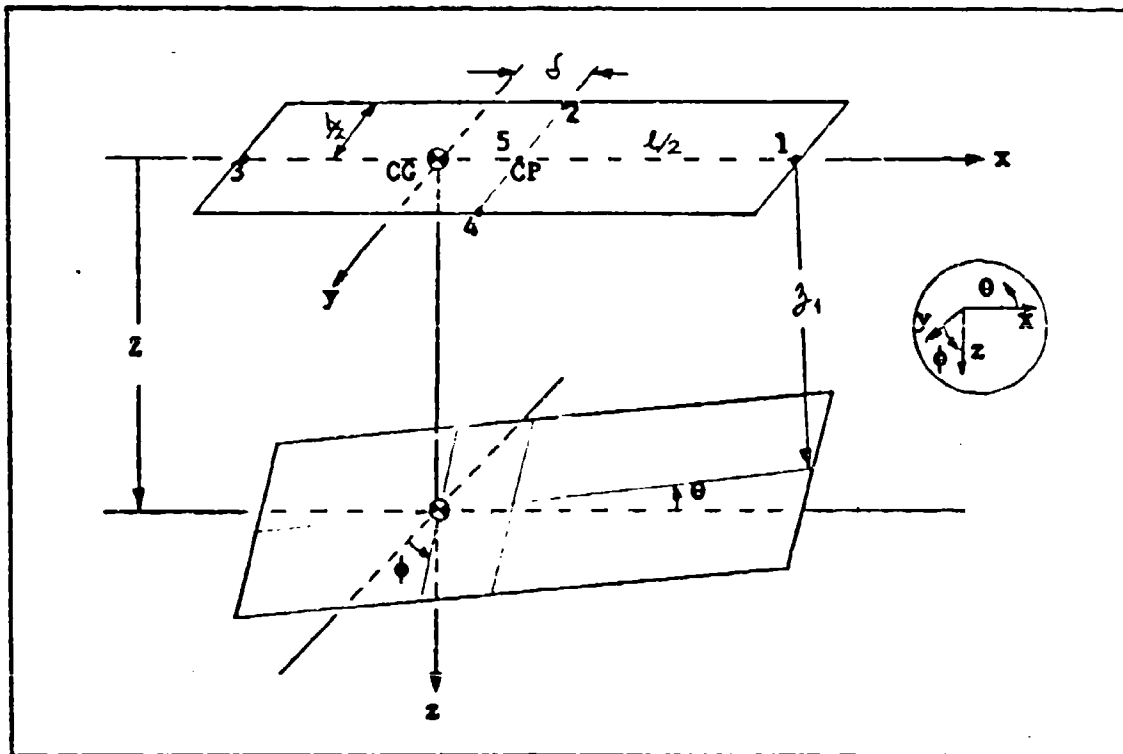


Fig. 13. The VEAM in Arbitrary Deflection (Heave, Pitch and Roll)

Figure 13 illustrates that the deflection at each s/d unit location is

$$\begin{aligned}
 z_1 &= z - \left(\frac{l}{2} + \delta\right) \theta \\
 z_2 &= z - b_2 \phi - \delta \theta \\
 z_3 &= z + \left(\frac{l}{2} - \delta\right) \theta \\
 z_4 &= z + b_2 \phi - \delta \theta \\
 z_5 &= z - \delta \theta
 \end{aligned} \tag{5}$$

The rate of deflection of each s/d unit point is the derivative of equations (5).

$$\begin{aligned}
 \dot{z}_1 &= \dot{z} - (b_2 + \delta) \dot{\theta} \\
 \dot{z}_2 &= \dot{z} - b_2 \dot{\phi} - \delta \dot{\theta} \\
 \dot{z}_3 &= \dot{z} + (b_2 - \delta) \dot{\theta} \\
 \dot{z}_4 &= \dot{z} + b_2 \dot{\phi} - \delta \dot{\theta} \\
 \dot{z}_5 &= \dot{z} - \delta \dot{\theta}
 \end{aligned} \tag{6}$$

Substitution of equations (5) and (6) into equation (4) provide the necessary information for a force and moment analysis.

The Heave Mode

Summing all forces in the vertical direction, where the forces are as previously described, results in

$$\sum F_z = m \ddot{z} = \sum_{i=1}^5 F_i \tag{7}$$

Substitution of the complete s/d unit force equations (the combination of equations (4), (5) and (6), into equation (7) and separating like orders of heave displacement and pitch angle results in the heave mode equation

$$\ddot{z} + \frac{c_E}{m} \dot{z} + \frac{h_E}{m} z = \frac{c_E}{m} \delta \dot{\theta} + \frac{h_E}{m} \delta \theta \tag{8}$$

where the effective spring and damper coefficients are

$$\begin{aligned}
 c_E &= \sum_{i=1}^5 c_i \\
 h_E &= \sum_{i=1}^5 h_i
 \end{aligned} \tag{9}$$

The Roll Mode

In a like manner, the roll equation develops from a summation of moments about the longitudinal x-axis.

$$\sum M_x = J_{xx} \ddot{\phi} = F_4 (b_2) - F_2 (b_2) \tag{10}$$

In this case, the physical symmetry of the trunk about the longitudinal axis suggests that the corresponding s/d units are also symmetric; or

$$\begin{aligned}
 c_2 &= c_4 = c_{2,4} \\
 h_2 &= h_4 = h_{2,4}
 \end{aligned} \tag{11}$$

The complete s/d unit force equations are substituted into (10) and

the coefficients of like order derivatives are collected to give

$$\ddot{\phi} + \phi \left[\frac{c_{2,4} b^2}{2 J_{xx}} \right] + \phi \left[\frac{h_{2,4} b^2}{2 J_{xx}} \right] = 0 \quad (12)$$

The Pitch Mode

Development of the pitch equation involves a bit more algebra, but the method is the same. Moments are summed about the lateral y-axis.

$$\sum M_y = J_y \ddot{\theta} = F_1 \left(\frac{l}{2} + \delta \right) + F_2 \delta - F_3 \left(\frac{l}{2} - \delta \right) + F_4 \delta + F_5 \delta \quad (13)$$

and the complete s/d unit force equations are substituted. To the assumption of the roll s/d units (equation 12) is added the more tenuous assumption that the fore-aft s/d units are also symmetric, or

$$\begin{aligned} c_1 &= c_3 = c_{1,3} \\ h_1 &= h_3 = h_{1,3} \end{aligned} \quad (14)$$

Equations (14) are considered more assumptive due to the slightly different volume between the fore and aft trunk sections (see the cross-sectional areas in Figure 7), but the difference is considered negligible. The complete pitch equation is

$$\begin{aligned} \ddot{\theta} + \dot{\theta} \left\{ \frac{1}{J_y} \left[2c_{1,3} \left[\left(\frac{l}{2} \right)^2 + \delta^2 \right] + 2c_{2,4} \delta^2 + c_5 \delta^2 \right] \right\} \\ + \theta \left\{ \frac{1}{J_y} \left[2h_{1,3} \left[\left(\frac{l}{2} \right)^2 + \delta^2 \right] + 2h_{2,4} \delta^2 + h_5 \delta^2 \right] \right\} \\ = \frac{\delta Z}{J_y} h_{2E} + \frac{\delta \dot{Z}}{J_y} c_E \end{aligned} \quad (15)$$

Free Fall Analysis

The free fall case requires a separate analysis in a different time frame. After implementing the mode assumptions presented in Chapter II, a free body diagram of the Jindivik Out of Ground Effect (OGE) shows that weight is the only force acting on the system as it falls in the vertical dimension. Time is measured from release and, so as not to confuse with the time domain for the model IGE, free fall time is designated τ . The height of the vehicle in free fall is designated (h) and follows the terminology presented in Figure 10.

It is measured positive down to maintain the same sign convention as the model.

The equations which describe free fall with no initial velocity are

$$\begin{aligned} z &= \frac{1}{2} g \tau^2 + h_I & (a) \\ \dot{z} &= g \tau & (b) \\ \ddot{z} &= +g & (c) \end{aligned} \quad (16)$$

This free fall analysis is used in conjunction with the heave tests as previously described. The values of the release height (h_I) and the time to initial contact (τ_c) are determined experimentally, and from (16a) the height at contact (h_c) is determined. Equation (16b) provides another initial condition, the velocity at contact. These values, with coordinate transformation, are then used in an analysis of the characteristics of the equations of motion.

Summary

The complete set of equations to describe the model in its three degrees of freedom is the combination of equation (8), (12) and (15). It should be noted that both the heave equation (8) and the pitch equation (15) are coupled to one another if the center of gravity of the vehicle is not at the center of pressure of the trunk, ie, $\delta \neq 0$. This is to say that a pure heave input motion will, in time, result in a pitch motion that may remain even after the heave motion has damped out, and vice-versa.

Solution of these equations of motion is the subject of the next chapter, but it must be remembered that the dynamic analysis is in reference to the equilibrium position of the vehicle. The equilibrium position can vary according to the vehicle configuration and/or flow rates into the trunk and cushion. In heave, the difference in height between equilibrium and the surface is constant for any given test. Program DATANYL in Appendix A computes this value. For roll, the equilibrium axis is parallel to the horizontal axis at all times due to the fact that the trunk is symmetrical. Pitch is the same as roll only if the center of gravity of the vehicle is coincident with the center of pressure of the trunk. For most pitch cases, where the CG is behind the CP, an equilibrium pitch angle (θ_{eq}), relative to the horizontal, will result. An expression for θ_{eq} is in Appendix B.

IV. Analysis of Jindivik Data (Theory)

Analysis of Roll and Pitch Data

The equations of motion developed in Chapter III can be related to a standard form for linear, constant coefficient, second order differential equations (Ref 1:244) where the coefficient of the displacement term is equal to ω_n^2 and the coefficient of the first derivative of displacement is equal to $2\zeta\omega_n$. For example, in the case of roll, these are written as

$$\begin{aligned}\frac{c_{2,4} b^2}{2 J_{xx}} &= 2\zeta\omega_n \\ \frac{k_{2,4}}{2 J_{xx}} &= \omega_n^2\end{aligned}\quad (17)$$

The parameters ω_n , the undamped natural frequency, and ζ , the damping ratio, serve to characterize the differential equation and thus the system. The solutions to the VEAM differential equations of motion (equations 8, 12 and 15) are of the form

$$D(t) = D_0 e^{-\zeta\omega_n t} \sin(\omega_d t + \phi') \quad (18)$$

where $D(t)$ is angular or linear displacement as a function of time, D_0 is a constant, and ω_d is the damped natural frequency. By definition,

$$\omega_d = \omega_n \sqrt{1 - \zeta^2} \quad (19)$$

The nature of the system being analyzed depends, to a large part, on the

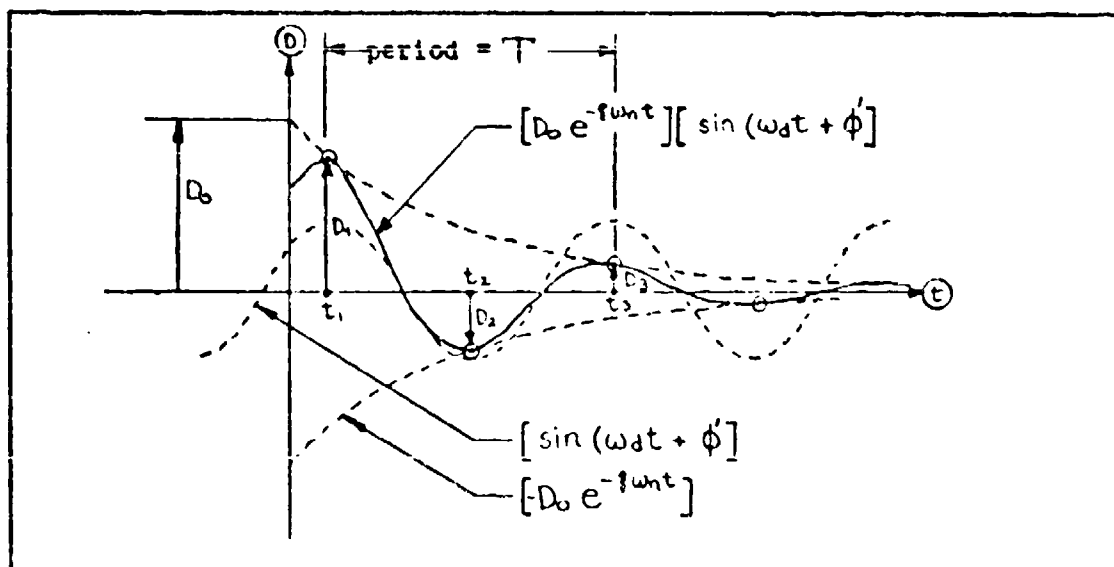


Fig. 14. General Underdamped Sinusoidal Response

value of ζ . For the case of this study where $\zeta < 1.0$, the system is called "underdamped" and the natural response appears as in Figure 14. The period of system response (T) is the time required to traverse one full cycle, thus $T = t_{P1} - t_{P1} = 1/f_d$ cps. From this, the following relationship is established

$$\omega_d (\text{rad/sec}) = 2\pi/T = 2\pi f_d (\text{cyc/sec}) \quad (20)$$

The period, which can be found from experimental data, leads directly to a value for the damped natural frequency.

A description of the system as it damps to the equilibrium position is available by comparing two adjacent peak amplitudes. This comparison is called the amplitude ratio and defined as D_1/D_2 . Combining equation (19) with (18) for two adjacent peaks and solving for the amplitude ratio gives

$$\frac{D_1}{D_2} = e^{(2\pi\zeta)/\sqrt{1-\zeta^2}} \quad (21)$$

The logarithmic decrement (d) is equal to the natural logarithm of the amplitude ratio, and

$$d \triangleq \ln \frac{D_1}{D_2} = \frac{2\pi\zeta}{\sqrt{1-\zeta^2}} \quad (22)$$

Alternately, the damping ratio is

$$\zeta = \left[\frac{d^2}{(2\pi)^2 + d^2} \right]^{1/2} \quad (23)$$

The preceding analysis was computerized to evaluate the system in roll and pitch, to provide the mode spring and damper coefficients, and to plot the data. This program and its results are presented in Appendix A.

Analysis of Heave Data

The initial analysis of Jindivik heave data indicated rapid damping of the heave mode with another mode remaining. This is illustrated in Figure 15. Evaluation of the data past the mode change point indicated that the pitch mode characteristics now predominated. Test results suggested that the heave mode damped out in about three peaks (0.75 to 1.45 seconds). With so few peak amplitude points, the heave data was considered too sparse to analyze in the same manner as pitch and roll. For this reason, an analysis based on percent overshoot and rise time was selected to characterize the system. This method of

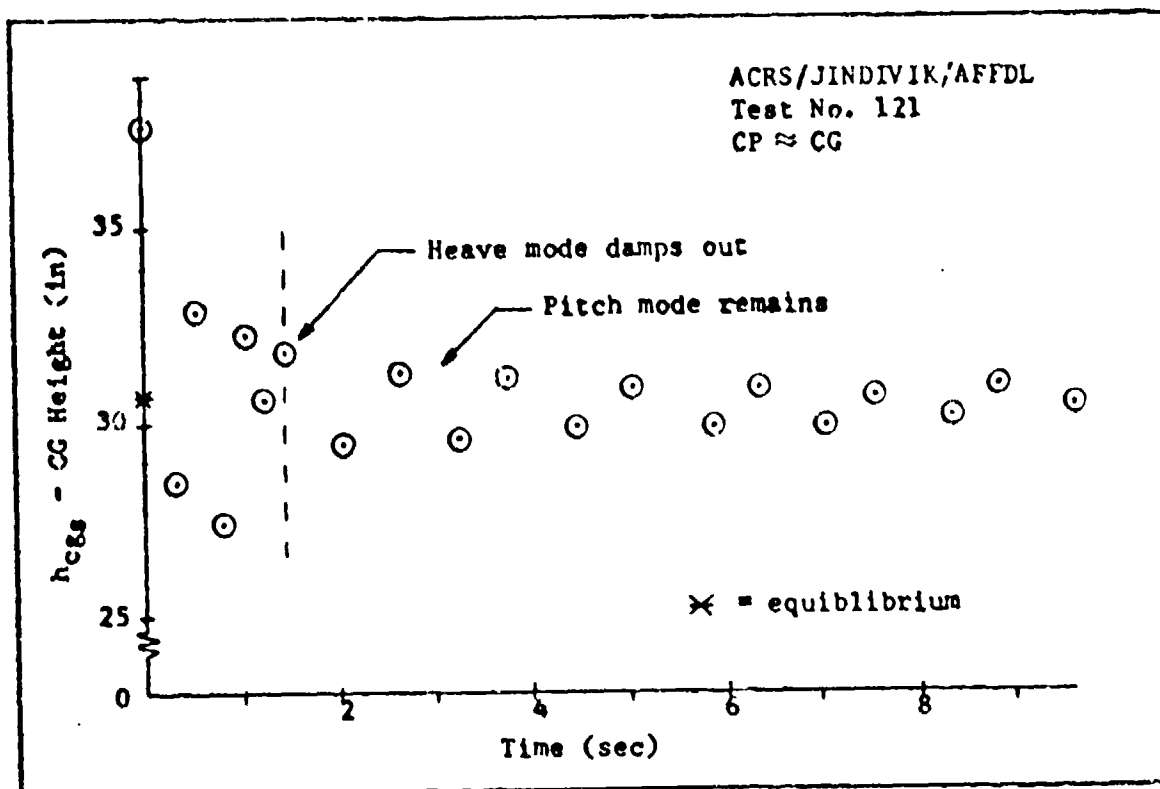


Fig. 15. Heave Test Data

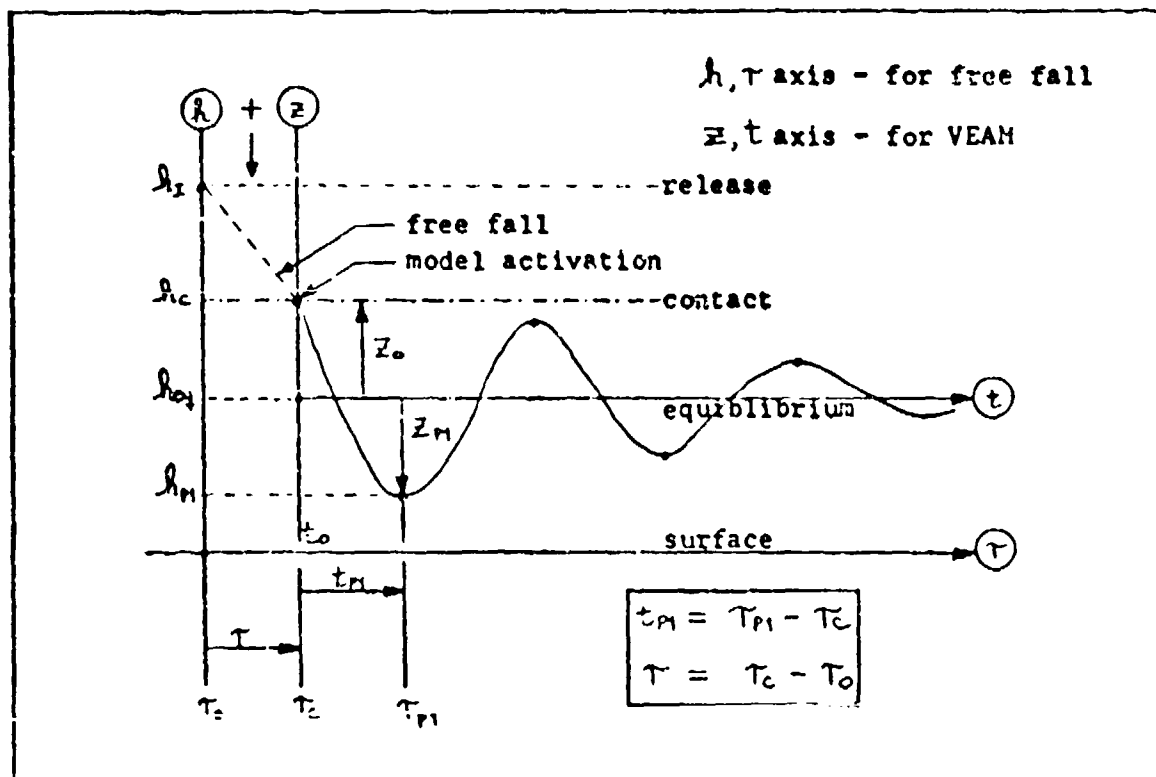


Fig. 16. Heave Data Analysis Coordinates

solution, which is illustrated in Figure 16, accounted for the fact that the model has both initial displacement and initial velocity at model activation (surface contact).

Starting with the heave differential equation of motion (8), Laplace transforms are used to find the solution

$$\frac{Z(t)}{Z_0} = e^{-\xi \omega_n t} (\cos \omega_d t + K \sin \omega_d t) \quad (24)$$

where

$$K = \frac{\xi}{\sqrt{1-\xi^2}} + \frac{\dot{Z}_0}{Z_0 \omega_n \sqrt{1-\xi^2}} \quad (25)$$

By using a trigonometric double-angle identity, (24) can be simplified to the form

$$\frac{Z(t)}{Z_0} = \sqrt{1+K^2} e^{-\xi \omega_n t} \sin(\omega_d t + \phi') \quad (26)$$

where

$$\phi' = \cot^{-1} K = \sin^{-1} \frac{1}{\sqrt{1+K^2}} \quad (27)$$

Maximum overshoot/undershoot occurs when $\sin(\omega_d t + \phi') = \pm 1.0$.

Thus,

$$\frac{Z(t)_{\max}}{Z_0} = \sqrt{1+K^2} e^{-\xi \omega_n t_p} \quad (28)$$

Equation (26) is differentiated with respect to time and solved in order to obtain a general expression for peak time (t_p) valid for any response peak depending on the value of the integer (n),

$$t_p = \dot{Z}_0 / \omega_n (\dot{Z}_0 \xi + Z_0 \omega_n) - n\pi / \omega_n \sqrt{1-\xi^2} \quad (29)$$

Equation (28) is solved for the damping ratio and equation (29) for the undamped natural frequency to provide two equations suitable for an iterative solution on a computer.

$$\xi = \frac{-\ln [|Z(t)_{\max} / Z_0| / \sqrt{1+K^2}]}{\omega_n t_p} \quad (30)$$

(a)

$$\omega_n = \frac{\dot{Z}_0 - \frac{n\pi}{\sqrt{1-\xi^2}} (\xi \dot{Z}_0 + Z_0 \omega_n)}{t_p (\xi \dot{Z}_0 + Z_0 \omega_n)} \quad (b)$$

The program which accomplishes this, called RISE, is presented in Appendix A.

Results

The results of the analysis of Jindivik data from both programs DATANYL and RISE are presented in the following tables. Table II characterizes the system for each mode for each AFFDL test, and Table III summarizes results that are peculiar to the heave mode only.

TABLE II

RESULTS OF ANALYSIS OF JINDIVIK DATA

Program DATANYL						
Mode	Case	Test No	Zeta	Wn (rad/sec)	Mode Coefficient	
					k_E (ft-lbf/rad)	C_E (ft-lbf/rad/sec)
Pitch	1	59	.0436	6.66	80,394.76	1,052.36
	2	60	.0462	6.20	69,524.92	1,036.00
	3	61	.0357	5.66	57,917.22	731.38
Roll	1	56	.0534	1.84	4,040.29	234.06
	2	55	.0577	1.64	3,077.99	221.05
	3	58	.0629	1.52	2,753.88	227.58
Program RISE						
			First Peak		(lbf/ft)	(lbf-sec/ft)
Heave	1	123	.3482	15.22	17,769.30	813.04
	3	122	.3533	16.61	21,163.15	900.29
	4	121	.3771	15.48	18,381.59	895.57
			Average			
Heave	1	123AV	.2616	14.90	17,029.96	597.99
	3	122AV	.1822	14.67	16,508.26	410.06
	4	121AV	.1799	14.24	15,554.68	393.02
Cases						
1 - Vent opened						
2 - Vent closed						
3 - Flow added ($\dot{m}_C = \frac{1}{2}\dot{m}_T$)						
4 - Flow added ($\dot{m}_C = \dot{m}_T$)						

TABLE III

PROGRAM RISE FREE FALL DATA
(Jindivik Tests/Heave Mode)

Heave Test No	TP1 (sec)	Z ϕ (in)	Z ϕ DOT (in/sec)	ZP1 (in)
123	0.220	-7.157	0.2683	2.230
122	0.202	-7.267	0.2630	2.220
121	0.2190	-7.111	0.2173	1.980

V. Analysis of the Spring/Damper Units (Theory)

General

The analysis of the model equations of motion is completed by computer solution. The computer analysis is presented in Appendix B. Prior to implementing this solution, the spring/damper units must be fully described.

Spring/Damper Unit Evaluation

If it were not for the coupling terms in the heave and pitch cases, the equations of motion could be solved with the mode characteristics only (ζ 's and ω_n 's). The coupling requires knowledge of the individual s/d units.

In Chapter II, it was emphasized that only one "spring" value and one "damper" value could be derived from the data of each mode. Analysis of two of the modes, pitch and roll, resulted in torsional springs and dampers, each of which now can be transformed into a pair of linear springs and dampers at an assumed moment arm to satisfy the model configuration. The moment arm chosen for this analysis is based on the Jindivik ACRS trunk (Figure 1). The tangential contact points of the trunk and the surface with the xz and yz planes define the points for measurement of trunk length and width. Assuming trunk symmetry, the proper moment arms are half of the length ($l/2$) and half the width ($b/2$).

In Chapter IV, the relations between the mode characteristics and the spring/damper coefficients were established. The example for the roll case is repeated here.

$$\begin{aligned} c_{2,4} &= (4 \zeta \omega_{nR} J_{xx}) / b^2 & (a) \\ k &= [J_{xx} \omega_{nR}^2] / b^2 & (b) \end{aligned} \quad (17)$$

Expressions for the heave and pitch cases can be found by similarly equating the coefficients of the differential equation, but the heave and pitch spring/damper coefficients are functions of each other. Simultaneous solution of the expressions result in a form that is in terms of the mode characteristics only. These are:

$$c_{1,3} = \frac{\xi_p \omega_{np} J_{yy} - \xi_H \omega_{nH} m \delta^2}{(\ell/2)^2} \quad (31)$$

$$k_{1,3} = \frac{(\omega_{np})^2 J_{yy} - m (\omega_{nH})^2 \delta^2}{2 (\ell/2)^2} \quad (32)$$

$$c_5 = 2 [\xi_H \omega_{nH} m - (c_{1,3} + c_{2,4})] \quad (33)$$

$$k_5 = m (\omega_{nH})^2 - 2 (k_{1,3} + k_{2,4}) \quad (34)$$

Numerical solution of the s/d units is accomplished in program MODANYL (Appendix B), the results of which are presented in Table IV.

TABLE IV			
LINEAR SPRING/DAMPER UNIT COEFFICIENTS (from Program MODANYL)			
Mode-Test No. ξ and ω_n	Linear s/d Units		
	Position	Spring Coefficients (K) (lb _f /ft)	Damper Coefficients (C) (lb _f /ft/sec)
H-122	1,3	1,174.8	6.9
P-61	2,4	639.1	52.9
R-58	5	17,340.1	772.4
H-122AV	1,3	1,232.9	13.0
P-61	2,4	639.1	52.9
R-58	5	12,623.1	274.6
H-123	1,3	1,804.9	16.7
P-59	2,4	936.5	54.4
R-56	5	9,434.6	599.5
H-123AV	1,3	1,780.2	18.6
P-59	2,4	936.5	54.3
R-56	5	11,439.4	466.5
<p>Note 1: For the heave case, calculations are based on data acquired where the CG was shifted above the trunk CP.</p> <p>Note 2: For the heave mode, the first peak analysis was used for ξ and ω_n unless subscripted by AV, in which case the average analysis was used.</p> <p>Note 3: Linear s/d unit values are based on the Jindivik Trunk, Figure 7, where $\ell/2 = 53.85$ inches and $b/L = 17.6$ inches.</p>			

VI. Analysis of the Vertical Energy Absorption Model

General

The Vertical Energy Absorption Model was exercised on a CDC 6600 computer with the goal to duplicate the Jindivik test of Table I. The model results, which compare favorably with the original tests and with one another, are presented in graphic form in Appendix B with the exception that the responses from a single test condition (flow added-tests 58, 61, and 123) are included in this chapter in order to analyze them more closely. A variable is present in these comparisons since the heave tests were conducted with the CG approximately above the center of pressure (CP) of the trunk, whereas the roll and pitch tests were in normal configuration with the CG aft of the CP. The exact effect of the change of the CG location on the heave data is not known.

Spring Coefficient Comparison

Before examining the model responses, it is worthwhile to compare the mode values of the spring coefficients from Table II with earlier experimental AFFDL static test results which are summarized in Appendix D. These values are plotted in Figure 17 in a kind of histogram where the abscissa represents the point cushion conditions of vent opened (VO), vent

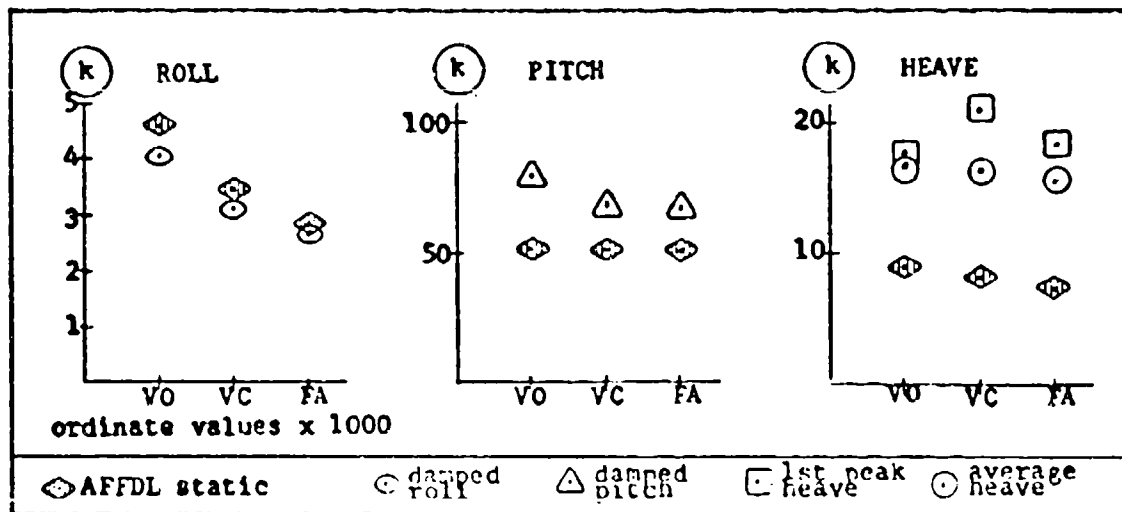


Fig. 17. Comparison of Spring Coefficients

closed (VC) and flow added (FA). Although point conditions, the abscissa does suggest a scale of increasing cushion effectiveness (P_c and \dot{m}_c increasing). This suggests that the dynamic roll spring coefficient and the static roll stiffness are comparable. Thus, for an approximation, the dynamic roll spring coefficient can be found from the easier and less expensive static tests. Another advantage is that the static analytic techniques are easier than the dynamic ones. The dynamic pitch stiffness also shows reasonable agreement between the dynamic and static values and does approach the static value.

The heave case shows dissimilar results. The first peak analysis values appear to increase while the average analysis values show the same decreasing trend with increasing mass flow as the static test values. In both cases, there is a definite magnitude difference in the values between the dynamic and static values of the spring coefficients for any given test configuration. This fact suggests the presence of a dynamic spring phenomenon that was not observable during the static testing.

Model Roll Response

The test values of the damping ratio ζ and undamped natural frequency ω_n used to characterize model response are those in Table II. In all roll tests, ζ generally increases and ω_n generally decreases with increasing mass flow to the cushion.

In Figure 18 for roll test 58, the response of the model shows excellent correlation to the test data in all respects.

Model Pitch Response

For the pitch tests, Table II, ζ 's show no decisive trend, while ω_n 's, like the roll mode, show a decreasing trend with increasing mass flow to the cushion.

Figure 19, for pitch test 61, generally shows good results except it appears that the equilibrium axis of the response is angled slightly to the equilibrium axis of the data. Referring momentarily to Figure 30, page 60, in Appendix A, the equilibrium plots \diamond of the original data show a definite increasing trend with time. The equilibrium height (HEQ) of each test was defined as the average value of these individual equilibrium positions. Back to Figure 19, it is the average equilibrium

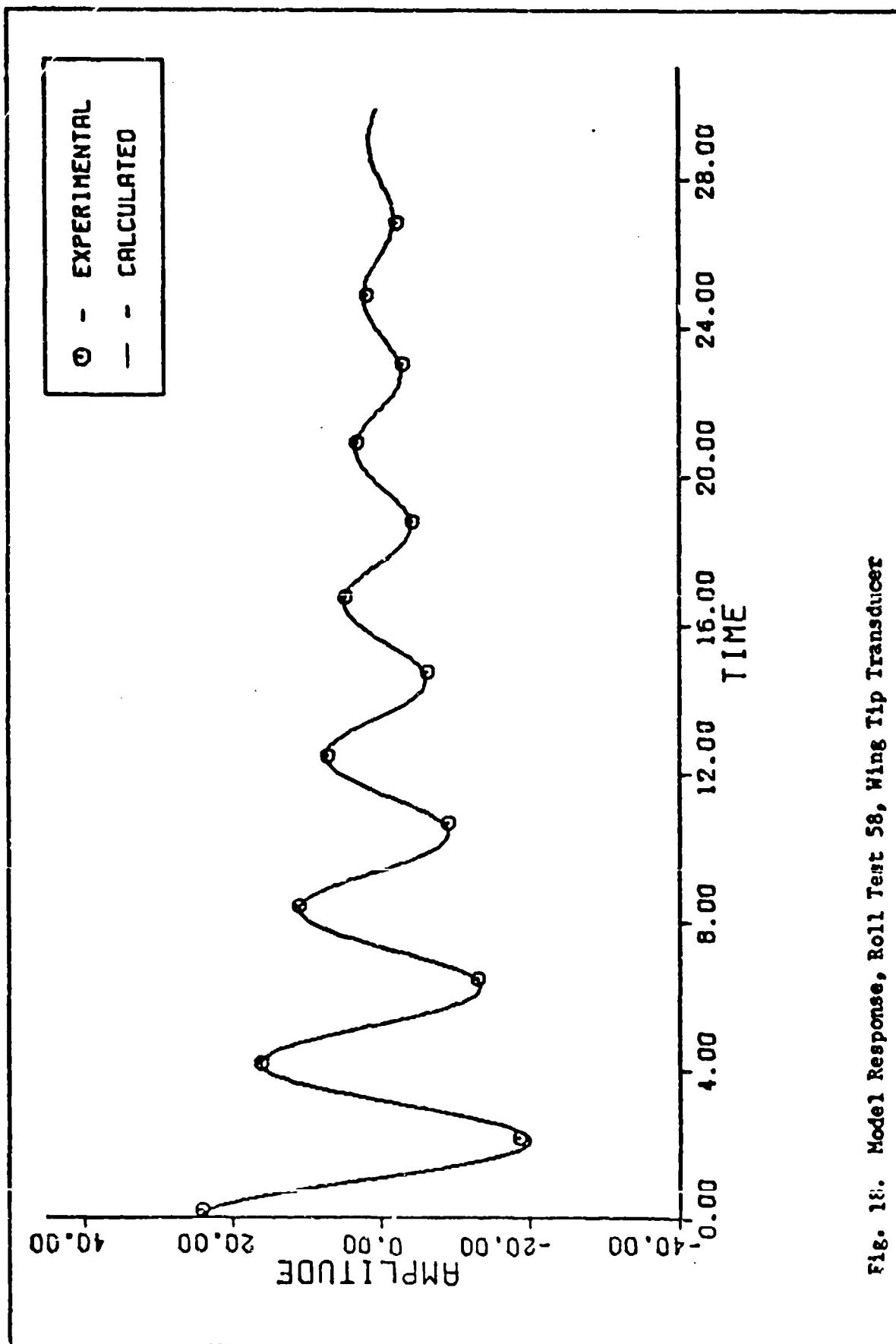


Fig. 18. Model Response, Roll Test 58, Wing Tip Transducer

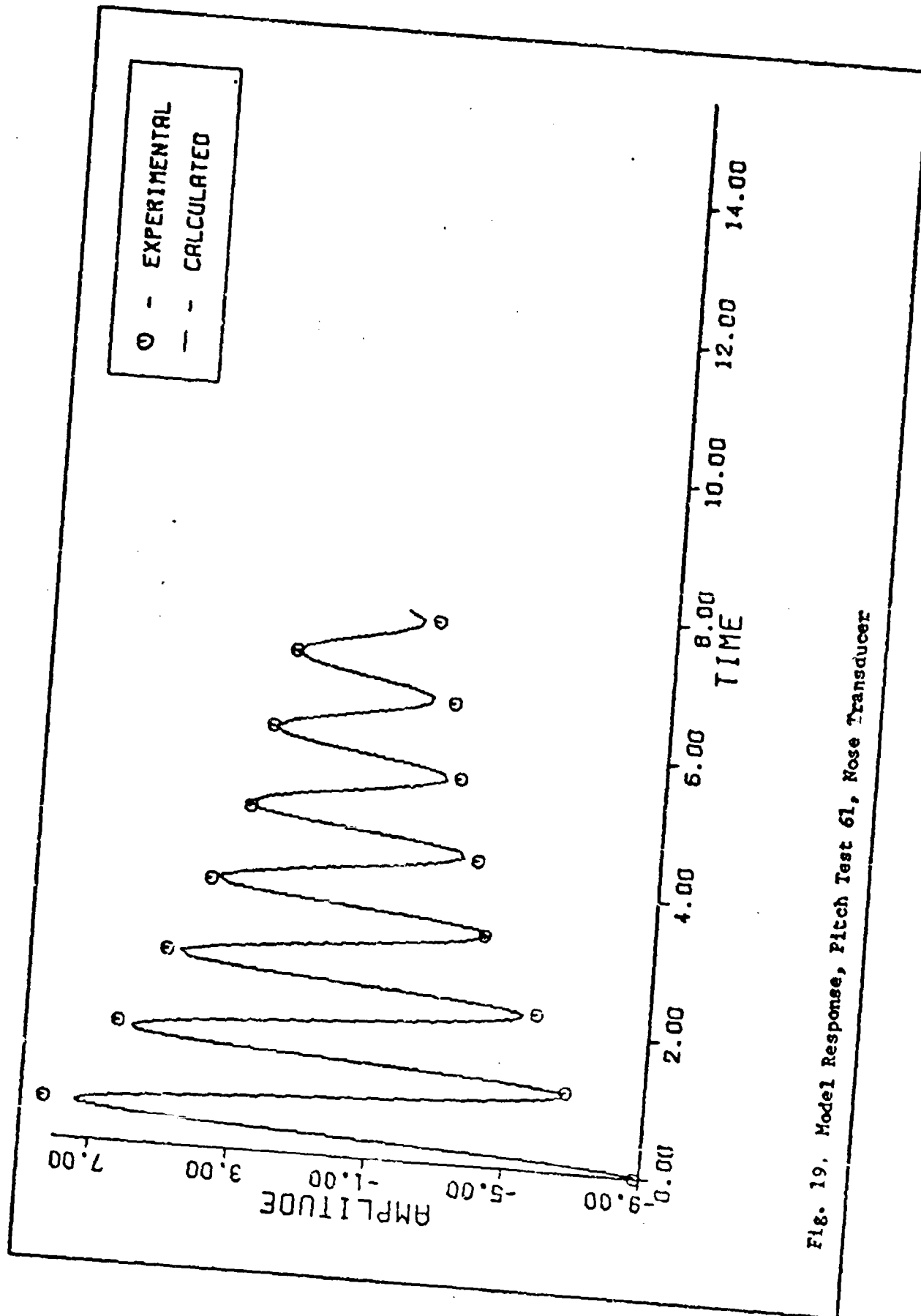


Fig. 19. Model Response, Pitch Test 61, Nose Transducer

height, a constant, that was used in program MODANYL to adjust the original data to the same equilibrium axis as the model response so that the two could be compared. Thus, a slight deviation is introduced to the plot. The magnitude of this deviation is equal to the difference between the average equilibrium height and the actual equilibrium height at any time.

Model Heave Response

The heave response requires several computer runs with different initial conditions in order to evaluate. In Chapter III, the axis chosen for the development of the equations of motion was based on the equilibrium position. Experimental data showed that the equilibrium longitudinal axis made an angle of about 3 - 4.5 degrees nose up from the horizontal plane when the CG was displaced aft of the CP. When the aircraft is dropped level with the surface, then an additional initial condition in pitch is established where $\Theta \approx -3.0$ degrees relative to the equilibrium axis of the model. The first peak and average ζ 's and ω_n 's used to examine the heave mode response are those calculated in program RISE (Appendix A) and presented in Table V.

TABLE V						
ZETA & ω_n COMPUTATIONS FOR HEAVE (Program RISE, modified)						
Peak	TEST 123		TEST 122		TEST 121	
	ZETA	ω_n	ZETA	ω_n	ZETA	ω_n
1	.3482	15.22	.3533	16.61	.3771	15.48
2	.2444	14.72	.1627	14.40	.1691	14.52
3	.1922	14.77	.1296	14.35	.0851	13.93
4			.1575	13.80	.1078	13.32
5			.1847	14.77	.2515	14.37
6			.1057	14.12	.0890	13.82
Average Values	.2616	14.90	.1822	14.675	.1799	14.24

In the first two heave responses presented, the model is exercised with initial conditions on heave only ($\phi = \theta = 0$) and thus no pitch coupling develops. The results of these initial conditions are what was expected from the Jindivik tests when the CG was moved to a position above the trunk CP. The fact that the Jindivik test data shows the heave test coupling into a pitch mode suggests that, during the actual tests, the CG was not exactly over the CP and/or the initial pitch condition was not exactly level at contact.

In Figure 20a, the ζ and ω_n from the first peak analysis are used. The response correlates well with the first data point but is too heavily damped to approach the other data points.

In Figure 20b, the average values for ζ and ω_n are used. Even though the response overshoots the first peak, a much better subsequent response is achieved.

In the next two cases, suspected actual Jindivik test conditions are duplicated; that is, the model is activated parallel to the surface, which puts an initial condition on pitch, and with initial conditions on heave. In these response examples, the model resembles normal Jindivik configuration where the CG is behind the CP.

In Figure 20c, the first peak analysis shows a degradation of response to the first peak due to pitch coupling and a tendency for the pitch mode to dominate the response; that is, heave is not effective after the first peak. It is obvious that the pitch peaks are nowhere near the data points, but this may not be too serious. The period of the pitch mode is constant and approximates the period of the data. This means that the damped natural frequencies (ω_d) do compare. In addition, the peak amplitudes of the pitch response fit exactly into the data exponential decay curve, thus suggesting a comparable logarithmic decrement and pitch damping ratio (ζ).

In Figure 20d, the same initial conditions as Figure 20c are used but with the average values for ζ and ω_n . The degradation of the first peak response actually assists toward matching the data point. Subsequent response is much improved in heave, with the heave mode matching or, at least, moving toward all data points.

A closer inspection of the character of the heave mode is possible with Table V which includes a summary of ζ and ω_n calculations from

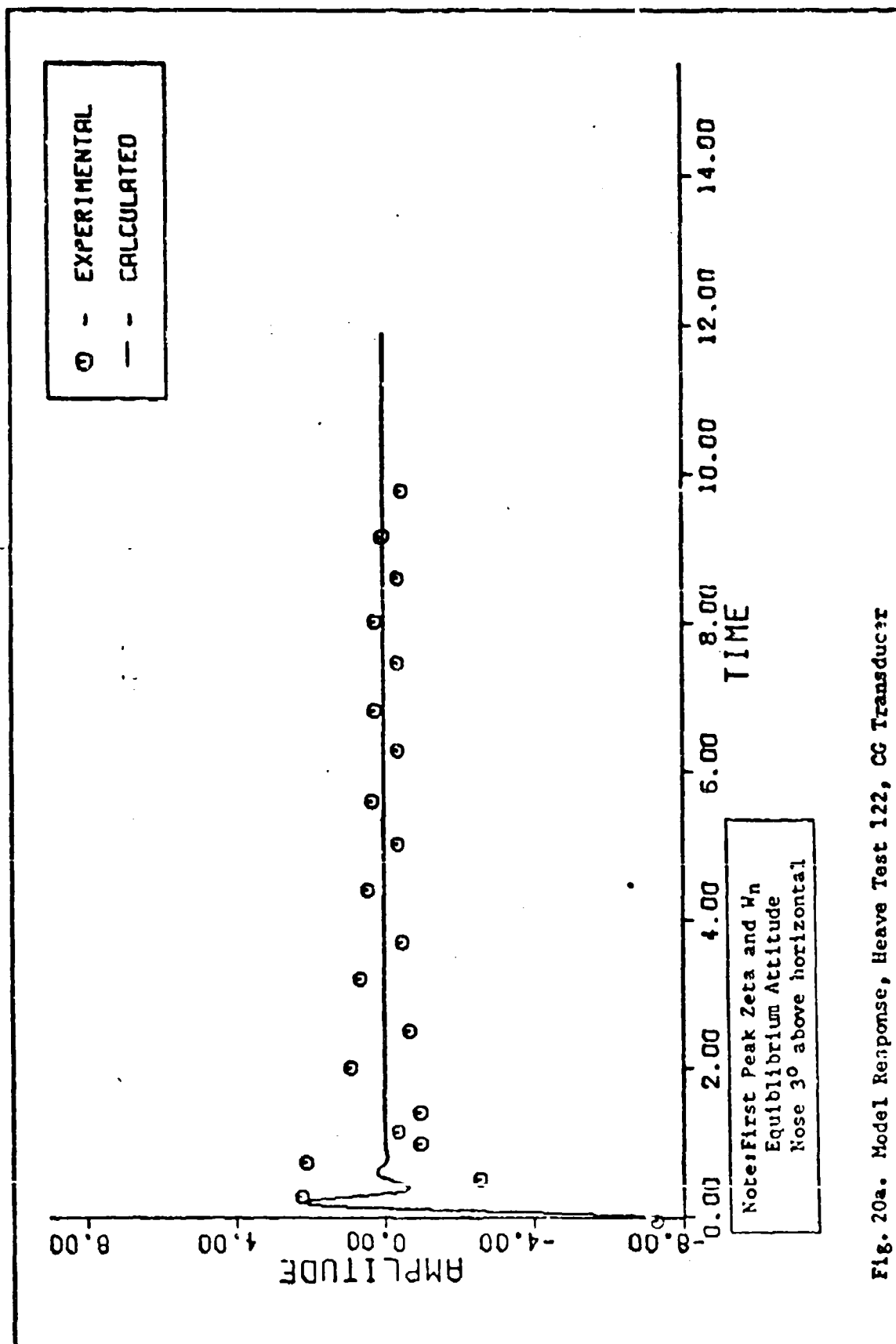


Fig. 20a. Model Response, Heave Test 122, CG Transducer

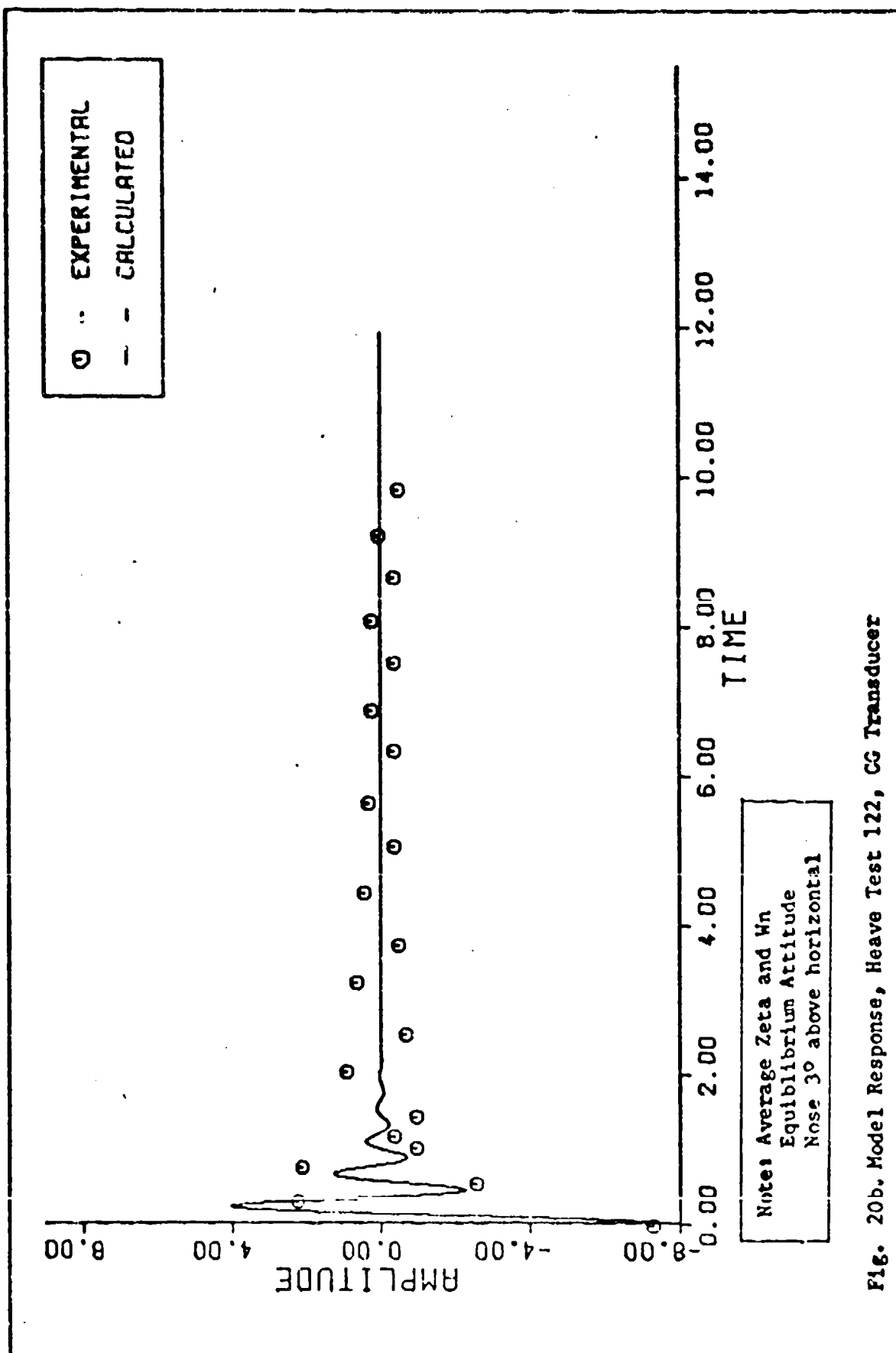


Fig. 20b. Model Response, Heave Test 122, CG Transducer

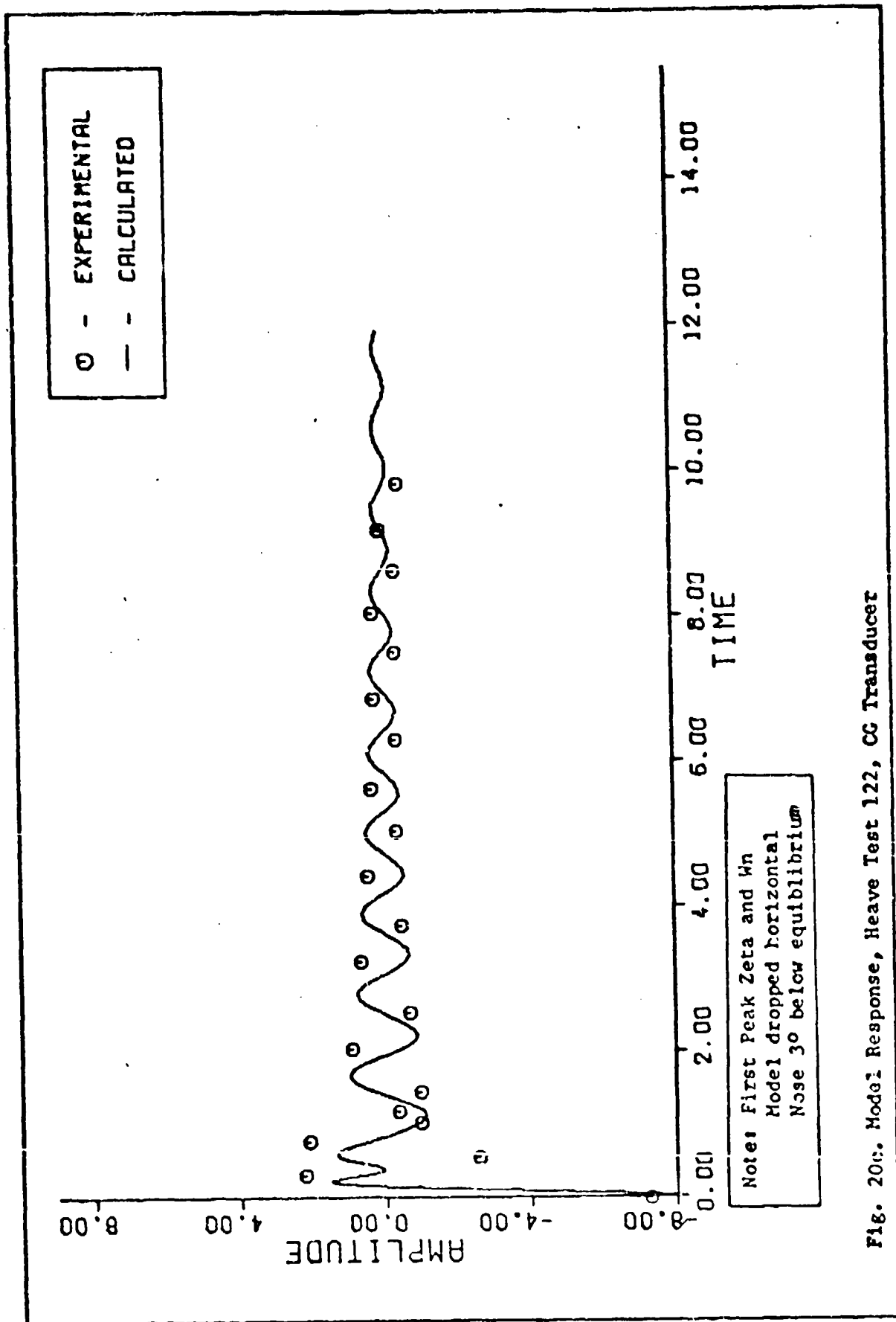


Fig. 20c. Model Response, Heave Test 122, CG Transducer

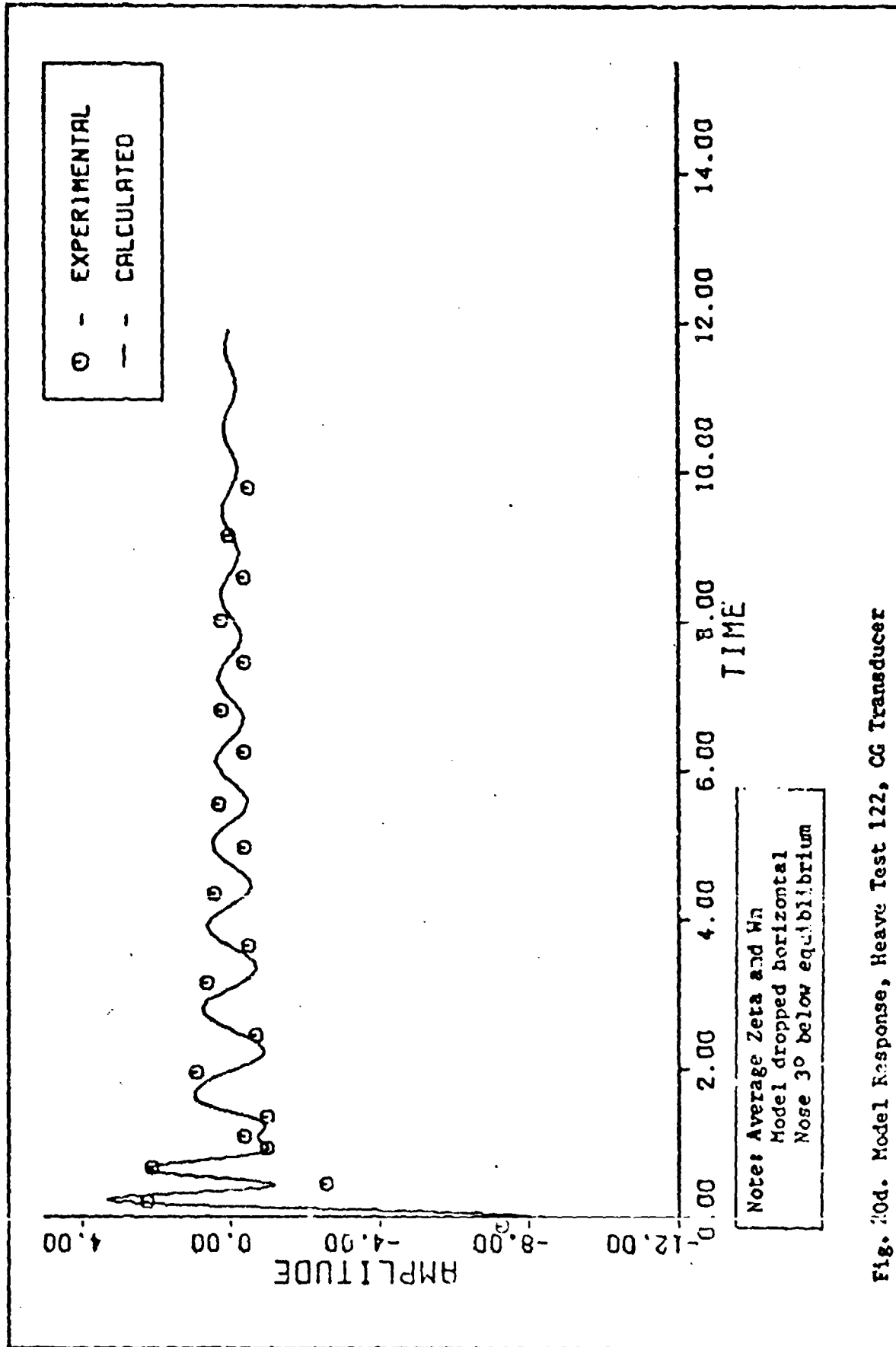


Fig. 20d. Model Response, Heave Test 122, CG Transducer

program RISE for all peaks. In all the leave test cases, the first peak values of ζ and ω_n are significantly higher than the subsequent values. The subsequent values of ω_n are essentially constant. Equations (17b), (32) and (34) imply that when ω_n is constant, then the spring coefficient is constant. The damping ratios (ζ), on the other hand vary erratically, suggesting a non-linear behavior. It can be seen from equations (17a), (31) and (33), that, given ω_n a constant, if ζ is non-linear, then the damper coefficients are non-linear.

VII. Conclusions and Recommendations

Conclusions

From the analysis in Chapter VI and with the supplementary response curves in Appendix B, the Vertical Energy Absorption Model demonstrates model response characteristics in the roll and pitch modes that correlate well to the Jindivik data. In the heave mode, results are satisfactory, but more important, the potential for continued development and more precise prediction has been demonstrated. The use of a mechanical analog prediction scheme for an Air Cushion Landing System has sufficient merit to warrant further investigation.

The linear assumption for both the spring and damper coefficients made in Chapter II is born out by analytic results and response curves in pitch and roll. The roll mode is superior in this respect.

Heave response of the model is reasonable, but care must be exercised in the selection of the proper damping ratio (ζ) and undamped natural frequency (ω_n). For an analytical means of finding ζ and ω_n , the method of averaging the values from a peak time analysis (program RISE) provides good results. Reference the heave equation (8), the terms on the right hand side indicate a coupling of the motion to the pitch mode. The amplitudes of the heave response curves in Figures 20a to 20d do not match the data consistently as ζ and ω_n are varied. Using the first peak values for ζ and ω_n results in a good response match at the first data point (Figure 20a), but the excessive damping ratio suppresses the amplitude of the response at subsequent data points. Using the average values of ζ and ω_n , the response approaches the subsequent data points but overshoots the first data point. These observations suggest that the heave response is non-linear. The non-linearity is in the exponential decay curve of Figure 14 and is due to the product $\zeta\omega_n$. However, from the summary of heave characteristics in Table V, it is shown that ω_n is approximately constant and is approximately equal to the average value of the heave ω_n . With the conclusion that the heave ω_n is a constant, then it is possible to conclude that the dynamic heave spring coefficient (k_E) is constant (linear) also. A further observation is possible. With a constant heave ω_n , if the product $\zeta\omega_n$ is non-linear, then the non-linearity must be due to the

damping ratio ($\frac{1}{2}$). Translating this observation to the model, it is now possible to conclude that the non-linearity in heave is due to the heave damper coefficient (C_E).

Of concern is the fact that the theoretical response peaks of the remaining pitch response after heave had damped out did not match the data in time (phase shift) even though there was correlation in period and amplitude of the exponential decay. Since the heave mode has violated the original model assumption of linearity, it is not possible to form a conclusion about the phase shift of the remaining pitch response without first investigating the heave non-linearity.

In Chapter I, it was noted that there are two categories of trunk material, stretchable and non-stretchable. Since this model investigation was based on data from an ACRS made of non-stretchable material, use of the model with stretchable material trunks must be accomplished with caution. The exact effect of a stretchable trunk on the linearity of the system characteristics is not known at this time; however, the model is expected to operate correctly if a proper expression for the spring and damper coefficients are provided.

The schematic of the VEAM in Figure 8 visually suggests that the peripheral springs represent sections of the trunk and that the center spring represents the cushion. This is not the case. The model requires a center spring (position 5) to account for the heave dynamics in addition to the roll and pitch linear springs which are derived from a torsional mode spring. This is illustrated in Table IV where the linear s/d unit coefficients are summarized from program MODANYL.

Recommendations

The following recommendations are derived from this study:

1. An investigation into the non-linear nature of the heave damping phenomenon should be made. A non-linear heave damper coefficient should be formulated and incorporated into the model to eliminate the deficiency of the linear assumption. These results should then be used to investigate the difference in phase shift between the theoretical curve and the experimental data of the heave response after heave damps out.

2. A method should be investigated which would allow the prediction of the spring and damper coefficients directly from trunk and cushion parameters so that this model can be used to investigate the dynamics of arbitrary trunk configurations without first building and testing on actual vehicle or scaled model.

Bibliography

1. Cannon, Robert H., Jr. Dynamics of Physical Systems. New York: McGraw-Hill Book Company, 1967.
2. Coles, A.V. Air Cushion Landing System CC-115 Aircraft. Technical Report AFFDL-TR-72-4, Part 1. Wright-Patterson Air Force Base, Ohio: Air Force Flight Dynamics Laboratory, May 1972.
3. Digges, Kennerly H. Theory of an Air Cushion Landing System for Aircraft. Technical Report AFFDL-TR-71-50. Wright-Patterson Air Force Base, Ohio: Air Force Flight Dynamics Laboratory, June 1971.
4. Doebelin, Ernest O. System Dynamics, Modeling and Response. Columbus, Ohio: Charles E. Merrill Publishing Company, 1972.
5. Dorf, Richard C. Modern Control Systems. Reading, Massachusetts: Addison-Wesley Publishing Company, 1967.
6. Rodrigues, Anthony. Drop and Static Tests on a Tenth-Scale Model of an Air Cushion Landing System (ACLS). Thesis for Master of Science. Wright-Patterson Air Force Base, Ohio: Air Force Institute of Technology, 1973.
7. Ryken, John M. Design of an Air Cushion Recovery System for the Jindivik Drone Aircraft. Technical Report AFFDL-TR-73-xx. Wright-Patterson Air Force Base, Ohio: Air Force Flight Dynamics Laboratory, 1973.
8. Saha, Hrishikesh. Air Cushion Landing Systems. Tullahoma, Tennessee: University of Tennessee, 1973.
9. Vaughn, John C., III and Steiger, James T. Vertical Energy Absorption Analysis of an Air Cushion Recovery System. Technical Memorandum AFFDL-TM-72-03-FEM. Wright-Patterson Air Force Base, Ohio: Air Force Flight Dynamics Laboratory, August 1972.

Appendix A

Analysis of Jindivik Data (Computer Solution)

Program DATANYL

The program for evaluating the Jindivik ACLS roll and pitch data according to the theory set forth in Chapter IV is called DATANYL. Table VI describes the method for entering data into the program and defines the symbols used. Table VII describes the output symbology and units. Following Table VII is a listing of DATANYL, a single example output from the line printer, and a plot of the test data of each of the roll and pitch tests of Table I.

TABLE VI			
PROGRAM DATANYL-INPUT DATA			
Data Group	No. of Data Cards in Group	Format	Input Symbol
1	1	I5	F
2	1	8F5,F10.3, A9	N,P,Q,R,S,W,U,NOTR,MASSEQ,TITLE
3	1-N	F10.3	T
4	1-N	F10.3	H
DEFINITIONS OF INPUT SYMBOLS			
F	The number of sets of data (data groups 2,3, & 4)*		
N	Total number of data points		
P	The data point number for the first positive peak (1 or 2)		
Q	Total number of positive peaks		
R	The data point number of the last positive peak		
S	The data point number of the first negative peak (1 or 2)		
W	Total number of negative peaks		
V	The data point number of the last negative peak		
NOTR	The integer number of the Jindivik test run		
MASSEQ	The moment of inertia (slugs-ft ²)		
TITLE	Enter "ROLL" or "PITCH"		
T	The time from t ₀ for all peaks in consecutive order		
H	The adjusted linear transducer heights		
* data groups 2,3, & 4 comprise a set of data for each Jindivik test run. Enter as many sets (F) as there are test runs to be analyzed on a single computer run.			

TABLE VII

PROGRAM DATANYL-OUTPUT DATA

Column Number	Column Title	Description
1	DATA POINT	The data point number for recorded positive and negative peaks in consecutive order
2	TIME (SEC)	The time occurrence of the positive and negative peaks
3	H (IN)	The recorded heights or perturbations from linear transducers for CG, Nose, and Wing
4	T (SEC)	The period, measured between adjacent positive peaks
5	FD (CPS)	The damped natural frequency in cycles/second
6	WD (RPS)	The damped natural frequency in radians/second
7	HEQ (IN)	The equilibrium height of the system in steady state
8	POSAR	The amplitude ratios of the positive peaks
9	NEGAR	The amplitude ratios of the negative peaks

The following values are averaged to obtain the final value used in the remainder of the calculations: T, FD, WD, HEQ, POSAR, NEGAR.

```

PROGRAM      DATANYL

      PROGRAM DATANYL (INPUT,OUTPUT, PLOT)

C THIS PROGRAM WILL ACCEPT INPUT 30 DATA POINTS MAXIMUM
      DIMENSION T(32), H(32), TF(16), FD(16), HEC(32), C(16), AFF(16), ARN(16)
5      1WD(16), FC(32), HE(32)
      INTEGER F,C,R,S,W,U,F
      REAL MASSEC,KE
      READ C,C,F
10      60 FORMAT (15)
      DO 61 J=1,F
      READ 1,N,F,O,P,S,W,U,ACTR,MASSEC,TITLE
1      1 FORMAT (E15,F10.3,A9)
      READ 2, (T(M),M=1,N)
15      45 READ 2, (F(N),M=1,N)
      2 FORMAT (F10.3)

C 7000 CUT MATRICES
      DO 5 I=1,N
      TF(I)=C.
      FC(I)=C.
      WC(I)=C.
      HE(I)=C.
      5 FEO(I)=C.

C 8000 COMPLETE PERICES & FREQUENCIES (T,FD,WD)
      SUMTF=C.
      SUMFC=C.
      K = F+2
      DO 10 I=K,P+2
20      TF(I) = T(I) - T(I-2)
      FC(I) = 1./TF(I)
      WF(I) = 2.*2.1415926*FC(I)
      SUMTF = SUMTF + TP(I)

```

Fig. 21a. Program DATANYL

```

35      10 SUMFD = SUMFD + FO(I)
        AVTF = SUMTF / (O-1)
        AVFC = SUMFD / (O-1)
        AVWC = 2.*2.1415926*AVFC

C      C COMPUTE EQUIBLIBRIUM POINTS (LINEAR FIT)
40      SUMHEC = 0.
        K=N-1
        FC 20 I=2,K
            L=I+1
            M=I-1
            HCP = ((H(L)-H(M))/(T(L)-T(M)))*(T(I)-T(M)))+H(M)
            HEN(I) = (H(I)+HCP)/2.
20      SUMHEC=SUMHEC+HEN(I)
        AVHLC=SUMHEC/(N-2)

C      C COMPUTE THE POSITIVE ASPECT RATIOS & POSITIVE DECREMENTS
50      K=O-1
        CALL TCRFE (F,K,R,N,AF,H,AVAFCS,POSDEC,AVHEC,FC)

C      C COMPUTE THE NEGATIVE AMPLITUDE RATIOS AND DECREMENTS
55      K=N-1

C      C COMPUTE THE OVERALL AMPLITUDE RATIO & DECREMENT
60      AVO=(AVAFCS+AVARNEG)/2.
        DEC=ALCC(AVC)

C      C COMPUTE DAMPING RATIO (ZETA)
        ZETA = SQRT(DEC**2/(35.4784176+DEC**2))

C      C COMPUTE CAPPER NATURAL FREQUENCY
65      WN = AVWC/SQRT(1.0-ZETA**2)

```

Fig. 21b. Program DATANL (cont.)


```

70      C COMPUTE SPRING/DAMPER COEFFICIENTS
      KE = MASSEC*(WN**2)
      CE = 2.*ZETA*W1*MASSEC
      C
      C
      PRINT 50,NCTR,TITLE
50      FORMAT ('1*4Y*ACLS/JINCLIVK/DATA ANALYSIS*/5X*TESY FUN *I3
1* - *F5//)
      PRINT 51
51      FORMAT (5) *DATA*4X*TIME*8X*W*9X*T*8X*FD*8X*DC*8X*FEC*5X*POSPR*5X
1*NEGAP*
2 /5X*FCINT*3X*(SEC)*6X*(IN)*5X*(SEC)*5X*(CFS)*5X*(RFS)*5X*(IN)*//)
      CC 100 J=1,N
      PRINT 101,I,T(I),H(I),TP(I),FD(I),WD(I),HEC(I),AFF(I),ARN(I)
101      FORMAT (5X12,F10.7,F10.2,4X,G10.7,5G10.4)
100      CONTINUE
      PRINT 52
52      FORMAT (32X*-----*4X*-----*4X*-----*4X*-----*
14X*-----*/)
      PRINT 53 ,AVTP,AVED,AVH0,AVHE0,AVARPOS,AVARNEG
53      FORMAT (12X*AVERAGE VALUES = *3XG10.4)
      PRINT 54,CFC,ZETA,W1,KE,CE
54      FORMAT (//5X*LOGARITHMETRIC INCREMENT (CEC) = * F12.4/5X
1*CAMPING RATIO*14X*(ZETA) = * F12.4/5X*UNCAFFEC NATURAL FREQUENCY
2 (WN) = * F10.2,5X*(RAD/SEC)*
35X*EFFECTIVE SPRING COEFFICIENT (KE) = *F10.2,5X*(FT-LBF/RAD)*5X
4*EFFECTIVE DAMPER COEFFICIENT (CE) = *F10.2,5X*(FT-LBF/(RAD/SEC)*
5)
      C
      C PLOT THE DATA
      K=N+2
      CALL DATAFLT (T,H,HEC,N,K,AVHE0)
      C1 CONTINUE
      STOP
      END

```

Fig. 21c. Program DATANYL (cont.)

```

SUBROUTINE DECRC
SUBROUTINE DECRC (J,K,L,N,D,H,AVD,DEC,AVFEC,PD)
DIMENSION C(K),H(N),HF(N)
INTEGER R,S
C
5  C ZERO OUT MATRICES
   CC 5 I=1,N
   S C(I)=0.
   SUMC=C.
C
10  C ADJUST AMPLITUDES TO EQUILIBRIUM POSITION
   DO 6 I=1,N
   6  PC(I) = P(I) - AVHEO
C
15  C COMPUTE AMPLITUDE RATIOS
   M=L-2
   DO 10 I=L,N,2
   R=I+1
   S=I+2
   C(R) = PC(I)/HD(S)
   10  SUMD = SUMC+D(R)
   AVD = SUMC/(K)
   DEC = ALCG(AVD)
   RETURN
END
20

```

Fig. 22. Program DATANYL, Subroutine DECRC

```

SUBROUTINE DATAPLT
  DIMENSION T(K),H(K),FEC(K)
  CALL FLOT (0.,-11.,-3)
  CALL FLOT (0.,1.5,-3)
  C DRAW FORCEF
    CALL FLOT (1.,1.,3)
    CALL FLOT (1.,7.,2)
    CALL FLOT (10.,7.,2)
    CALL FLOT (10.,1.,2)
    CALL FLOT (1.,1.,2)
  C DRAW AXIS
    CALL FLOT (1.875,2.5,-3)
    CALL SCALE (T,7.75,N,1)
    CALL SCALE (H,4.25,N,1)
    CALL AXIS (0.,0.,4PTIME,-4,7.75,0.,T(N+1),T(N+2))
    CALL AXIS (0.,0.,9HAMFLITUDE,+9,4.25,90.,F(N+1),F(N+2))
  C PLOT THE DATA
    HEC (N+1) = H(N+1)
    FEC (N+2) = F(N+2)
  C PLOT H EQUILIBRIUM POINTS
  C PRINT THE LEGENDS
    CALL FLOT (5.5,3.45,+2)
    CALL FLOT (7.75,3.45,2)
    CALL FLOT (7.75,4.25,2)
    CALL FLOT (5.5,4.25,2)
    CALL FLOT (5.5,3.45,2)
    CALL SYMPL (5.75,4.,1,1,0.,-1)
    CALL SYMPL (6.,3.95,1,12H- AMPLITUDE,C.,12)
    CALL SYMPL (5.75,3.7,1,5,0.,-1)
    CALL SYMPL (6.,3.65,1,17H- H EQUILIBRIUM,0.,17)

```

Fig. 23a. Program DATAPLT, Subroutine DATAPLT

```

35      CALL FLCT (4.75,.1,3)
        CALL FLCT (7.75,.1,2)
        CALL FLCT (7.75,.3,2)
        CALL FLCT (4.75,.3,2)
        CALL FLCT (4.75,.1,2)
        CALL SYMECT (4.9,.2,.1,4,0,-1)
        CALL SYMECT (5.05,.15,.1,24,A= AVERAGE H EQUILJERIUM,0.,24)
40      CALL FLCT (12.,0.,-3)
        CALL FLCTE
        RETURN
        END

```

Fig. 23b. Program DATANYL, Subroutine DATAPLI (cont.)

ACLS/JINDIVIK/ATA ANALYSIS
TEST RUN 55 - PITCH

DATA POINT	TIME (SEC)	H (IN)	T (SEC)	FD (CPS)	WD (RPS)	HEC (IN)	FCSAR	NEGAR
1	0.000	-0.30	0.	0.	0.	0.	0.	0.
2	0.550	17.70	0.	0.	0.	9.415	0.	1.380
3	1.000	2.30	0.	0.	0.	9.448	1.390	0.
4	1.525	15.30	0.975	1.026	6.444	9.177	0.	1.257
5	1.975	3.70	0.	0.	0.	9.168	1.295	0.
6	2.475	13.90	0.950	1.052	6.614	9.175	0.	1.350
7	2.975	5.20	0.	0.	0.	9.127	1.507	0.
8	3.420	12.30	0.945	1.058	6.649	8.961	0.	1.255
9	3.825	6.10	0.	0.	0.	8.942	1.395	0.
10	4.730	11.40	0.880	1.136	7.140	8.928	0.	1.356
11	4.875	6.90	0.	0.	0.	9.121	1.046	0.
12	5.075	11.30	0.975	1.026	6.444	9.171	0.	1.151
13	5.725	7.20	0.	0.	0.	0.	0.	0.

AVERAGE VALUES =			0.9450	1.063	6.656	9.106	1.328	1.304

LOGARITHMIC DECREMENT (DEC) = 0.2743
 DAMPING RATIO (ZETA) = 0.2436
 UNCAMPED NATURAL FREQUENCY (1/2) = 6.66 (RAD/SEC)
 EFFECTIVE SPRING COEFFICIENT (KB) = 80354.78 (FT-LBF/RAD)
 EFFECTIVE DAMPER COEFFICIENT (CF) = 1052.36 (FT-LBF/(RAD/SEC))

Fig. 14. Sample Output of Program DATANYL

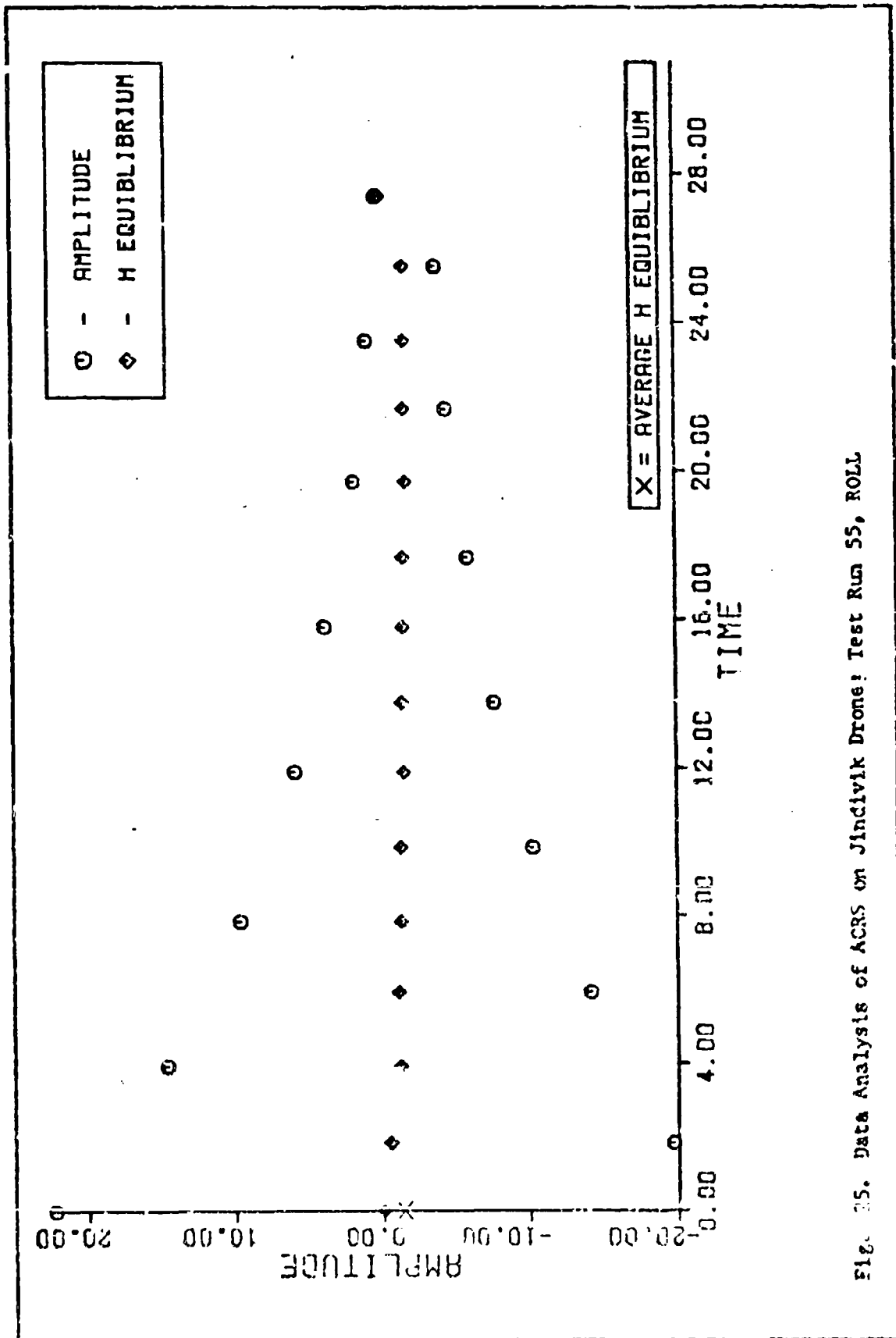


Fig. 25. Data Analysis of ACRS on Jindivik Drone: Test Run 55, ROLL

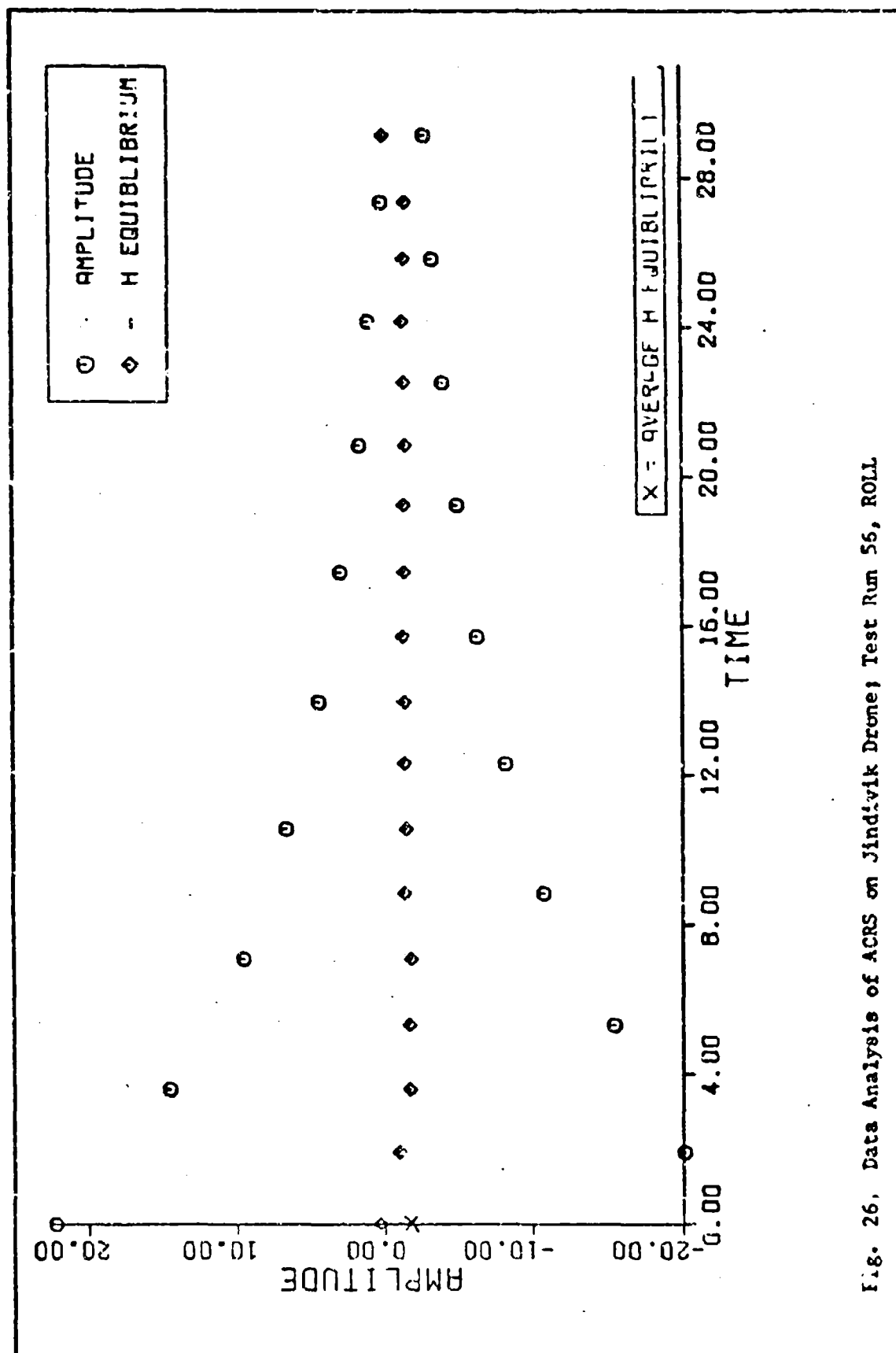


Fig. 26. Data Analysis of ACRS on Jindivik Drone; Test Run 56, ROLL

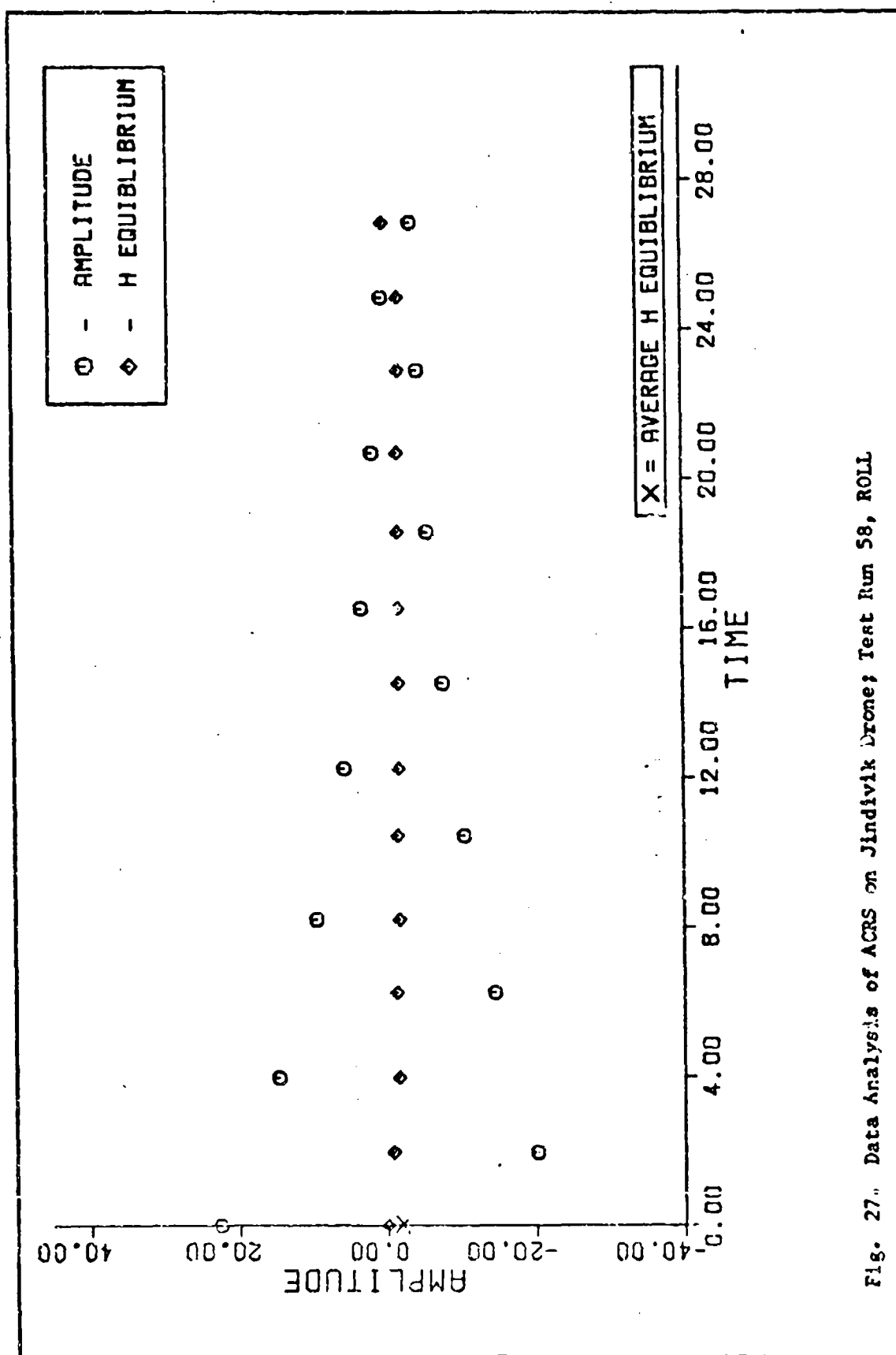


Fig. 27. Data Analysis of ACRS on Jindivik Drone; Test Run 58, ROLL

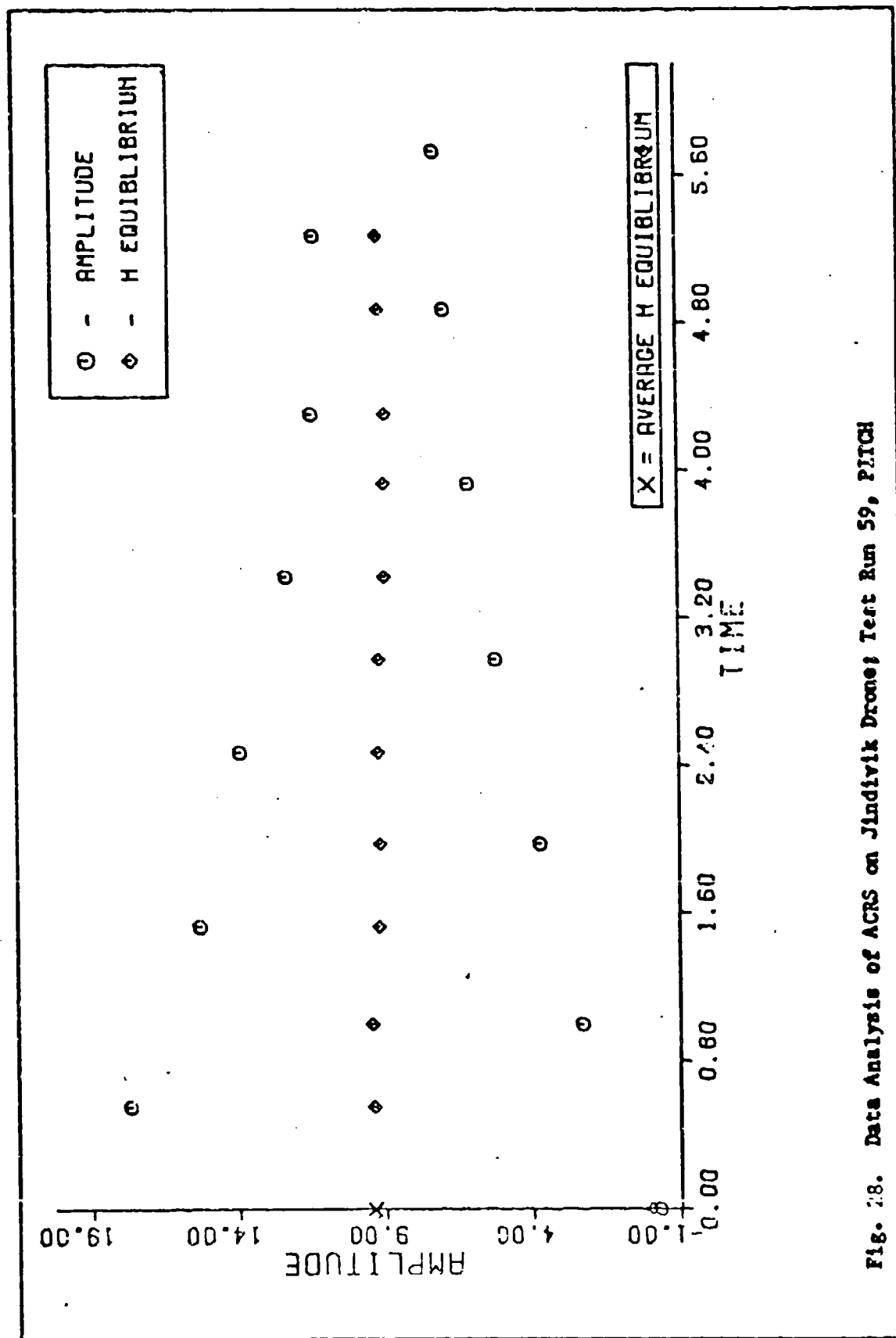


Fig. 28. Data Analysis of ACRS on Jindivik Drone; Test Run 59, PITCH

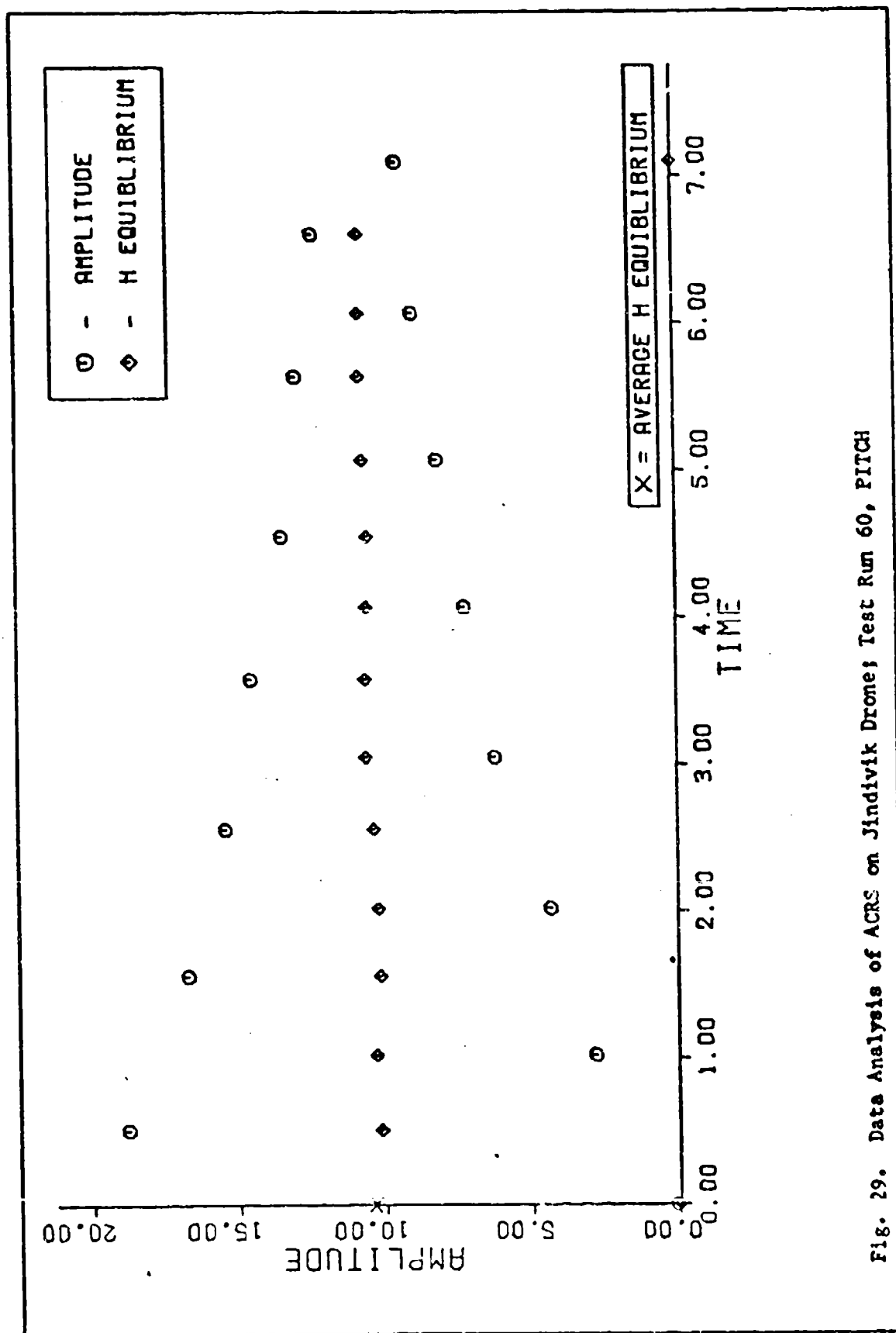


Fig. 29. Data Analysis of ACRS on Jindivik Drone; Test Run 60, PITCH

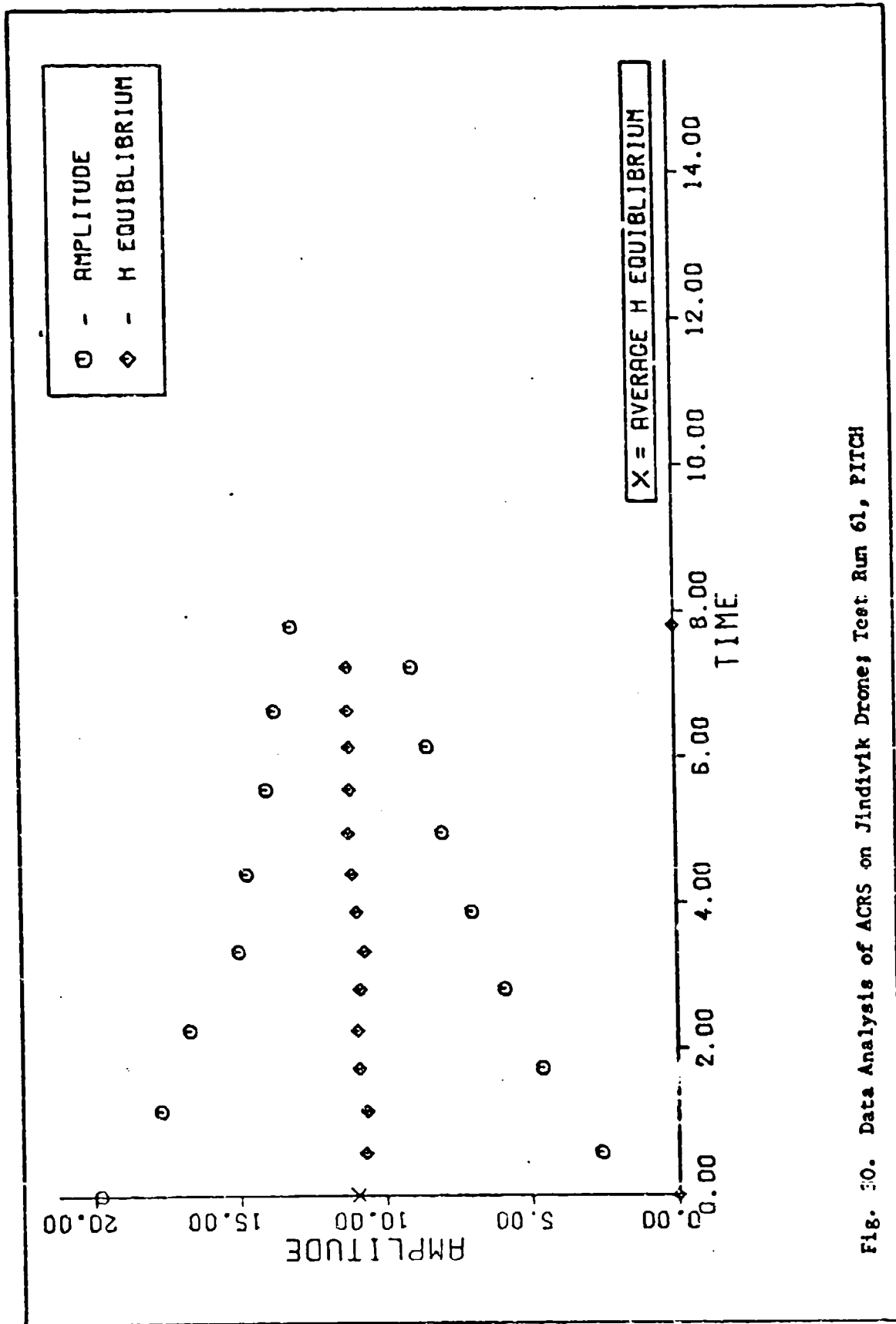


Fig. 30. Data Analysis of ACRS on Jindivik Drone; Test Run 61, PITCH

Program RISE

Program RISE computes the damping ration (ζ) and undamped natural frequency (ω_n) of the Jindivik heave mode using the method of percent overshoot and rise time to the first peak (Chapter IV) and accounts for an initial condition on velocity as well as displacement at model activation. The free fall equations are included to provide values required by the analysis. To check linearity in heave, RISE can be modified (lines 381-384) to allow computation of ζ and ω_n at peak times subsequent to the first peak. The program is designed for use on the teletype remote terminal. Table VIII provides the method for reading data into the program. Table IX describes the symbols and units for output. Symbols in both Tables are in accord with Figure 16. Figure 31 presents a listing of the program RISE. A summary of all calculations from program RISE can be found in Tables II and III of Chapter IV.

TABLE VIII						
PROGRAM RISE-INPUT DATA						
Input Statement	Format	Input Symbol				
Read 1	5F10.3	TAU	TAUPI	HI	HEQ	HPI
Read 4	2F10.4,2I5	ZETA	WN	N	L	
DEFINITIONS OF INPUT SYMBOLS*						
TAU	Time of free fall (sec.)					
TAUPI	Time from release to the first peak (sec.)					
HI	Height of release point from surface (in.)					
HEQ	Equilibrium height from surface (in.)					
HPI	Height of first peak from surface (in.)					
ZETA	Damping ratio - assumed or guess for iteration (N/D)					
WN	Undamped natural frequency - assumed or guess for iteration (rad./sec.)					
N	Integer value of cycles - i for first peak					
L	Integer value of number of iterations desired					
* Symbols are in accordance with Figure 16, Chapter IV.						

TABLE IX
PROGRAM RISE - OUTPUT DATA

Output Statement	Output Symbol	Output Definition	Units
Print 11	TP	Time to first peak	sec.
	Z ϕ	Initial displacement from equilibrium, positive measured down	in.
	Z ϕ D ϕ T	Initial velocity at t ₀	in./sec.
	ZP1	Displacement of the first peak from equilibrium	in.
Print 15	N	The N value read in	N/D
	ZETA1	The first guess for ZETA	N/D
	WN1	The first guess for WN	rad./sec.
Print 13	ZETA	The iterative solution for ZETA	N/D
	WN	The iterative solution for WN	rad./sec.

```

100= PROGRAM RISE (INPUT, OUTPUT)
110= INTEGER K
120= PRINT 20
130=20 FORMAT (/5X*READ IN DATA - TAU,TAU*P1,HI,HEQ,HPI*)
140= READ 1,TAU,TAU*P1,HI,HEQ,HPI
150=1 FORMAT (5F10.3)
170= PRINT 21
130=21 FORMAT (/5X*READ IN DATA - ZETA,WN,N,L*)
190= READ 4,ZETA,WN,N,L
200=4 FORMAT (2F10.4,2I5)
210=0 AXIS: H POSITIVE DOWN FROM SURFACE
220=0 TAU FROM RELEASE
230=0 FREE FALL TO HC
240= HC=((32.2/(12.*2.))* (TAU**2))+HI
250=0 CHANGE AXIS: H POSITIVE DOWN FROM EQUILIBRIUM, I FROM CONTACT
260= ZO=HC-HEQ
270= ZODOT=((32.2/12.)*TAU
280= ZPI=HPI-HEQ
290= IPI=TAU*P1-TAU
300= PRINT 10
310=0
320=10 FORMAT(/9X*P1*6X*ZO*7X*ZODOT*6X*ZPI*)
330= PRINT 11,IPI,ZO,ZODOT,ZPI
340=11 FORMAT(5X4G10.4/)
350= PRINT 15
360=15 FORMAT (9X*N*5X*ZETA1*6X*WN1*)
370= PRINT 16,N,ZETA,WN
380=16 FORMAT (5X15,2F10.5//)

```

Fig. 31a. Program RISE

```

381=3      CONTINUE
382=      PRINT 22
383=22     FORMAT (5X*READ IN TPI,ZPI,N*)
384=      READ 23,TPI,ZPI,N
385=23     FORMAT (2F10.4,I5)

390=      PRINT 13
400=13     FORMAT (9X*ZETA*9X*WN*)
410=C
420=      DO 2 I=1,L
430=      A=(ZODOT*ZETA)+(ZO*WN)
440=      B=SQRT(1.0-ZETA**2)
450=      C=N*3.1415926
460=      K=(ZETA/B)+(ZODOT/(ZO*WN*B))
470=      ZETA=(-1.0*ALOG((ABS(ZPI/ZO))/SQRT(1.0+K**2)))/(WN*TPI)
480=      WN=(ZODOT-(C/B*A))/(TPI*A)
490=      PRINT 12,ZETA,WN
500=12     FORMAT (2F15.5)
510=2      CONTINUE
520=C      THE "GO TO 3" STATEMENT ALLOWS SEQUENTIAL USE OF "READ 4"
530=C      THE "READ 1" DATA REMAINS CONSTANT
540=C      IF EQUATIONS DO NOT CONVERGE IN "L CYCLES" THEN ENTER LAST VALUES OF "ZETA & WN" AND TRY AGAIN
550=C
560=C      THIS METHOD REQUIRES USER ABORT TO TERMINATE
570=      GO TO 3
580=      END

```

Fig. 31b. Program RISE (cont.)

Appendix B
Analysis of the Equations of Motion
(Computer Solution)

Program MODANYL

The evaluation of the equations of motion of the Vertical Energy Absorption Model (VEAM) in its three degrees of freedom (DOF) is accomplished by program MODANYL. A listing of the program is presented in Figure 32. Due to program volume, only the graphical results are included in this study.

This program is designed to solve the VEAM equations with the use of AFIT Subroutine RKDES, a differential equation solver using a variable step fourth-order Runge-Kutta method. In addition, the mode springs and dampers are converted to linear spring/damper units with the equations developed in Chapter V.

The total vertical displacement as a result of movement in the 3 DOF of any arbitrary point in the plane of the model is computed by Subroutine LOCATE. Displacement of any point (P) relative to the CG

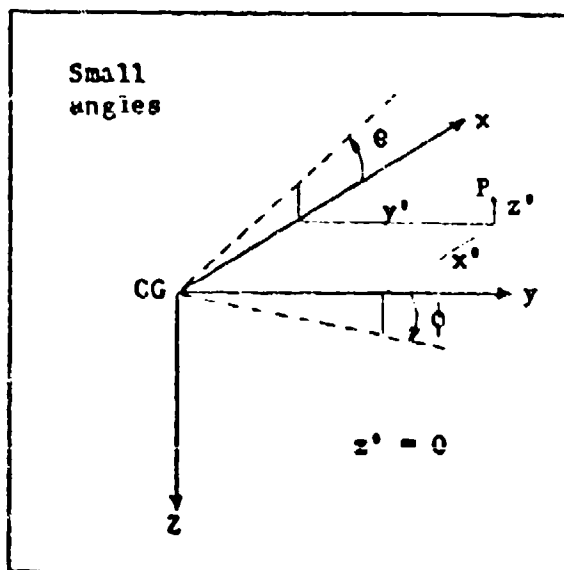


Fig. 32. Vertical Displacement
for Subroutine LOCATE

could be accomplished by LOCATE, but the model assumptions of Chapter II permit limiting the arbitrary point to the horizontal plane ($z' = 0$). For this study, the three positions in the xy plane that coincided with the locations of the Jindivik linear displacement transducers were chosen for output in order to compare with the test data.

A subroutine called ANAPLT plots the theoretical curve and the experimental data points for

comparison. Since this plot routine is similar to DATAPLT of Appendix A, a listing is omitted.

The equations of motion solve a dynamic force balance relative to the equilibrium axis. All initial conditions on displacement that are applied to the equations of motion must be referenced to the equilibrium axis also. Collecting data relative to the equilibrium axis is difficult since the equilibrium position changes according to test configuration. Therefore, data is measured from a known horizontal such as the surface or the spring-neutral/contact plane. For the purposes of these calculations, the spring-neutral or contact plane is chosen as the reference. A total force and moment balance is accomplished and the equilibrium displacement of the model from the spring neutral plane is calculated for each mode. The following relationships provide the means to reference the initial conditions to the equilibrium axis.

$$z_{eq} = \frac{W}{k_E} + \frac{W \delta^2}{2 k_{1,3} (l/2)^2} \quad (35)$$

$$\theta_{eq} = \frac{\delta W}{2 k_{1,3} (l/2)^2} \quad (36)$$

$$\phi_{eq} = \frac{z_4 - z_2}{b/2} = 0 \text{ for all times; that is,} \quad (37)$$

the equilibrium axis and the contact axis measure roll relative to the horizontal.

```

PROGRAM MODANAL TRACE
      PROGRAM M(JANAL (IMPLT,CLIPUT,FLOT)
      DIMENSION C(6),F(5), Z(6,2),ZDOT(6,2),THA(6,2),THADCT(6,2)
      1,FUI(6,2),SWIDOT(6,2),TIME(6,2),ZFN(6,2),ZFW(6,2),ZFINAL(6,2),
      2,EXPTH(32),EXPTH(32),EXPTH(32),EXPTH(32),EXPTH(32),EXPTH(32),
      3,ZOC(6,2)
      REAL JXX,JYY,K13,K24,K5
      INTEGER F,C,C
      COMMON/FLMA/7CTAH,WNT,ZETAP,WNP,ZETAS,WNR,KE,CE,DELTA,MASS,JY)
      5
      10 C INPUT DATA
      READ 10,C(1),C(2),C(3),D(4),D(5),D(6)
      11 FORMAT (F10.5)
      READ 14,F,C,WNT,H,HEGF,PEGR
      14 FORMAT (3I5,3F10.4)
      READ 11,INIT,ISTOP,DT,TAU,K
      11 FORMAT (6F10.3,I5)
      READ 12,ZETAP,WNP,ZETAF,WNP,ZETAR,WNP
      12 FORMAT (6F10.5)
      READ 13,TKLGTH1,TKG1,JXX,JYY,WEIGHT,DELTA1
      13 FORMAT (6F10.3)
      READ 15,X,Y,YH,XP,YP,XR,YR
      15 FORMAT (6F10.3)
      READ 60,EXPTH(1),N=1,F)
      READ 60,EXPTH(M),M=1,F)
      READ 60,EXPTH(4),M=1,C)
      READ 60,EXPTH(1),N=1,C)
      READ 60,EXPTH(M),N=1,C)
      READ 60,EXPTH(M),M=1,C)
      20 FORMAT (F10.3)
      20 C CHANGE DATA TO EQUIBLIBRIUM AXIS
      DO 61 1=1,F

```

Fig. 13a. Program MODANAL

```

35      61 EXPHF(I) = EXPHH(I) - PECH
        CC 62 I=1,C
        62 EXPHF(I) = EXPHH(I) - PECH
        CC 63 I=1,C
        63 EXPHF(I) = EXPHH(I) - PECH
        C CORRECT PLATE TIME TO ACCOUNT FOR FREE FALL
        CC 64 I=1,F
        64 EXPHF(I) = EXPHH(I) - YAU
        C
        C INITIALIZERS
        I=0
        CT1 = 0
        TI=0.0
        LE=0
        NE=0
        51 JC(1)
        52 JC(2)
        53 JH(1)=0
        54 JH(2)=0
        55 PH(1)=0
        56 PH(2)=0
        C UNIT CONVERSIONS FOR COMPUTATIONS
        C CHANGE DIMENSIONS FROM (INCHES) TO (FEET)
        TKLGT = TKLGT/12.0
        TMR = TMR/12.0
        CELTA = CELTA/12.0
        C CHANGE HEIGHT (LRF) TO MASS (SLUGS)
        MASS = HEIGHT/32.2

```

Fig. 33b. Program MODANYL (cont.)

```

60      C COMPLETE THE INDIVIDUAL S/C UNIT LINEAR S/D COEFFICIENTS
      C24=(4.0*(ZFTAR*WNR*JX))/(TKP**2)
      K24=(2.0*(JYX*(WNR**2))/(TKP**2)
      DLNOM= (TKLGTH/2.0)**2
      C13 = ((75TAP*WNR*JY)-(75TAP*WNR*MASS*(DELTA**2)))/(CENOM*2.0)
      K13 = ((14WNR**2)*JY)-(MASS*(WNR**2)*(DELTA**2))/(CENOM*2.0)
      C22=2.0*(75TAP*WNR*JX)-((C13+C24))
      K2=(MASS*(WNR**2))-(2.0*(13+K24))
      K8 = (K13*2.0) + (K24*2.0) + K5
      C8 = (C13*2.0) + (C24*2.0) + C5

70      C SOLVE EQUATIONS & CREATE MATRICES
      C2 CONTINUE
      CALL ARCES (I,D,N,DT)
      L=L+1
      TIME(I)=T
      Z(L)=C(1)
      ZOOT(L)=C(2)
      TPA(L)=C(3)
      TPADEL(L)=C(4)
      PHI(L)=C(5)
      PHICOT(L)=C(6)
      IF (I.LT.TM10) GO TO 2
      IF (TIME(L-1).LT.TM10) CT = 10.0*DT
      IF (I.LT.ISTOP) GO TO 2
      CALL LOCATE (TIME,Z,TPA,PHI,K,XH,YH,ZCG)
      CALL LOCATE (TIME,Z,TPA,PHI,K,XF,YF,ZFN)
      CALL LOCATE (TIME,Z,TPA,PHI,K,XF,YR,ZFW)

80      C PRINT OUTPUT

```

Fig. 33c. Program MOEANYL (cont.)

```

SUBROUTINE F      1FCE
    SUBROUTINE F(T,D,P)
    DIMENSION C(6),P(6)
    COMMON/BLK/7ZTAH,WNP,ZETAP,WLP,ZETAR,WNR,KE,CE,DELTA,MASS,JYY
    P(1)=C(2)
    P(2)=(-2.*ZETAP*WNP*C(2))-((WNP**2)*D(1))+((CE*DELTA*D(4))*12.0)
    1 /MASS) + ((KL*DELTA*C(3))*12.0)/MASS)
    P(3)=C(4)
    P(4)=(-2.*ZETAP*WNP*C(4))-((WNP**2)*D(3))+((CL*DELTA*D(2)))/(JYY
    1 *12.0) + ((KE*DELTA*D(1)))/(JYY*12.0)
    1 -((KL*DELTA*D(1))/JYY)
    P(5)=C(6)
    P(6)=(-2.*ZETAR*WNR*C(6))-((WNP**2)*C(5))
    RETURN
    END

SUBROUTINE LOCATE
    SUBROUTINE LOCATE (TIME,Z,THA,PHI,K,XP,YP,ZFINAL)
    DIMENSION ZFINAL(K),IPE(K),Z(K),IHA(K),PHI(K)
    DO 1 I=1,K
    1 ZFINAL(I) = Z(I) - (XP*(SIN(THA(I)))) + (YP*(SIN(PHI(I))))
    RETURN
    END

```

Fig. 34. Program MODINV, Subroutines F and LOCATE

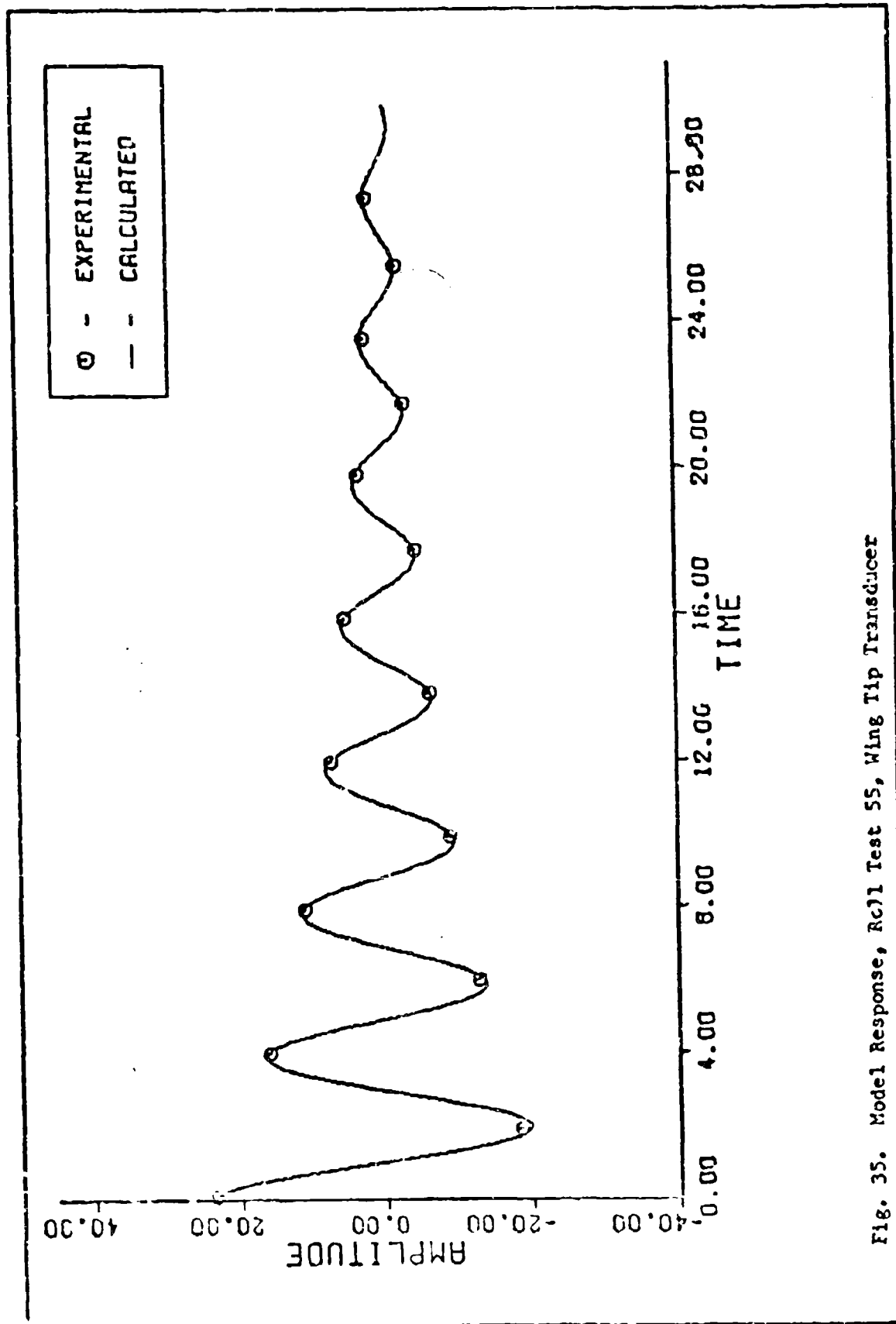


Fig. 35. Model Response, Rc71 Test 55, Wing Tip Transducer

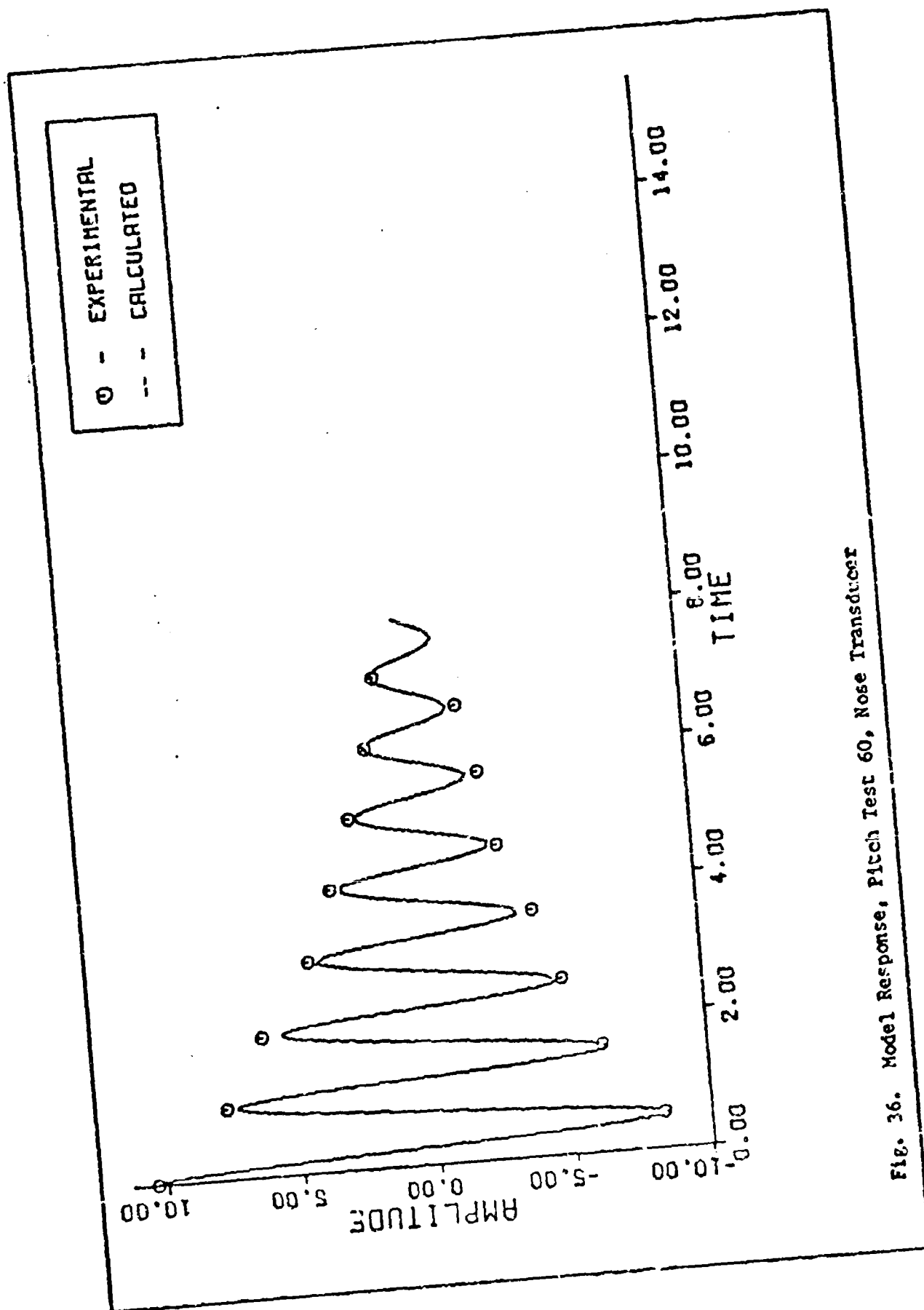


Fig. 36. Model Response, Pitch Test 60, Nose Transducer

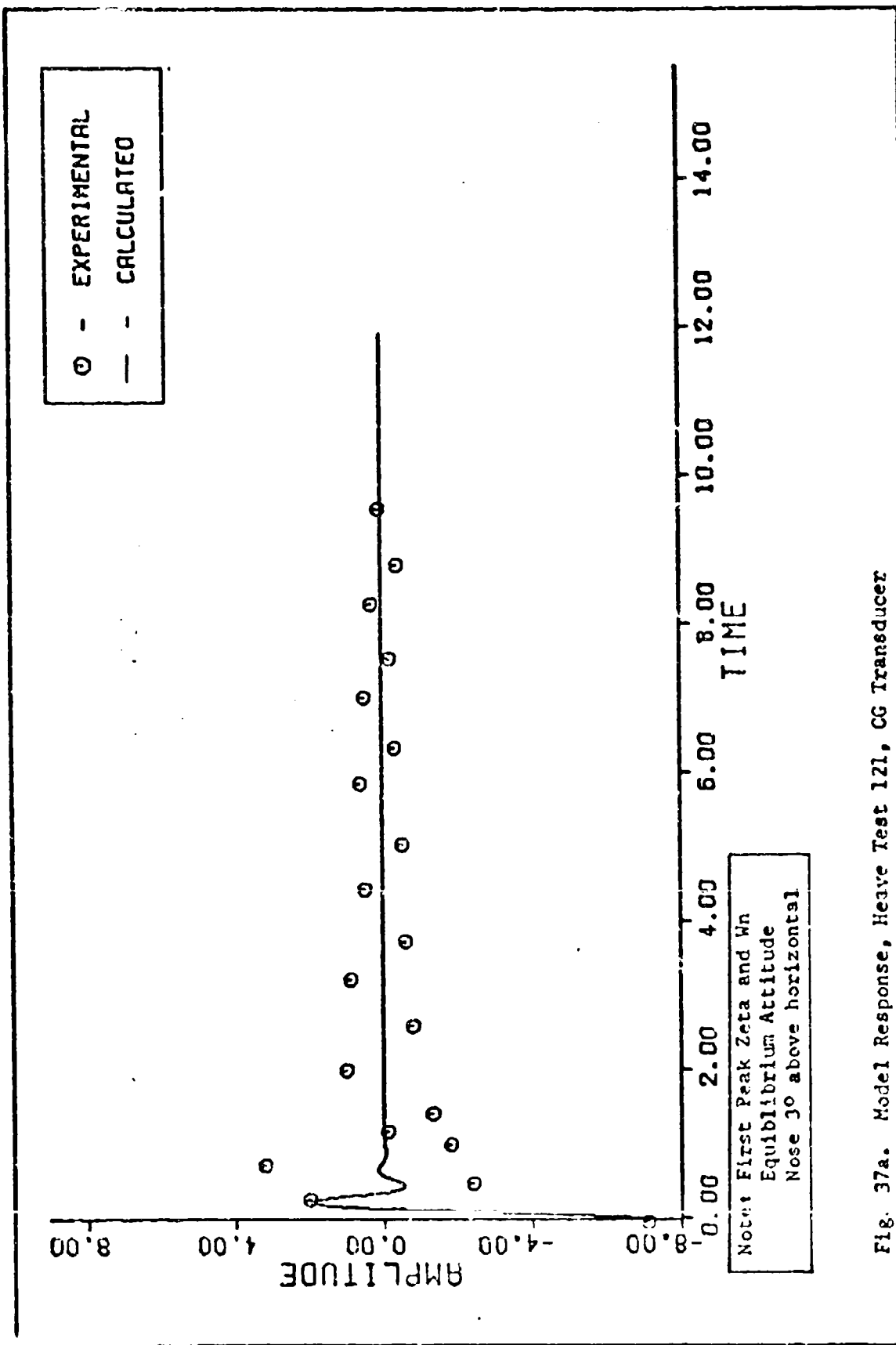


Fig. 37a. Model Response, Heave Test 121, CG Transducer

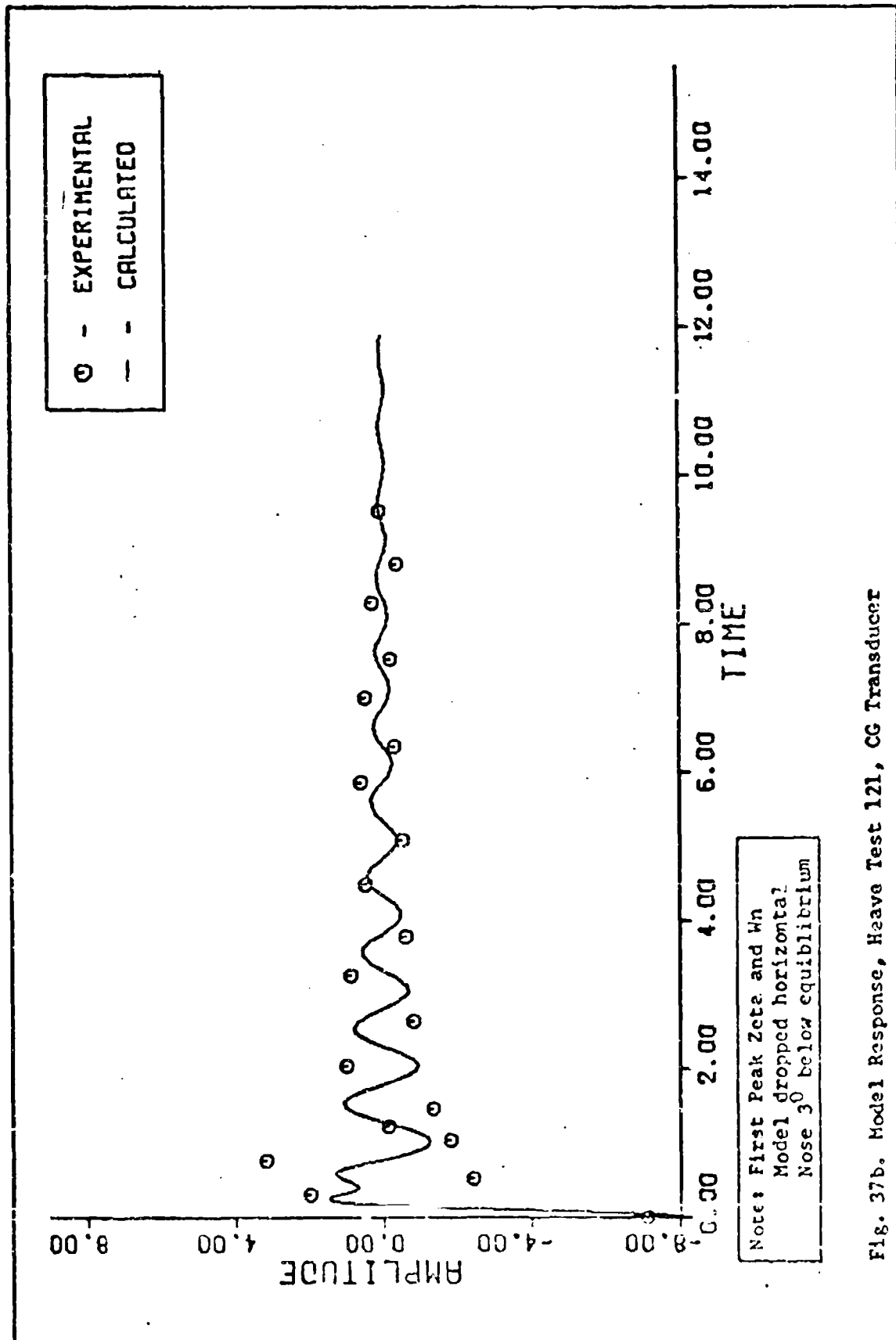
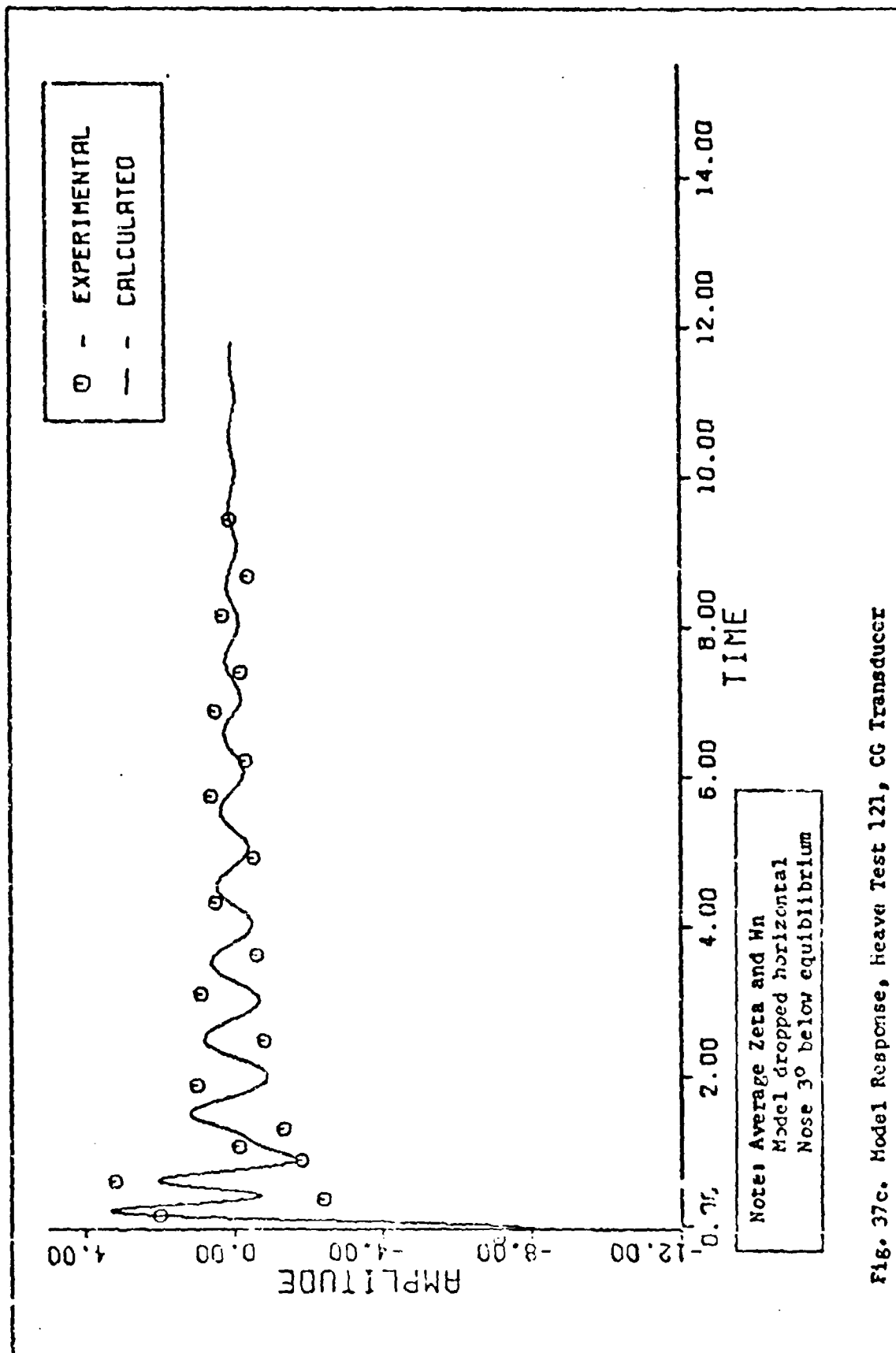


Fig. 37b. Model Response, Heave Test 121, CG Transducer



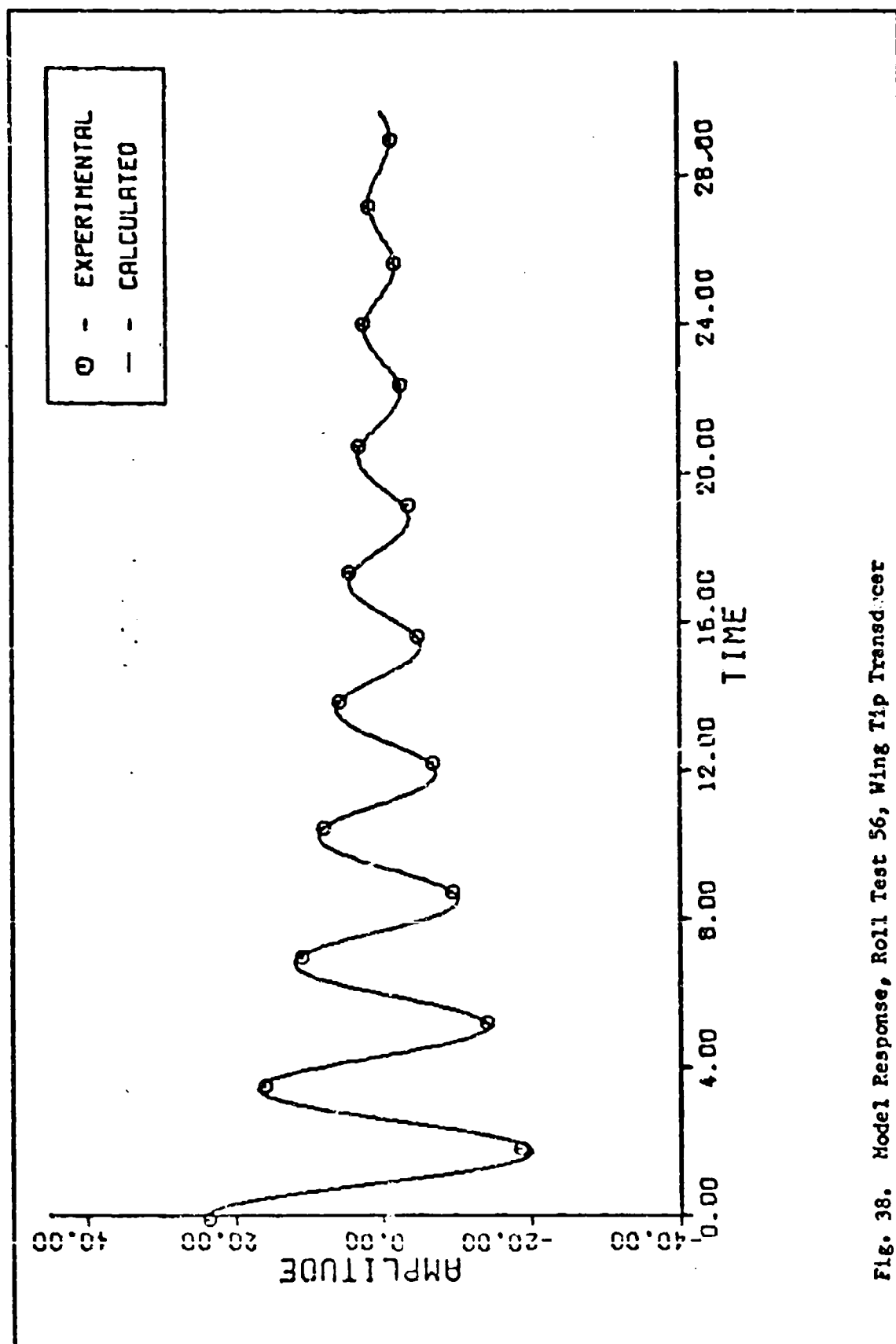


Fig. 38. Model Response, Roll Test 56, Wing Tip Transducer

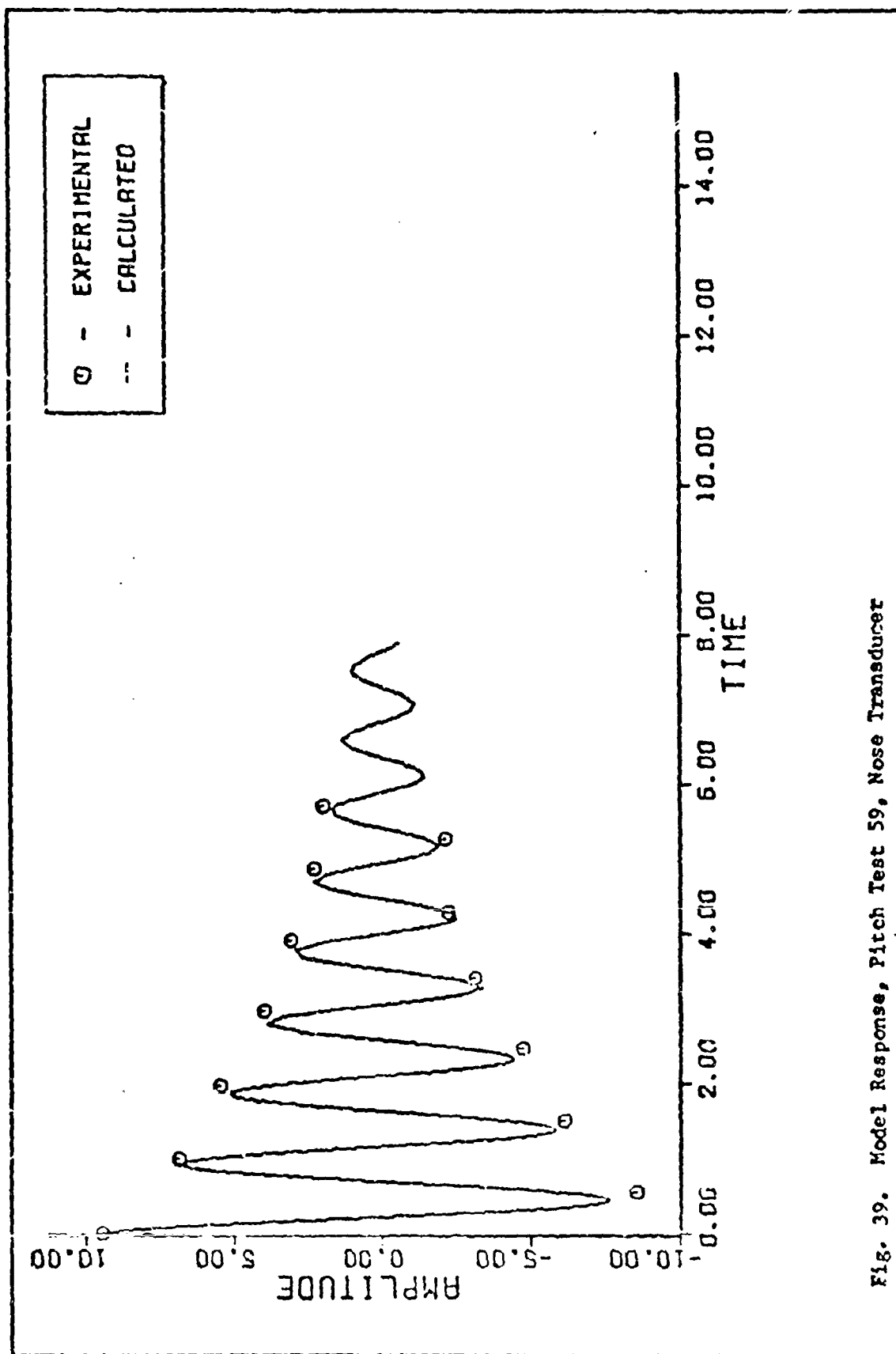


Fig. 39. Model Response, Pitch Test 59, Nose Transducer

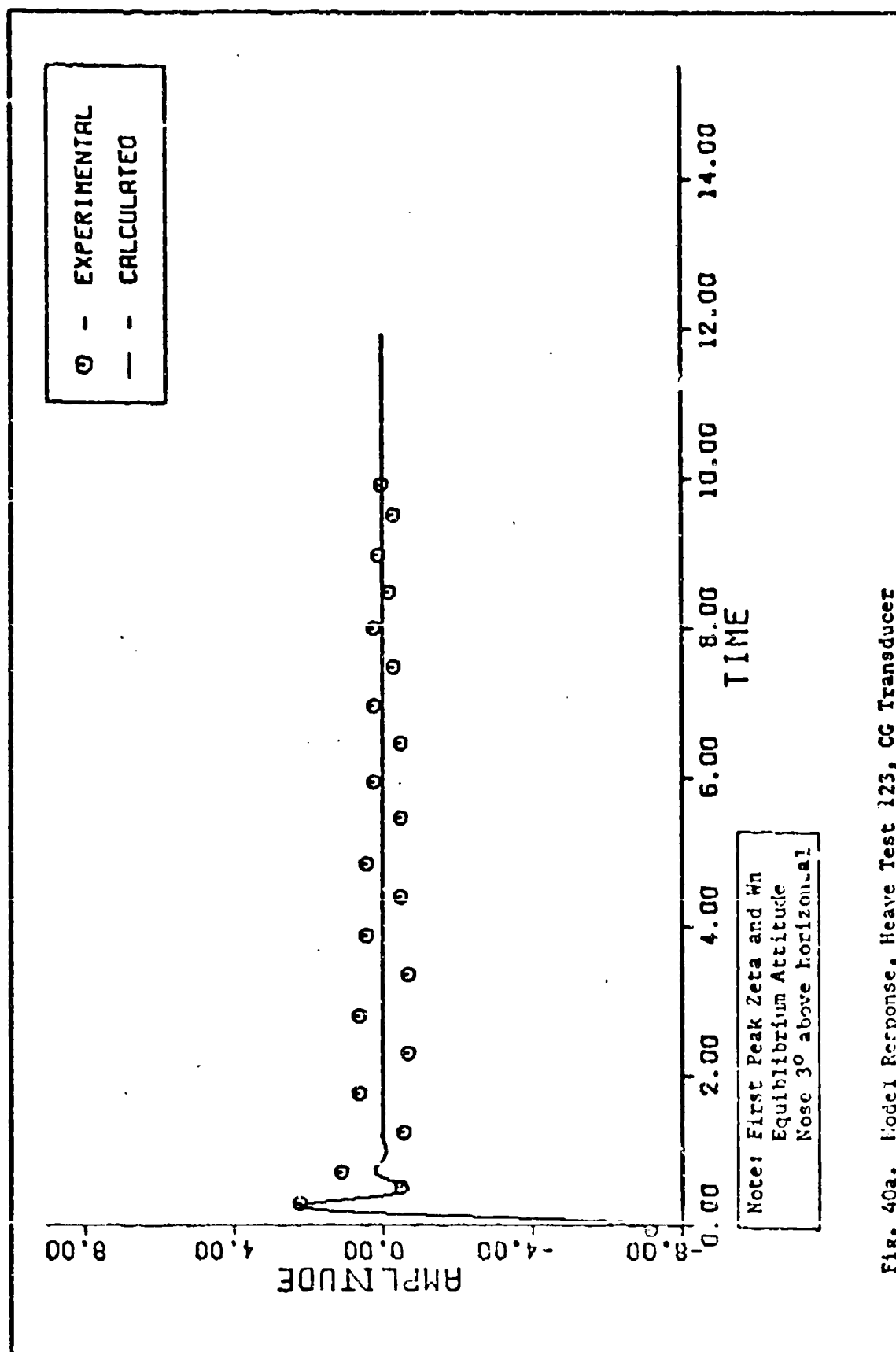


Fig. 40a. Model Response, Heave Test 123, CG Transducer

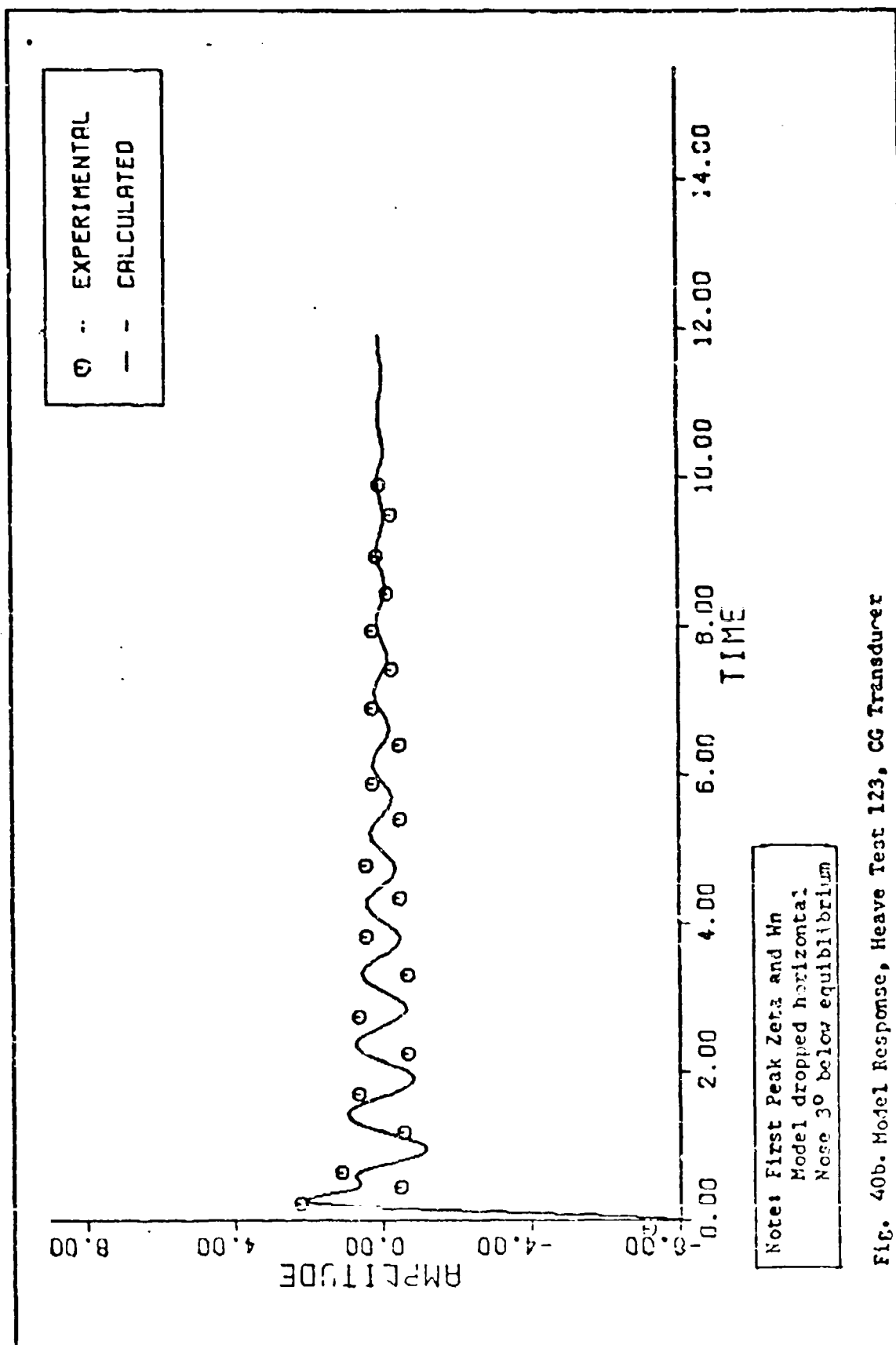


Fig. 40b. Model Response, Heave Test 123, CG Transducer

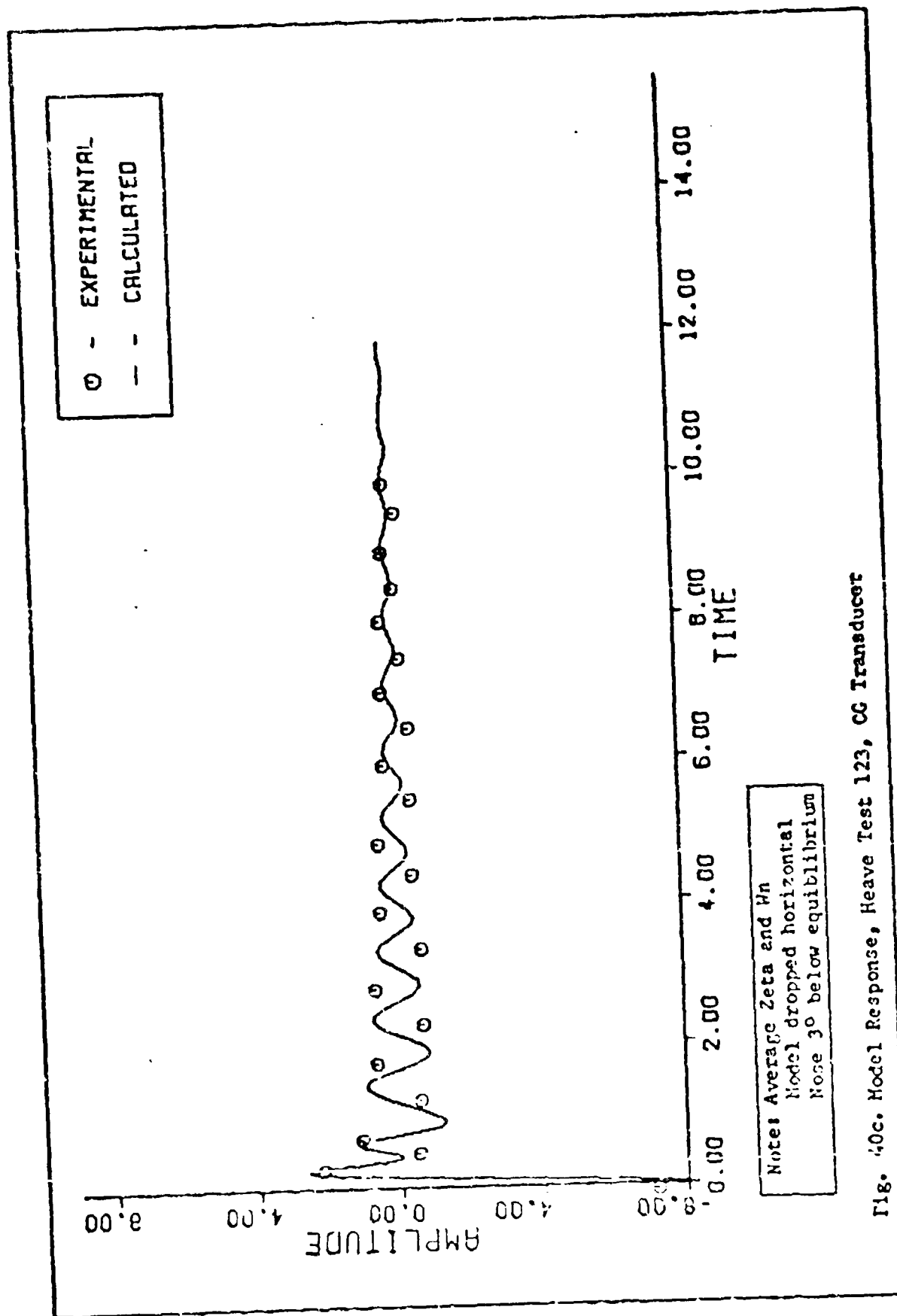


Fig. 40c. Model Response, Heave Test 123, CG Transducer

Appendix C

Justification of the Small Angle and
Horizontal Displacement Assumptions
in Pitch and Roll

General

In the main text, simplifications were made to the pitch and roll analysis that were based upon the assumption that the respective angles were small and/or the assumption that the horizontal displacement of a point during pitch or roll was negligible. Justification of these assumptions in the text would have been unwieldy, and would have detracted from the primary analysis. The roll mode has been chosen for this detailed illustration because it has the maximum motion.

Geometry

The roll linear displacement transducer was affixed to the Jindivik suspension frame a distance (L) above the horizontal surface through the center of gravity. A wire on inertia-reel from the transducer was attached to the wing tip at point a . Figure 41 shows the wing in deflection from equilibrium (ϕ). The transducer records a vertical displacement (h), but the attachment point is constrained by the wing and must sweep out the arc $w-w$. The wire, originally of length (L), is reduced to a length ($L-h$). Point a , attached to the wire, must be on arc $t-t$ also, where arc $t-t$ is part of a circle centered

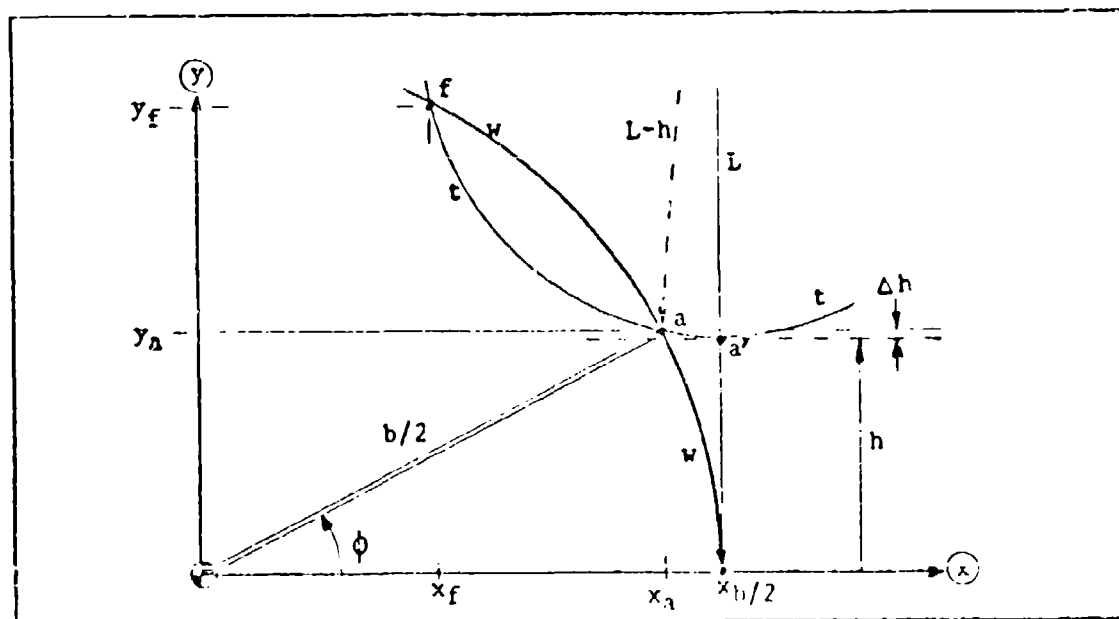


Fig. 41. Vertical and Translational Transducer Errors

at the transducer with radius $(L-h)$. If the movement were truly vertical, the point of attachment would be at a' , but it is at position a instead. This results in a vertical error (Δh) , and a horizontal error $(X_{b/2} - X_a)$.

Analysis

An origin is created at the center of gravity with an x, y axis defined for this problem as illustrated. Equations are then written which describe the arcs.

$$\text{For arc w-w: } x^2 + y^2 = (b/2)^2 \quad (38)$$

$$\text{For arc t-t: } (x - b/2)^2 + (y - L)^2 = (L - h)^2 \quad (39)$$

Simultaneous solution of these equations will yield the coordinates for points a and f . From (38), solve for $x = [(b/2)^2 - y^2]^{1/2}$ and substitute into (39) to solve for

$$y_{a,f} = \frac{LK \pm \sqrt{(LK)^2 - 4[L^2 + (b/2)^2][K^2/4 - (b/2)^4]}}{2[L^2 + (b/2)^2]} \quad (40)$$

where

$$K = 2(b/2)^2 + 2hL - h^2 \quad (41)$$

For the maximum roll case

$$L = 14 \text{ ft.} = 168 \text{ in.}$$

$$b/2 = 164.75 \text{ in.}$$

$$h = 22 \text{ in.}$$

from which

$$y_a = 22.005 \text{ in.}$$

$$\Delta h = .005 \text{ in.}$$

This calculation shows that the vertical error is negligible.

Substituting y_a into equation (38) results in a solution for

$$X_a = 163.268 \text{ in.}$$

Point a translates by the amount $b/2 - X_a = 1.482 \text{ in.}$ Thus, the horizontal translation is only about 1% of the half span $(b/2)$, and can thus be considered negligible.

The method above allows a precise calculation of the roll angle, also, where

$$\phi = \tan^{-1} y_a / x_a$$

For roll, $\phi_{\max} = 7.68$ degrees, which supports the small angle assumption.

The pitch case follows the same analysis except the half-span is

replaced by the distance between the nose transducer attachment point and the center of gravity (166.51 in.), and the maximum vertical displacement is 19.80 inches. The analysis shows that

$$\Delta h = 19.8047 \text{ in.}$$

$$X_G = 165.328 \text{ in.}$$

$$\Delta h = .0047 \text{ in.}$$

$$\theta_m = 6.23 \text{ degrees}$$

$$\text{Translation} = 1.182 \text{ in.}$$

which together support the original assumptions.

Although the above analysis used the displacement transducers as the example, the same assumptions hold true for the trunk. The x-displacement changes magnitude but their relationships and the maximum angles remain the same. The results of this analysis were used during development of the ACLS model as described in Chapter II and in subsequent calculations.

Appendix D
AFFDL Jindavik and Test Data

Certain data required in various computations was provided by the Air Force Flight Dynamics Laboratory, Mechanical Branch.

1. Ejector Test Results

Equilibrium Hover Conditions	Vent Opened	Vent Closed	Flow Added $P_c \approx 12.5$ psi	Flow Added $P_c \approx 30.4$ psi
Trunk pressure (P_t)	1.94	1.70	1.64	1.56
Cushion pressure (P_c)	0.03	0.61	0.65	0.68
Trunk flow (\dot{m}_t) lb _m /sec	0.79	0.97	1.02	1.07
Cushion flow (\dot{m}_c) lb _m /sec	UNK	0.0	0.46	1.32
Trunk footprint (A_t)	1238	612	579	565

2. Static Stiffness

Roll (R_R) ft-lb/rad	4583.66	3437.75	2864.79	-
Pitch (R_P) ft-lb/rad	51,566.2	51,566.2	51,566.2	-
Heave (R_H) lb/ft	9000	8400	7200	-

3. Heave Test

Drop Time, Release to contact (sec)	0.1	-	0.098	0.081
--	-----	---	-------	-------

4. Jindivik and ACRS

Moment of Inertia (J_{xx})	slug-ft ²	1190
Moment of Inertia (J_{yy})	slug-ft ²	1810
Weight	lb _f	2470
Trunk width	in	35.2
Trunk length	in	107.7
CP to CG Displacement (S)	in	8.56

VITA

Frederick C. Bauer was born on 20 May 1942 in Malden, Massachusetts, the son of Philip R. Bauer and Nita M. Bauer. He graduated from the United States Air Force Academy in 1963 with a Bachelor of Science degree and a commission as a Second Lieutenant in the United States Air Force. In 1964, he completed Undergraduate Pilot Training at Williams Air Force Base, Arizona, from which he received his pilot rating. While operationally assigned to Tactical Air Command (TAC), Pacific Air Command (PACAF), and the United States Air Forces in Europe (USAFE) from 1964-1972, he has flown C-130, CH-3, H-19, T39, and UH-1P mission aircraft. In 1971, he received the degree of Master of Science in Systems Management from the University of Southern California.

Permanent address: 4365 Antioch Drive
Enon, Ohio 45323

This thesis was typed by Mrs. Dorothy T. Bauer.